Supplementary information

A rigid phenyl-based covalently interlocked macrocycle with inherent porosity

Biao Xia[ab], Hartmut Komber[c], Sven M. Elbert*[d], Michael Mastalerz*[d], Junzhi Liu*[abe]

[a]Department of Chemistry, HKU-CAS Joint Laboratory on New Materials and Shanghai-Hong Kong Joint Laboratory on Chemical Synthesis, The University of Hong Kong, Pokfulam Road, Hong Kong, China

[b]Materials Innovation Institute for Life Sciences and Energy (MILES), HKU-SIRI, Shenzhen, China

[c]Leibniz-Institut for Polymerforschung Dresden e. V., Hohe Straße 6, 01069 Dresden, Germany

[d]Organisch-Chemisches Institut, Ruprecht-Karls-Universität Heidelberg, Im Neuenheimer Feld 270, 69120 Heidelberg, Germany

[e]State Key Laboratory of Synthetic Chemistry, The University of Hong Kong, Pokfulam Road, Hong Kong, China

*Corresponding author: sven.elbert@oci.uni-heidelberg.de; michael.mastalerz@oci.uni-heidelberg.de; juliu@hku.hk

Table of Contents

1. Materials and methods

All reactions were run under nitrogen atmosphere. Dichloromethane (DCM) and toluene were dried by solvent purification system (Inert) prior to use. All other chemicals were used without any further purification. 3-Chloro-5-*tert*-butyl-phenylboronic acid pinacol ester (**1**)[1], 4''-bromo-5'-(4-(*tert*-butyl)phenyl)-4-iodo-3'-(4-iodophenyl)-1,1':2',1''-terphenyl (**5**)[2] and 1,3-dibromo-5-chloro-2-iodobenzene (**10**)[3] were synthesized according to the reported procedures.

Recycling gel permeation chromatography (rGPC) was performed on a LaboACE LC-5060 (JAL, Japan) recycling preparative gel permeation chromatography (rGPC) device with UV detectors assembled with JAIGEL 2.0HR and 2.5HR columns and HPLC grade tetrahydrofuran (THF) as solvent. Preparative thin layer chromatography (P02015, Analtech Brand Silica Gel GF TLC Plates 2000μm 20x20cm) was bought form Miles Scientific company and used as received. The ultraviolet–visible (UV-vis) spectroscopy was conducted on the Agilent Cary 60. High-resolution mass spectra were obtained on a Bruker Q-Tof Maxis II mass spectrometer and a DFS high resolution magnetic sector mass spectrometer and Bruker Autoflex MALDI-TOF. Accurate masses from high-resolution mass spectra were reported for the molecular ion $[M+Na]^+$, $[M+K]^+$, $[M]^+$ or $[M+H]^+$. ^1H NMR and ^{13}C NMR spectra were obtained on a Bruker 400 or 500 spectrometer (400/500 MHz for ^1H, 101/125 MHz for ^{13}C). Chemical shifts are reported as parts per million (ppm) with residual solvent signals as internal standard (chloroform-*d* ($CDCl_3$): δ = 7.26 ppm (^1H), δ = 77.16 ppm (^{13}C); dimethyl sulfoxide-d_6 (d_6-DMSO): δ = 2.50 ppm (^1H), δ = 39.52 ppm (^{13}C); dichloromethane-d_2 (CD_2Cl_2): δ = 5.32 ppm (^1H), δ = 53.84 ppm (^{13}C), tetrachloroethane-d_2 ($C_2D_2Cl_4$): δ = 5.98 ppm (^1H), δ = 75.7 ppm (^{13}C)). Data for ^1H NMR were presented as following: chemical shifts (δ, ppm), multiplicity (br = broad, s = singlet, d = doublet, t = triplet, q = quartet, dd = doublet of doublets, tt = triplet of triplets, td = triplet of doublets, m = multiplet), coupling constant (Hz), and integration. Powder diffractometry was performed on Rigaku SmartLab diffractometer operated at

9 kW and equipped with a HyPix-3000 detector with incident CuKα radiation at λ = 1.54059 Å using a Debye-Scherrer geometry. The samples have been ground prior to measurements and have been measured in special glass mark-tubes with a 0.6 mm inner diameter at a capillary spin stage with 60 rpm. A background was collected using an empty capillary with the same measurement conditions and this was used for baseline correction by subtraction.

The surface areas and porosity was characterised by nitrogen and argon sorption analyses with autosorb computer-controlled surface analysers (AUTOSORB-IQ3, Quantachrome). Cooling was accomplished using a compressed helium CryoCooler (IQ3). The IQ3 is equipped with 1000, 10 and 0.1 torr sensors for low pressure measurements. For the measurements, 38.5 mg of **[2]CIM** were loaded intor 6 mm cryo cooler tubes (IQ3). The Brunauer-Emmett-Teller (BET) surface areas were calculated assuming a cross sectional area of 0.162 nm^2 for nitrogen molecules and 0.142 nm^2 for argon molecules at 77 K (N_2) and 87 K (Ar). The corresponding pressure ranges have been determined using Rouquerol plots; here only the relative pressure values with a positive slope in the Rouquerol plot were taken into account. The specific properties of the corresponding gases can be found in the gas sorption chapter of this Supporting Information. Gas selectivities were calculated using 3P's 3P Sim software (Version 1.1.0.9; 2018).

2. General procedures for the synthesis of compounds 3, 4, 5, 6, 8-13

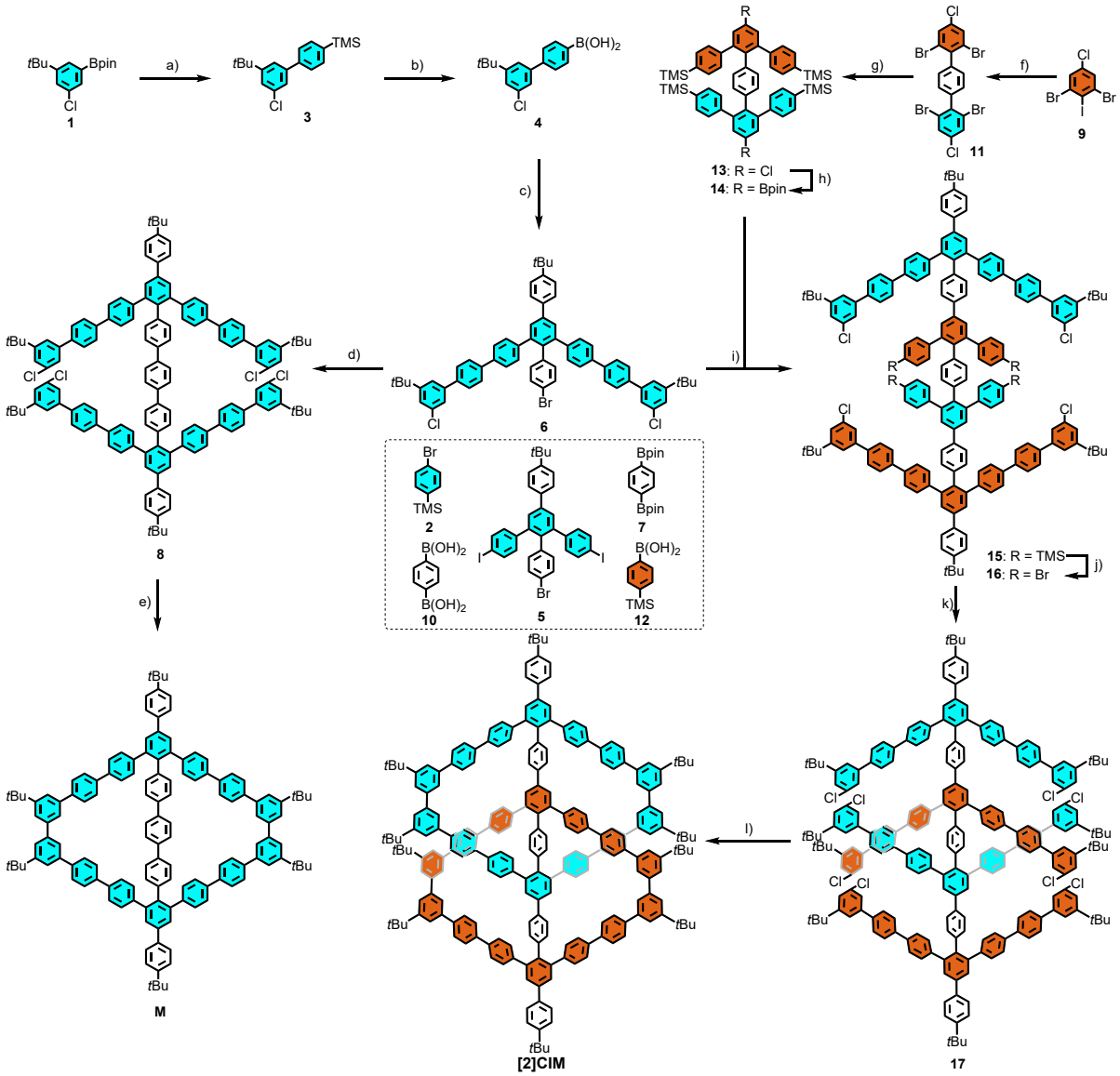

Synthesis of **(3'-(*tert*-butyl)-5'-chloro-[1,1'-biphenyl]-4-yl)trimethylsilane (3)**

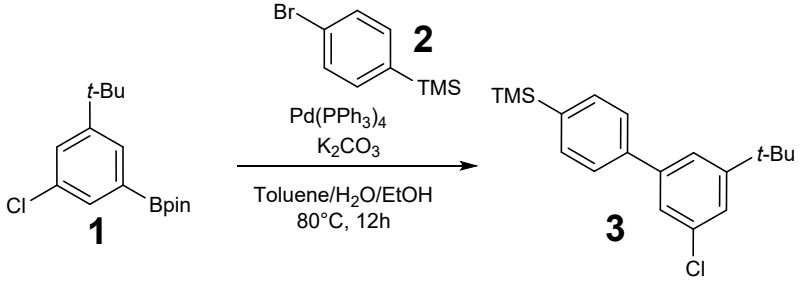

A mixture of 3-chloro-5-*tert*-butyl-phenylboronic acid pinacol ester (**1**)[1] (3.0 g, 10.18 mmol, 1.0 eq), (4-bromophenyl)trimethylsilane (**2**) (2.33 g, 10.18 mmol, 1.0 eq), and potassium carbonate (K_2CO_3) (4.22 g, 30.55 mmol, 3.0 eq) in toluene, ethanol and water (60 mL/10 mL/10 mL) was bubbled by N_2 for 30 minutes before the addition of tetrakis(triphenylphosphine)palladium(0) (588.3 mg, 0.509 mmol, 0.05 eq), then it was heated at 80 °C under N_2 atmosphere for 12 hours. The reaction mixture was poured into water, and the product was extracted with DCM (50 mL × 3) and the organic layer was dried over sodium sulfate (Na_2SO_4), concentrated, then the crude material was purified by silica gel column chromatography (eluent: hexane) to afford (3'-(*tert*-butyl)-5'-chloro-[1,1'-biphenyl]-4-yl)trimethylsilane **(3)** in 90 % yield (2.91 g, 9.18 mmol) as a colorless oil.

^{1}H NMR ($CDCl_3$, 400 MHz, 30 °C) δ 7.62 (d, J = 8.0 Hz, 2H), 7.55 (d, J = 8.0 Hz, 2H), 7.47 (s, 1H), 7.39 (s, 1H), 7.35 (s, 1H), 1.36 (s, 9H), 0.31 (s, 9H); ^{13}C NMR ($CDCl_3$, 101 MHz, 30 °C) δ 153.73, 142.83, 141.01, 140.03, 134.47, 134.01, 126.71, 124.75, 124.58, 122.90, 35.18, 31.39, 0.96; HRMS (ESI): calcd. for $C_{19}H_{25}ClSiNa$ ([M + Na]$^+$): 339.1306, found: 339.1295, error: 3.2 ppm.

Synthesis of **(3'-(*tert*-butyl)-5'-chloro-[1,1'-biphenyl]-4-yl)boronic acid (4)**

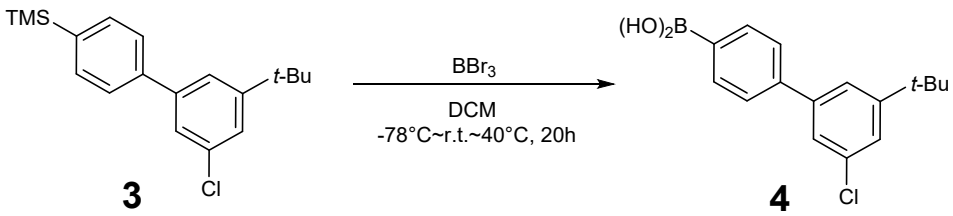

3 (2.91 g, 9.18 mmol, 1.0 eq) and 30 mL dry DCM were added to a 250 mL round bottle, then the boron tribromide (BBr_3) (13.8 mL, 1 M in DCM, 13.8 mmol, 1.5 eq) was added to the bottle at -78 °C dropwise. This reaction was kept at -78 °C for 2 hours, then warm to room temperature, stirred for another 2 hours, then it was heated at 40 °C and stirred for another 18 hours. This reaction was quenched by 5 M KOH aqueous

solution (11.0 mL, 55.1 mmol, 6.0 eq) at -78 °C, then it was brought to room temperature, acidified by 2 M HCl aqueous solution (41.3 mL, 82.6 mmol, 9.0 eq), stirred for 2 hours, then DCM was removed under reduced pressure, dimethyl ether (Et_2O) (50 mL) was added to the reaction mixture to dilute the product and the organic phase was washed by water (100 mL × 3). The organic layer was dried by Na_2SO_4, concentrated, the obtained organic material was washed by hexane (10 mL × 3) to afford (3'-(*tert*-butyl)-5'-chloro-[1,1'-biphenyl]-4-yl)boronic acid **(4)** (1.94 g, 73 %) as a white solid and used for the next step directly.

Synthesis of **6**

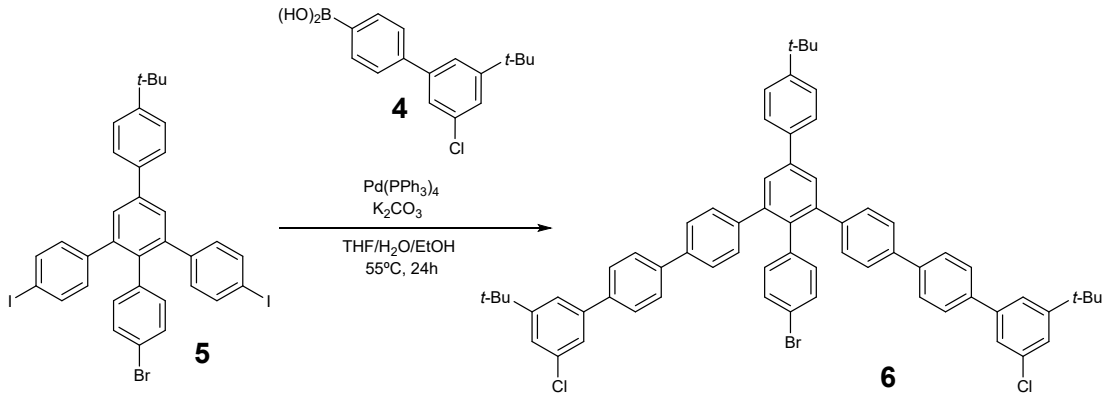

A mixture of **4** (787.7 mg, 2.73 mmol, 2.1 eq), **5**[2] (1.0 g, 1.3 mmol, 1.0 eq), and K_2CO_3 (1.8 g, 13.0 mmol) were dissolved in THF, ethanol and water (60 mL/10 mL/10 mL), the solution was purged with N_2 for 30 minutes, then tetrakis(triphenylphosphine)palladium(0) (75.1 mg, 0.065 mmol) was added to the mixture. The reaction mixture was then heated to 55 °C for 24 hours. After cooling, the reaction mixture was diluted with 30 mL water, extracted with CH_2Cl_2 (30 mL × 3) and the organic layer was dried with Na_2SO_4, concentrated, and purified by silica gel column chromatography (eluent: hexane/DCM = 10/1 to 8/1 to 6/1) to afford the desired product **6** (1.07 g, 82 %) as a white solid.

^{1}H NMR (CD_2Cl_2, 400 MHz, 30 °C) δ 7.75 (s, 2H), 7.72-7.65 (10H), 7.57-7.52 (8H), 7.46 (t, J = 1.6 Hz, 2H), 7.39 (t, J = 1.6 Hz, 2H), 7.26 (t, J = 4.0 Hz, 4H), 7.21 (d, J = 10.8 Hz, 2H), 6.90 (d, J = 10.8 Hz, 2H), 1.38 (s, 27H); ^{13}C NMR (CD_2Cl_2, 101

MHz, 30 °C) δ 154.32, 151.38, 142.47, 142.43, 141.39, 140.75, 140.18, 139.63, 139.01, 138.75, 137.58, 136.94, 134.67, 133.89, 131.01, 130.90, 128.67, 127.93, 127.67, 127.11, 126.64, 126.35, 125.06, 124.50, 123.00, 120.74, 35.38, 34.90, 31.49, 31.38; HRMS (ESI): calcd. for $C_{66}H_{59}BrCl_2K$ ([M + K]$^+$): 1041.2797, found: 1041.2744, error: 5.1 ppm.

Synthesis of **8**

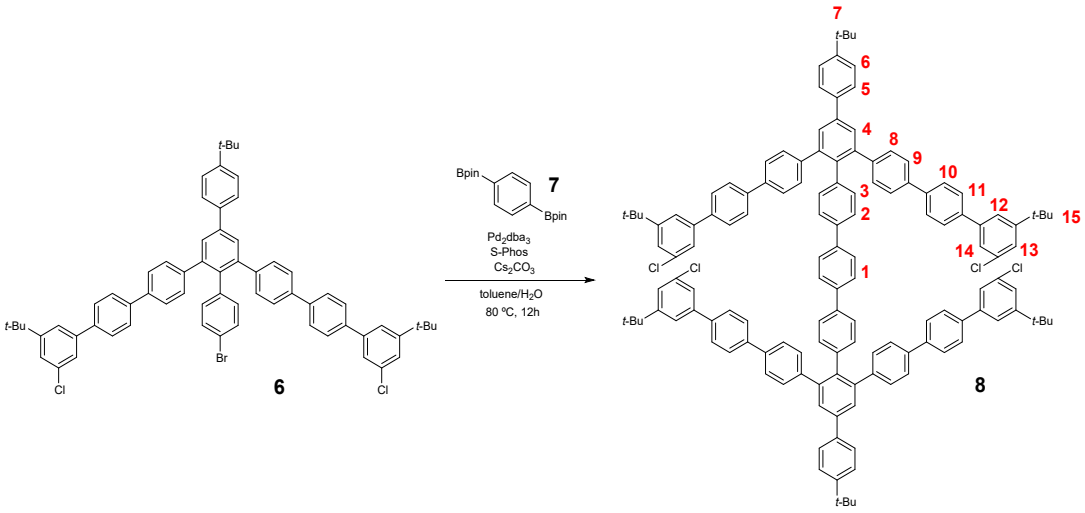

To a mixture of **6** (200.0 mg, 0.199 mmol, 2.1 eq), 1,4-benzenediboronic acid bis(pinacol) ester (**7**) (31.3 mg, 0.095 mmol, 1.0 eq), Cs_2CO_3 (309.4 mg, 0.950 mmol, 10.0 eq), 2-dicyclohexylphosphino-2',6'-dimethoxybiphenyl (31.2 mg, 0.076 mmol, 0.8 eq) and tris(dibenzylideneacetone)dipalladium (0) (34.8 mg, 0.038 mmol, 0.4 eq) were added degassed toluene and water (10 mL/5 mL), then it was heated at 80 °C under N_2 atmosphere for 12 h. The reaction mixture was poured into water and extracted with DCM (30 mL × 3); the organic layer was dried over Na_2SO_4, concentrated, then the crude material was purified by silica gel column chromatography (eluent: hexane/DCM = 6/1 to 5:1) to give **8** (115 mg, 0.060 mmol, 63 %) as a white solid.

^{1}H NMR ($C_2D_2Cl_2$, 500 MHz, 30 °C) δ 7.78 (s, 4H; 4), 7.71 (d, *J* = 8.6 Hz, 4H; 5), 7.68 (d, *J* = 8.3 Hz, 8H; 10), 7.60 (d, *J* = 8.3 Hz, 8H; 11), 7.58 (s, 4H; 1), 7.51 (d, *J* = 8.6 Hz, 12H; 6, 9), 7.48 (t, *J* = 1.4 Hz, 4H; 12), 7.40 (t, *J* = 1.4 Hz, 4H; 14), 7.35 (d, *J* = 8.2 Hz, 4H; 2), 7.33 (t, *J* = 1.4 Hz, 4H; 13), 7.28 (d, *J* = 8.2 Hz, 8H; 8), 7.01 (d, *J* = 8.2 Hz, 4H; 3), 1.38 (s, 18H; 7), 1.34 (s, 36H; 15); ^{13}C NMR ($C_2D_2Cl_2$, 125 MHz, 30 °C) δ 153.5, 150.5, 141.7, 141.6, 140.9, 139.5, 139.0, 138.8, 138.2, 137.5, 137.2, 137.1, 136.8, 133.9, 132.0 (3), 130.3 (8), 127.9 (4), 127.3 (11), 127.0 (10), 126.7 (1), 126.4 (5), 125.9 (9), 125.6 (6), 125.4 (2), 124.4 (13), 123.9 (14), 122.2 (12), 34.7, 34.2, 31.1 (7), 31.0 (15); HRMS (ESI): calcd. for $C_{138}H_{122}Cl_4$([M]$^+$): 1921.8300, found: 1921.8377, error: 4.0 ppm.

Synthesis of **11**

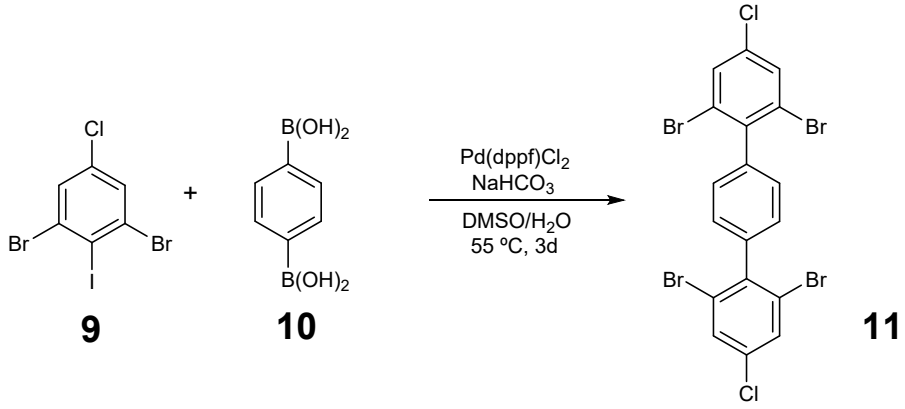

9 **10** **11**

To a mixture of **9**[3] (4.0 g, 10.09 mmol, 1.0 eq), 1,4-phenylenediboronic acid (**10**) (870.1 mg, 5.25 mmol, 0.52 eq), $NaHCO_3$ (2.54 g, 30.3 mmol, 3.0 eq) and [1,1′-bis(diphenylphosphino)ferrocene]dichloropalladium(II) (330.0 mg, 0.404 mmol, 0.04 eq) were added degassed DMSO and water (125 mL/20 mL), then it was heated at 55 °C under N_2 atmosphere for 3 days. The reaction mixture was poured into water and extracted with DCM (50 mL × 3); the organic layer was dried over Na_2SO_4, concentrated, then the crude material was purified by silica gel column chromatography (eluent: hexane) to give **11** (565 mg, 0.919 mmol, 18 %) as a white solid.

^{1}H NMR (CD_2Cl_2, 400 MHz, 30 °C) δ 7.72 (s, 4H), 7.29 (s, 4H); ^{13}C NMR (CD_2Cl_2, 101 MHz, 30 °C) δ 141.72, 140.54, 134.85, 132.05, 129.63, 124.81; HRMS (ESI): calcd. for $C_{18}H_8Br_4Cl_2$ ([M + Na]$^+$): 636.6588, found: 636.6538, error: 7.8 ppm.

Synthesis of **13**

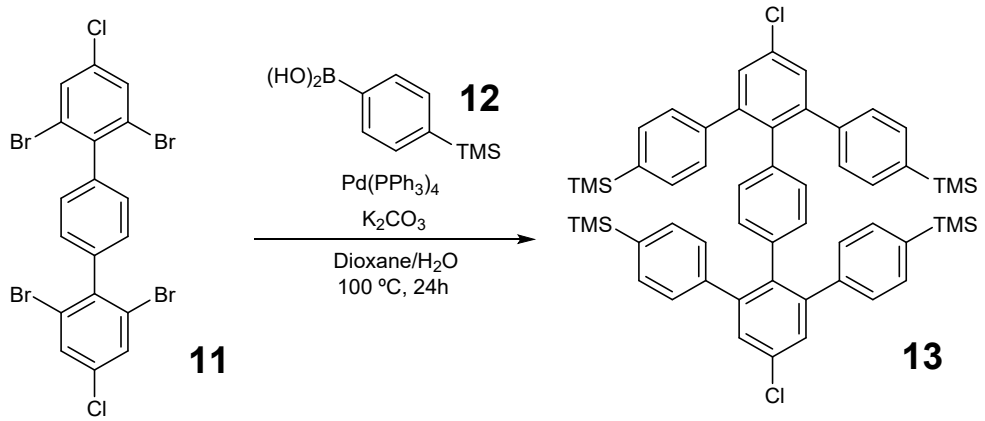

Under N_2 atmosphere, **11** (500 mg, 0.813 mmol, 1.0 eq), 4-trimethylsilylbenzeneboronic acid (**12**) (1.29 g, 6.67 mmol, 8.2 eq) and potassium carbonate (1.73 g, 12.5 mmol, 15.4 eq) were dissolved in a degassed mixed solvent of dioxane and H_2O (10 mL/1.5 mL), then tetrakis(triphenylphosphine)palladium(0) (117.5 mg, 0.102 mmol, 0.125 eq) was added to the mixture. The resulting solution was heated to 100 ºC and stirred for 1 day. the reaction mixture was diluted with water and extracted by DCM (50 mL × 3). The organic phase was dried over Na_2SO_4 and evaporated to dryness. The residue was purified by silica gel column chromatography (eluent: hexane:DCM 20:1) and **13** (585 mg, 0.813 mmol, 81%) was obtained as a white solid.

^{1}H NMR ($CDCl_3$, 400 MHz, 30 °C) δ 7.38 (d, J = 8.0 Hz, 8H), 7.36 (s, 4H), 6.94 (d, J = 8.0 Hz, 8H), 6.39 (s, 4H), 0.24 (s, 36H); ^{13}C NMR ($CDCl_3$, 101 MHz, 30 °C) δ 143.49, 141.28, 138.93, 137.21, 135.97, 132.95, 132.57, 131.12, 129.56, 129.30, -0.99; HRMS (ESI): calcd. $C_{54}H_{60}Cl_2Si_4K$([M + K]$^+$): 931.2772, found: 931.2746, error: 2.8 ppm.

Synthesis of **14**

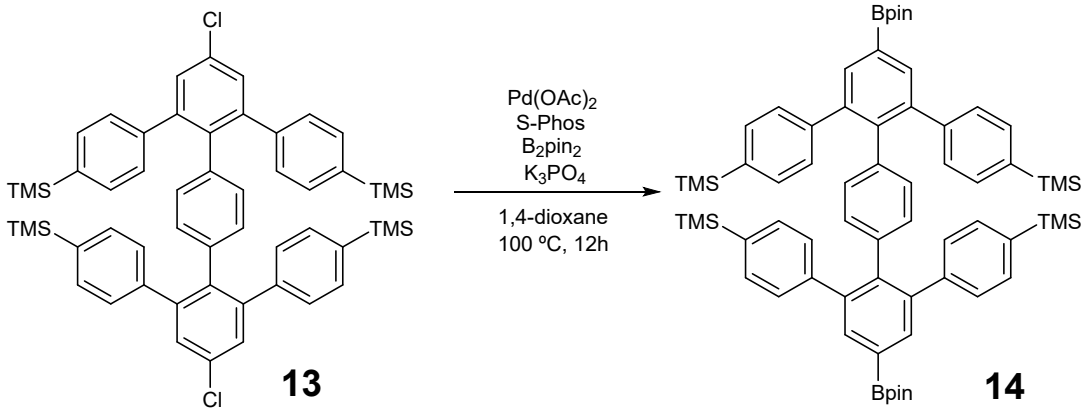

To the mixture of **13** (500 mg, 0.560 mmol, 1.0 equiv.), bis(pinacolato)diboron (853.8 mg, 3.36 mmol, 6.00 equiv.), potassium acetate (713.6 mg, 3.36 mmol, 6.00 equiv.), palladium(II) acetate ($Pd(OAc)_2$, 12.6 mg, 0.056 mmol, 0.1 eq), and 2-dicyclohexylphosphino-2',6'-dimethoxybiphenyl (S-Phos, 59.8 mg, 0.146 mmol, 0.26 eq) was added degassed anhydrous 1,4-dioxane (20 mL) in glove box. The reaction was heated to 100 °C for 12 hours and filtered over a plug of Celite, then washed by DCM. The solvent was concentrated, and the obtained material was washed by cold ethanol for several times to give product **14** (571 mg, 0.532 mmol, 95 %) as a white solid.

^{1}H NMR (CD_2Cl_2, 400 MHz, 30 °C) δ 7.74 (s, 4H), 7.40 (d, J = 7.2 Hz, 8H), 6.98 (d, J = 7.2 Hz, 8H), 6.43 (s, 4H), 1.32 (s, 24H), 0.24 (s, 36H); ^{13}C NMR (CD_2Cl_2, 101 MHz, 30 °C) δ 142.78, 141.58, 141.56, 138.40, 137.19, 136.44, 132.75, 131.16, 129.75, 84.31, 25.04, -1.03; HRMS (ESI): calcd. for $C_{66}H_{85}B_2O_4Si_4$([M + H]$^+$): 1075.5727, found: 1075.5715, error: 1.1 ppm.

Synthesis of **15**

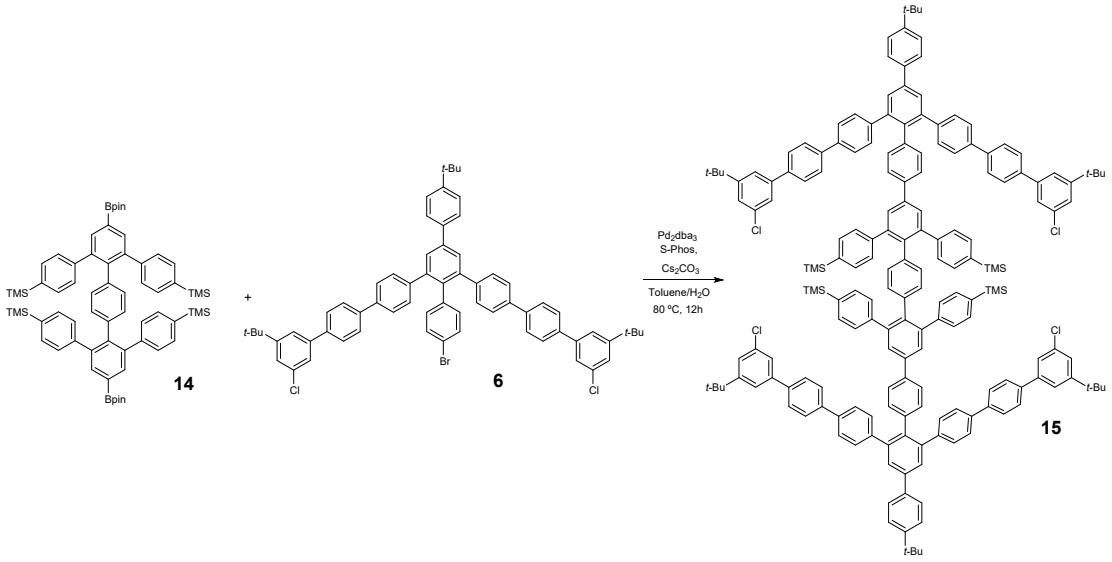

To a mixture of **14** (81.7 mg, 0.076 mmol, 1.0 eq), **6** (160.0 mg, 159.5 mmol, 2.1 eq), cesium carbonate (Cs_2CO_3) (247.5 mg, 0.760 mmol, 10.0 eq), 2-dicyclohexylphosphino-2',6'-dimethoxybiphenyl (25.0 mg, 0.061 mmol, 0.8 eq), and tris(dibenzylideneacetone)dipalladium(0) (27.8 mg, 0.030 mmol, 0.4 eq) was added degassed toluene and water (12 mL/6 mL), then it was heated at 80 °C under N_2 atmosphere for 12 hours. The reaction mixture was poured into water and extracted with DCM (30 mL × 3); then the organic layer was dried over Na_2SO_4, concentrated, then the crude material was purified by silica gel column chromatography (eluent: hexane/DCM = 6/1 to 5/1 to 4/1). To give **15** (116 mg, 0.042 mmol, 55%) as a white solid.

^{1}H NMR (CD_2Cl_2, 500 MHz, 30 °C) δ 7.76 (s, 4H), 7.71 (d, J = 6.8 Hz, 4H), 7.68 (d, J = 6.4 Hz, 8H), 7.63 (d, J = 6.8 Hz, 8H), 7.54-7.52 (20H), 7.44-7.42 (8H), 7.39-7.36 (12H), 7.31 (d, J = 6.4 Hz, 8H), 7.07 (d, J = 6.4 Hz, 4H), 6.97 (d, J = 6.0 Hz, 8H), 6.39 (s, 4H), 1.38-1.37 (54H), 0.19 (s, 36H); ^{13}C NMR (CD_2Cl_2, 125 MHz, 30 °C) δ 154.29, 151.29, 142.80, 142.62, 142.55, 142.50, 141.70, 140.52, 140.25, 139.54, 139.30, 138.60, 138.13, 137.95, 137.88, 137.73, 136.86, 134.67, 132.75, 132.68, 131.24, 130.93, 129.72, 129.12, 128.65, 128.43, 127.88, 127.64, 127.12, 126.54, 126.33, 126.26, 125.03, 124.48, 123.00, 35.38, 34.90, 31.50, 31.39, -1.06; HRMS (ESI): calcd. for $C_{186}H_{178}Cl_4Si_4$([M]$^+$): 2667.1792, found: 2667.1865, error: 2.7 ppm.

Synthesis of **16**

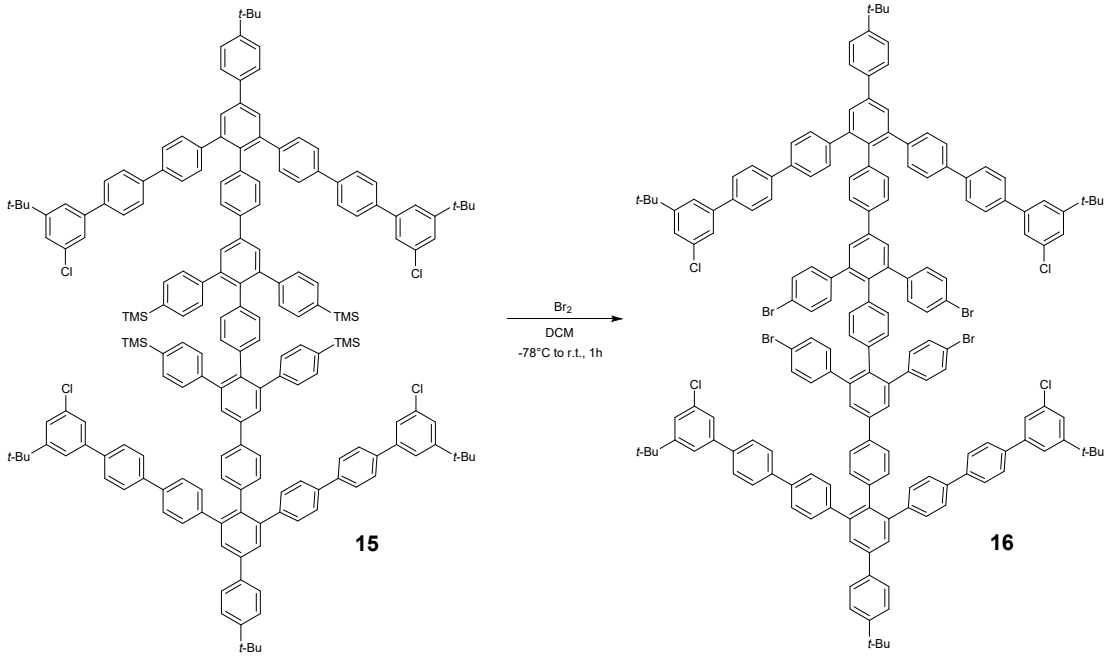

To a solution of **15** (100.0 mg, 0.037 mmol, 1.0 eq) in DCM (20 mL) was added bromine (38 μL, 0.750 mmol, 20.0 eq) at -78 °C dropwise. The reaction mixture was stirred for 1 hour before warmed to room temperature. After stirred for another 5 minutes, saturated aqueous solution of $Na_2S_2O_3$ was added to quench excess Br_2. The mixture was diluted with CH_2Cl_2 (50 mL), and the combined organic layer was washed by water (100 mL × 3) and dried over Na_2SO_4, then concentrated in vacuo. The compound **16** (92 mg, 0.034 mmol, 91%) was obtained as a white solid and used for the next step directly.

^{1}H NMR (CD_2Cl_2, 400 MHz, 30 °C) δ 7.75 (s, 4H), 7.70 (d, J = 8.0 Hz, 4H), 7.66-7.60 (16H), 7.53-7.50 (16H), 7.45 (s, 4H), 7.42 (s, 4H), 7.39-7.37 (8H), 7.30-7.25 (16H), 7.09 (d, J = 8.0 Hz, 4H), 6.83 (d, J = 8.0 Hz, 8H), 6.51 (s, 4H), 1.38-1.37 (54H); ^{13}C NMR (CD_2Cl_2, 101 MHz, 30 °C) δ 154.28, 151.31, 142.53, 142.41, 141.69, 141.65, 141.20, 140.55, 140.17, 139.61, 139.55, 138.59, 137.73, 137.67, 137.52, 137.05, 134.66, 132.75, 131.89, 131.09, 131.03, 130.93, 128.68, 128.41, 127.87, 127.62, 127.59, 127.11, 126.55, 126.34, 126.26, 125.05, 124.47, 122.96, 120.91, 35.37, 34.89,

31.49, 31.38; HRMS (ESI): calcd. $C_{174}H_{142}Br_4Cl_4$ ($[M]^+$): 2694.6584, found: 2694.8747, error: 80.3 ppm.

Synthesis of **17**

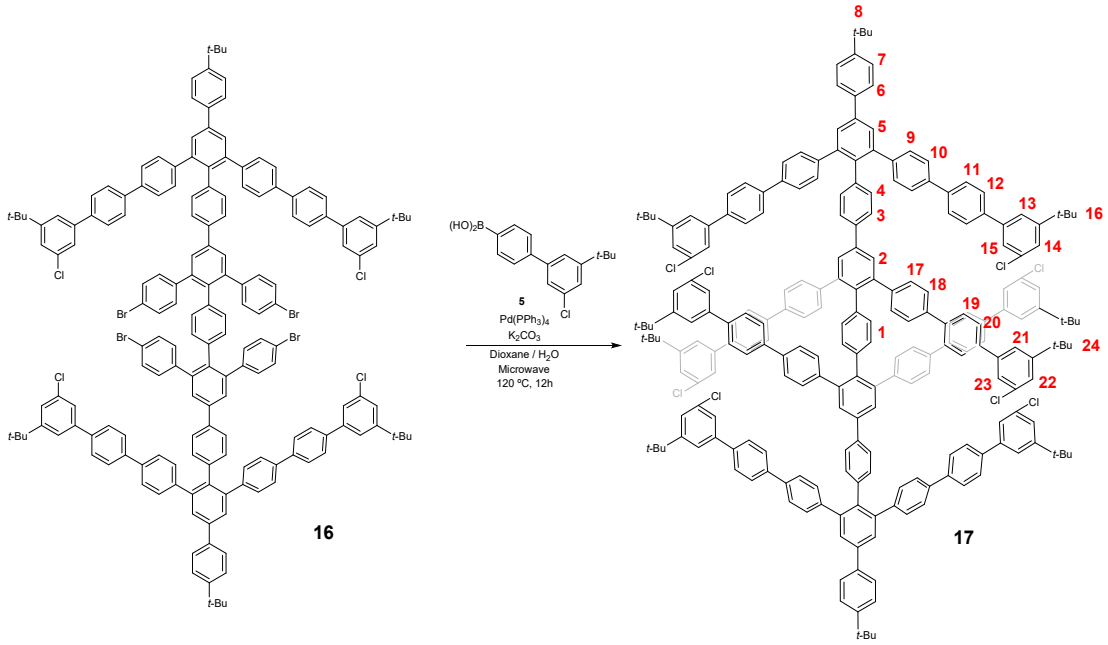

In a 35 mL microwave tube was added **16** (20.0 mg, 0.0074 mmol, 1.0 eq), **4** (42.8 mg, 0.149 mmol, 20.0 eq) and potassium carbonate (20.52 mg, 0.149 mmol), then dioxane (8 mL) and water (0.5 mL) were added. The solution was purged with N_2 for 30 minutes and tetrakis(triphenylphosphine)palladium(0) (1 mg, 0.001 mmol, 0.1 eq) was added. The reaction mixture was heated to 120 °C for 12 hours using microwave (maxpower model, 300W). After cooling, the reaction mixture was diluted with 20 mL water, extracted with DCM (30 mL × 3), the organic layer was dried with Na_2SO_4, and purified by silica gel column chromatography (eluent: hexane/DCM = 3/1) to afford the desired product **17** (10 mg, 0.003 mmol, 40 %) as a white solid.

^{1}H NMR (CD_2Cl_2, 500 MHz, 30 °C) δ 7.77 (s, 4H; 5), 7.71 (d, J = 8.5 Hz, 4H; 6), 7.69 (d, J = 8.4 Hz, 8H; 11), 7.62 (d, J = 8.4 Hz, 8H; 12), 7.61 (s, 4H; 2), 7.57 (AB spin system, 16H; 19, 20), 7.54 (d, J = 8.2 Hz, 8H; 10), 7.53 (d, J = 8.5 Hz, 4H; 7), 7.52 (t, J = 1.4 Hz, 4H; 13), 7.48 (t, J = 1.4 Hz, 4H; 21), 7.47 (d, J = 8.3 Hz, 4H; 3), 7.46 (d, J

= 8.0 Hz, 8H; 18), 7.42 (t, *J* = 1.4 Hz, 4H; 15), 7.38 (t, *J* = 1.4 Hz, 4H; 23), 7.35 (8H; 14, 22), 7.32 (d, *J* = 8.2 Hz, 8H; 9), 7.16 (d, *J* = 8.8 Hz, 8H; 17), 7.11 (d, *J* = 8.3 Hz, 4H; 4), 6.68 (s, 4H; 1), 1.39 (s, 18H; 8), 1.33 (s, 72H; 16, 24); ^{13}C NMR (CD_2Cl_2, 125 MHz, 30 °C) δ 154.2, 151.2, 142.5, 142.3, 142.2, 141.6, 141.5, 140.4, 140.1, 139.7, 139.5, 139.3, 138.7, 138.5, 138.1, 137.8, 137.7, 137.6, 137.1, 134.6, 132.6 (4), 131.4 (1), 130.9 (17), 130.8 (9), 128.6 (2, 5), 127.8 (12, 20), 127.5 (11, 19), 127.0 (6), 126.4 (10), 126.2 (3, 7, 18), 124.9 (14, 22), 124.3 (15, 23), 122.9 (13), 122.8 (21), 35.2, 34.8, 31.4 (8), 31.2 (16, 24); HRMS (ESI): calcd. $C_{238}H_{208}Cl_8([M]^+)$: 3343.3622, found: 3343.3433, error: 5.7 ppm.

3. General procedures for the synthesis of macrocycle M and [2]CIM

Synthesis of **M**

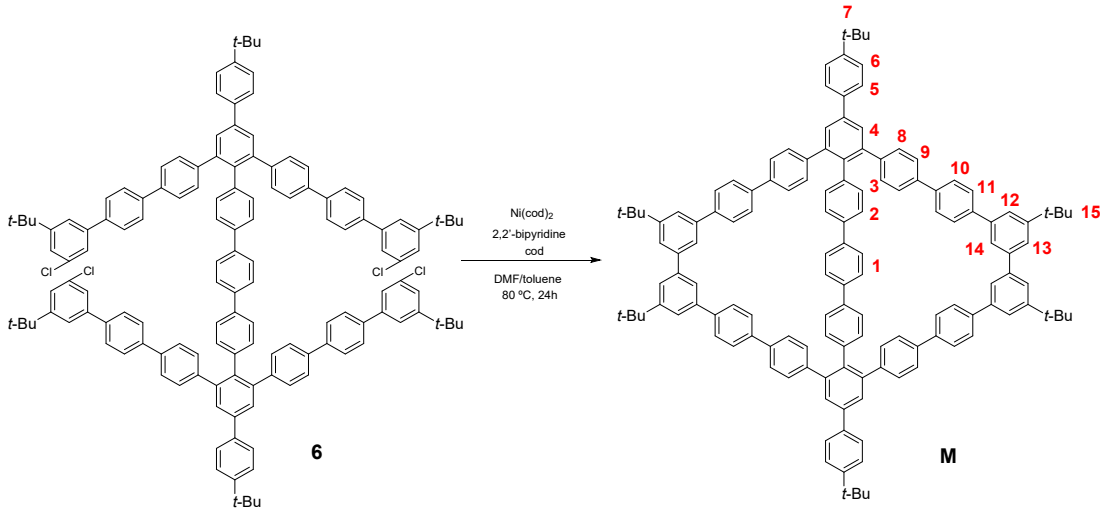

A mixture of 2,2'-bipyridyl (162.5 mg, 1.04 mmol, 40.0 eq), 1,5-cyclooctadiene (112.6 mg, 1.04 mmol, 40.0 eq) and bis(1,5-cyclooctadiene)nickel(0) ($Ni(cod)_2$) (286.2 mg, 1.04 mmol, 40.0 eq, 10 eq per C-Cl bond) in DMF (13.0 mL) was stirred at 80 °C for 40 minutes. To the mixture was added a solution of **8** (50.0 mg, 0.026 mmol, 1.0 eq) in toluene (13.0 mL), and the reaction mixture was stirred at 80 °C for another 18 hours. The mixture was then cooled to room temperature and stirred for 1h after the addition of 2 M aqueous HCl solution (3 mL). This mixture was poured into 100 mL of saturated aqueous NaCl solution and was extracted by DCM (50 mL × 3), the combined organic layer was washed with brine, dried over anhydrous Na_2SO_4, and concentrated in vacuo. After passed through a flash silica column, the organic part was concentrated and the crude material was washed by methanol (20 mL), acetone (20 mL) and DCM (1 mL) to afford **M** (37.2 mg, 0.022 mmol, 80 %) as a white solid.

^{1}H NMR ($C_2D_2Cl_2$, 500 MHz, 30 °C) δ 7.87 (s, 4H; 4), 7.75 (d, J = 8.4 Hz, 4H; 5), 7.70-7.65 (24H; 10 – 13), 7.63 (s, 4H; 1), 7.58 (s, 4H; 14), 7.53 (d, J = 8.4 Hz, 4H; 6), 7.47 (d, J = 8.1 Hz, 8H; 9), 7.29 (d, J = 8.2 Hz, 4H; 2), 7.24 (d, J = 8.1 Hz, 8H; 8), 6.84 (d, J = 8.2 Hz, 4H; 3), 1.46 (s, 36H; 15), 1.40 (s, 18H; 7); ^{13}C NMR ($C_2D_2Cl_2$, 125 MHz 30 °C) δ 151.9, 150.5, 141.8, 141.4, 140.9, 140.5, 140.3, 139.7, 139.1, 138.5, 138.1,

138.0 136.9, 136.7, 132.0 (3), 130.4 (8), 127.5 (10 or 11), 127.2 (4), 127.1 (10 or 11), 126.8 (1), 126.5 (5), 125.9 (9), 125.7 (6), 125.4 (2), 123.8 (14), 123.0 (12,13), 34.7, 34.3, 31.3 (15), 31.2 (7); HRMS (ESI): calcd. For $C_{138}H_{122}$([M]$^+$): 1779.9573, found: 1779.9597, error: 1.3 ppm.

Synthesis of **[2]CIM**

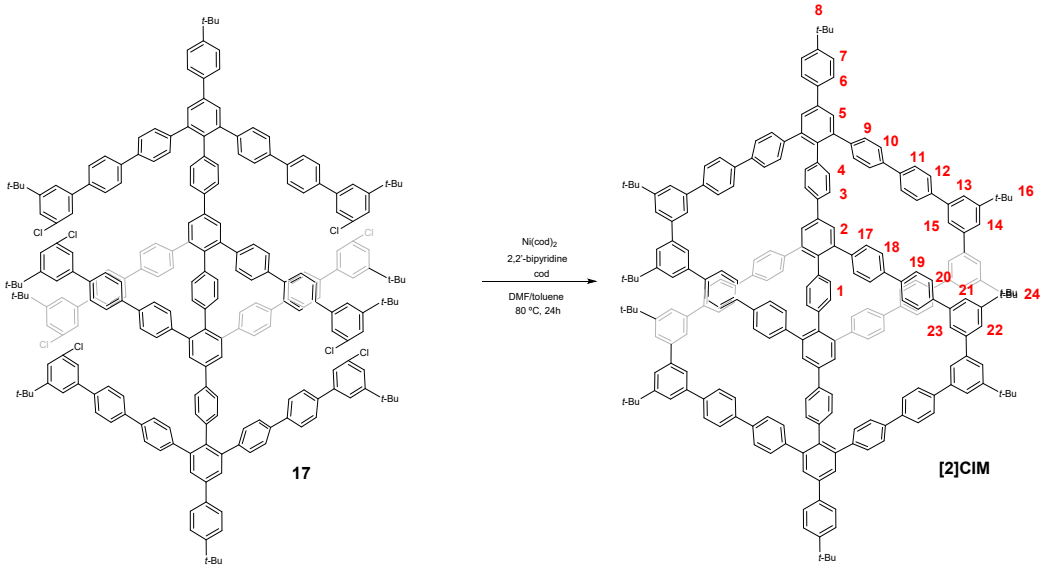

A mixture of 2,2'-bipyridyl (164.1 mg, 0.597 mmol, 100.0 eq), 1,5-cyclooctadiene (64.6 mg, 0.597 mmol, 100.0 eq) and $Ni(cod)_2$ (187.9 mg, 0.683 mmol, 100.0 eq, 12.5 eq per C-Cl bond) in DMF (3.0 mL) was stirred at 80 °C for 30 minutes. To the mixture was added a solution of **17** (20.0 mg, 0.006 mmol) in toluene (3.0 mL), and the reaction mixture was stirred at 80 °C for another 18 hours. The mixture was then cooled to room temperature and stirred for 1hours after the addition of 2 M HCl aqueous solution (3 mL). This mixture was poured into 100 mL of saturated aqueous NaCl solution and was extracted by DCM (50 mL × 3), the combined organic layer was washed with brine, dried over anhydrous Na_2SO_4, and concentrated in vacuo. After passed through a flash silica column, the organic part was concentrated and the crude material was purified by preparative recycling gel permeation chromatography (THF), then further purified by

PTLC (eluent: hexane/DCM = 3/1) to afford **[2]CIM** (3.8 mg, 1.25 μmol, 21 %) as a white solid.

^{1}H NMR (CD_2Cl_2, 500 MHz, 30 °C) δ 7.88 (s, 4H; 5), 7.79 (s, 4H; 2), 7.77 (d, J = 8.0 Hz, 4H; 6), 7.75-7.60 (56H; 11 - 15, 19 - 23), 7.58 (d, J = 8.0 Hz, 4H; 7), 7.52 (20H; 3, 10, 18), 7.32 (d, J = 8.0 Hz, 8H; 9), 7.19 (d, J = 8.0 Hz, 8H; 17), 6.99 (d, J = 8.2 Hz, 4H; 4), 6.37 (s, 4H; 1), 1.47 (s, 36H; 16 or 24), 1.45 (s, 36H; 16 or 24), 1.42 (s, 18H; 8);^{13}C NMR (CD_2Cl_2, 125 MHz, 30 °C) δ 152.8, 152.7, 151.2, 142.5, 142.1, 141.5, 141.4, 141.3, 141.2, 140.9, 140.6, 140.1, 139.8, 139.7, 139.6, 138.9, 138.8, 138.4, 137.9, 137.6, 136.5, 132.6 (4), 131.5 (1), 131.0 (17), 130.9 (9), 128.0 (12 or 20), 127.9 (12 or 20), 127.7 (5), 127.5 (2), 127.5 (11, 19), 127.1 (6), 126.4 (18), 126.3 (7, 10), 125.9 (3), 124.2 (15, 23), 123.4 (13, 14, 21, 22), 35.2, 34.8, 31.5 (16, 24), 31.4 (8); HRMS(MALDI-TOF): calcd. for $C_{238}H_{206}$ ($[M]^+$): 3065.6092, found: 3065.6182, error: 2.9 ppm.

4. X-ray crystallography

Table S1. Crystal data and structure refinement for **[2]CIM**.

Identification code	CCDC 2172868
Empirical formula	$C_{233.75}H_{194.75}$
Formula weight	3003.63
Temperature/K	101(2)
Crystal system	triclinic
Space group	P-1
a/Å	17.9824(8)
b/Å	25.6746(11)
c/Å	32.8671(10)
α/°	95.933(3)
β/°	93.030(3)
γ/°	96.569(4)
Volume/Å^3	14961.9(10)
Z	2
ρ_{calc}g/cm^3	0.667
μ/mm^{-1}	0.283
F(000)	3194.0
Crystal size/mm^3	0.1 × 0.08 × 0.03
Radiation	CuKα (λ = 1.54184)
2Θ range for data collection/°	4.644 to 129.996
Index ranges	-21 ≤ h ≤ 21, -30 ≤ k ≤ 30, -29 ≤ l ≤ 38
Reflections collected	175441
Independent reflections	50188 [R_{int} = 0.1795, R_{sigma} = 0.1431]
Data/restraints/parameters	50188/158/2102
Goodness-of-fit on F^2	0.997
Final R indexes [I>=2σ (I)]	R_1 = 0.1108, wR_2 = 0.2746
Final R indexes [all data]	R_1 = 0.2193, wR_2 = 0.3463
Largest diff. peak/hole / e Å^{-3}	0.51/-0.29

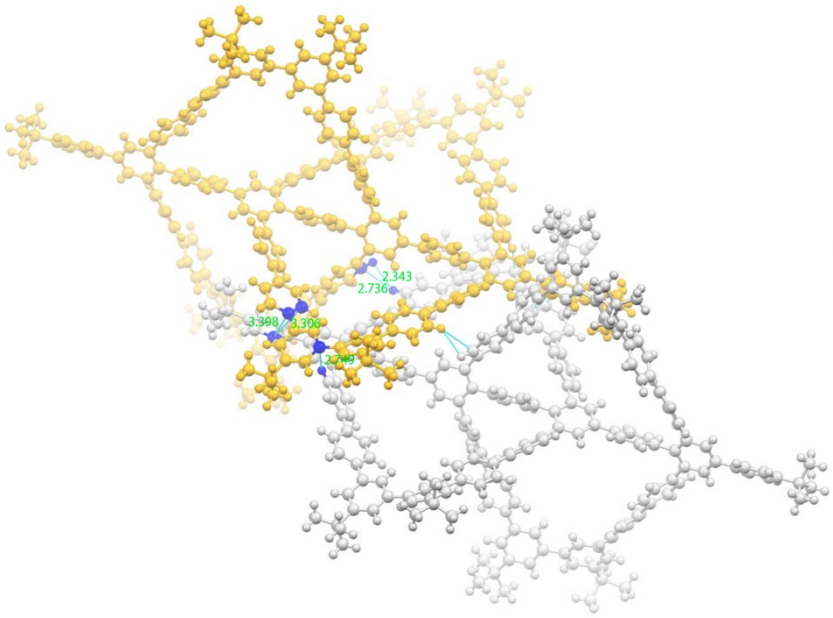

Fig. S1. Weak interactions inside the unit cell: π-π interactions (3.398 Å & 3.306 Å), C-H···π (2.736 Å & 2.749 Å) and C-H···H-C (2.343 Å) (highlighted in blue). Symmetric interactions were not marked.

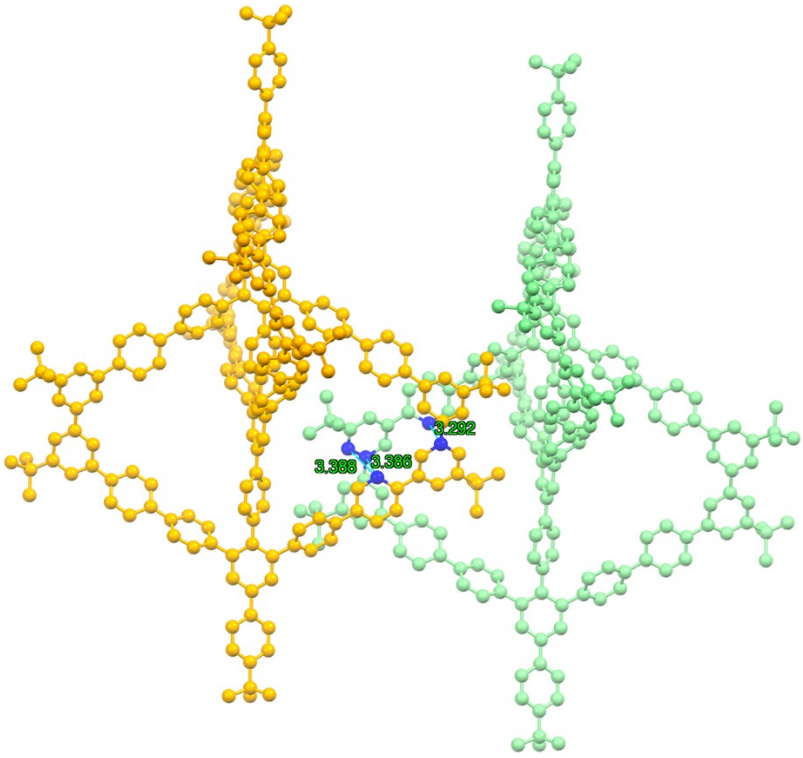

Fig. S2. *a*-axis packing of **[2]CIM**: dominated by strong π-π (3.292 Å to 3.388 Å) interactions (highlighted in blue). Hydrogen atoms have been omitted for clarity.

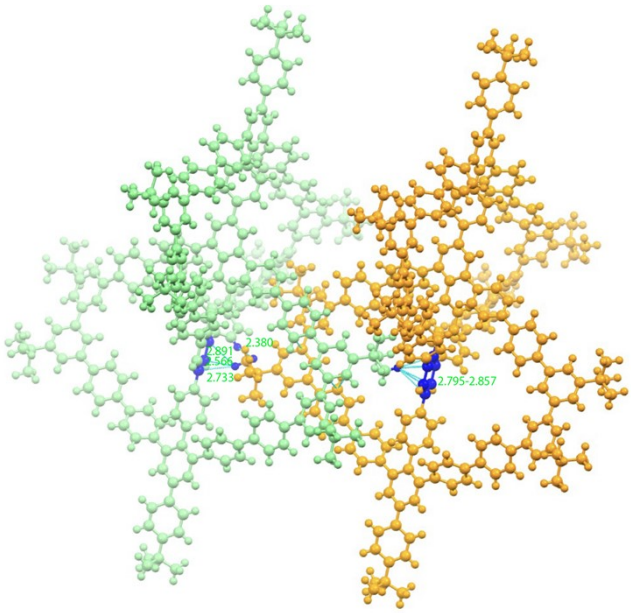

Fig. S3. *a*-axis packing of **[2]CIM**: C-H···π (2.566 Å to 2.891 Å) and C-H···H-C (2.380 Å) weak interactions (highlighted in blue).

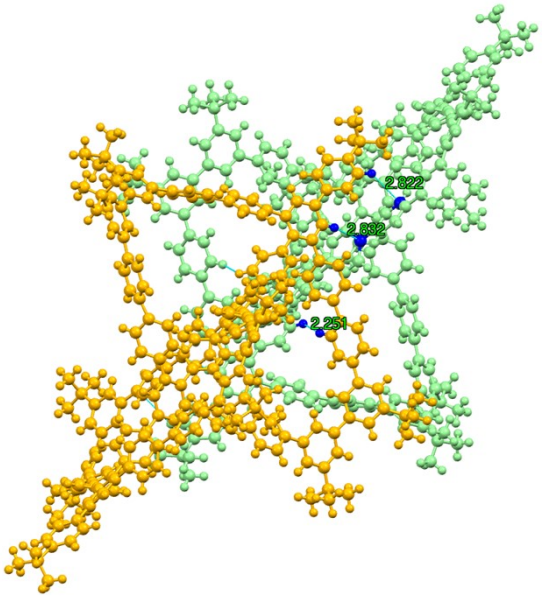

Fig. S4. *ac*-axis packing of **[2]CIM** dominated by weak C-H···π (2.822 Å & 2.832 Å) and C-H···H-C (2.251 Å) weak interactions (highlighted in blue).

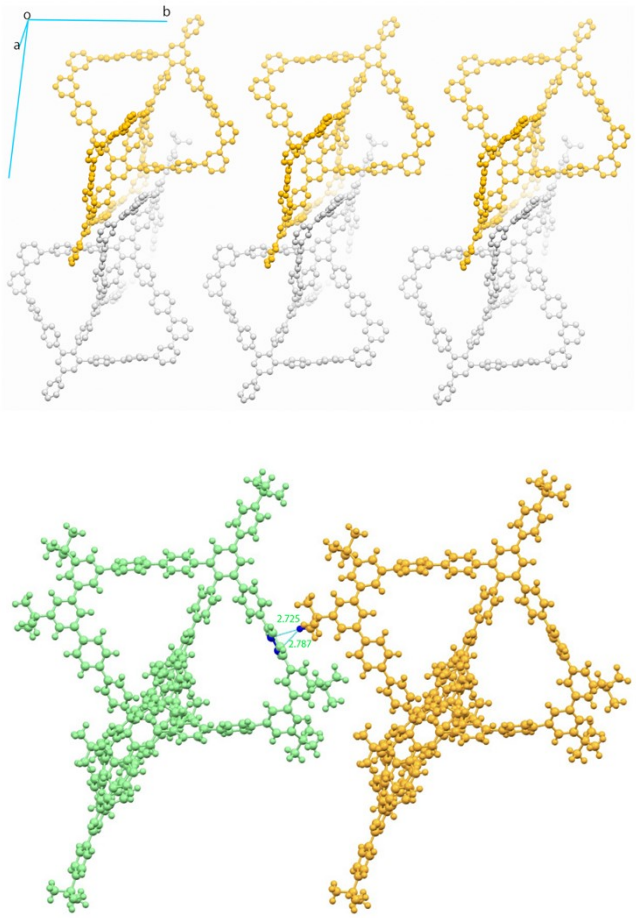

Fig. S5. *b*-axis packing of **[2]CIM**: dominated by weak C-H···π (2.725 Å & 2.787 Å) weak interactions (highlighted in blue).

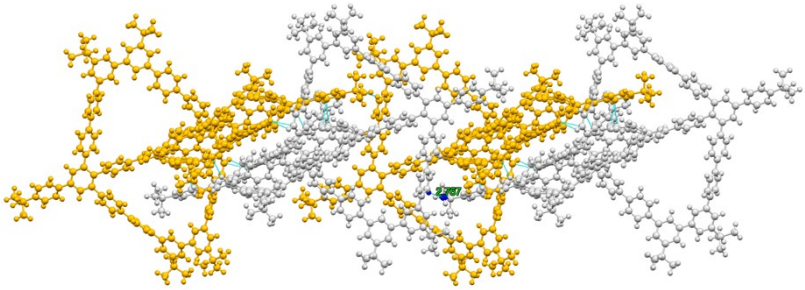

Fig. S6. Interdigitating ***c***-axis stack arrangement of **[2]CIM** showing C-H···π (2.767 Å) weak interaction (highlighted in blue) between different unit cells was observed.

5. Theoretical calculation

All theoretical calculations for this work were performed with Gaussian16[4] software package by selecting the 6-31G(d) basis set. The prevalent B3LYP with exchange-correlation functional with D3 correction was selected to optimize the ground-state geometries. Structure of **M** was optimized without any symmetry assumptions. The energy of geometry of **[2]CIM** was optimized from the gas-phase studies with the geometry in single crystal as initial input geometry.

6. UV-vis absorption spectra and fluorescence spectra

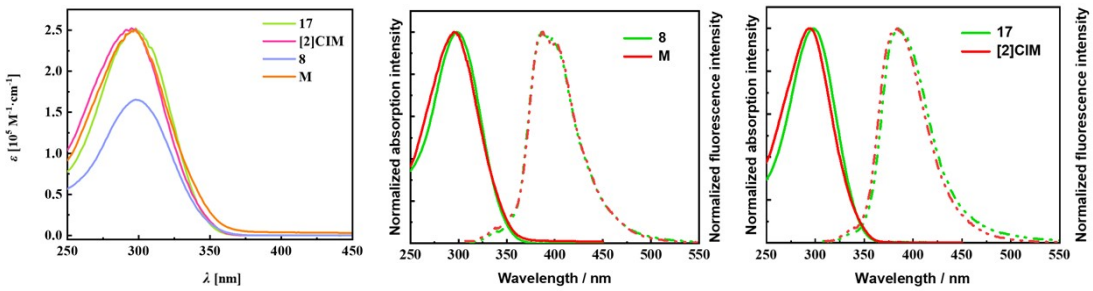

Fig. S7. Left, UV-vis absorption spectra of **8**, **17**, **M**, and **[2]CIM** in DCM (10 μM). **Middle**, UV–vis absorption (solid line) and fluorescence (broken line) spectra of **8** and **M** in DCM (10 μM). **Right**, UV–vis absorption (solid line) and fluorescence (broken line) spectra of **17** and **[2]CIM** in DCM (10 μM).

7. NMR spectra

7.1. ^{1}H NMR and ^{13}C NMR spectra of compounds **3**, **6**, **8, 11, 13-17.**

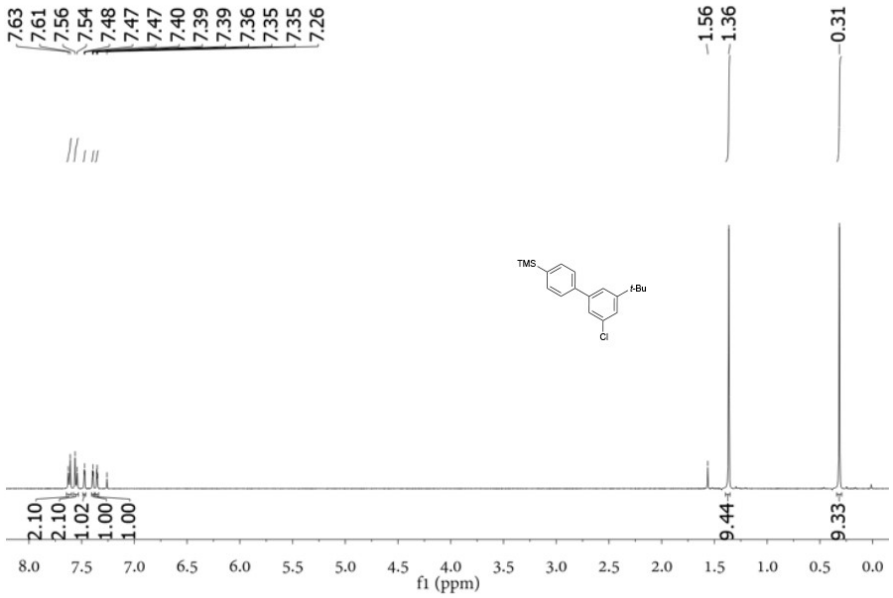

Fig. S8. ^{1}H NMR spectrum (400 MHz) of **3** in $CDCl_3$ at room temperature.

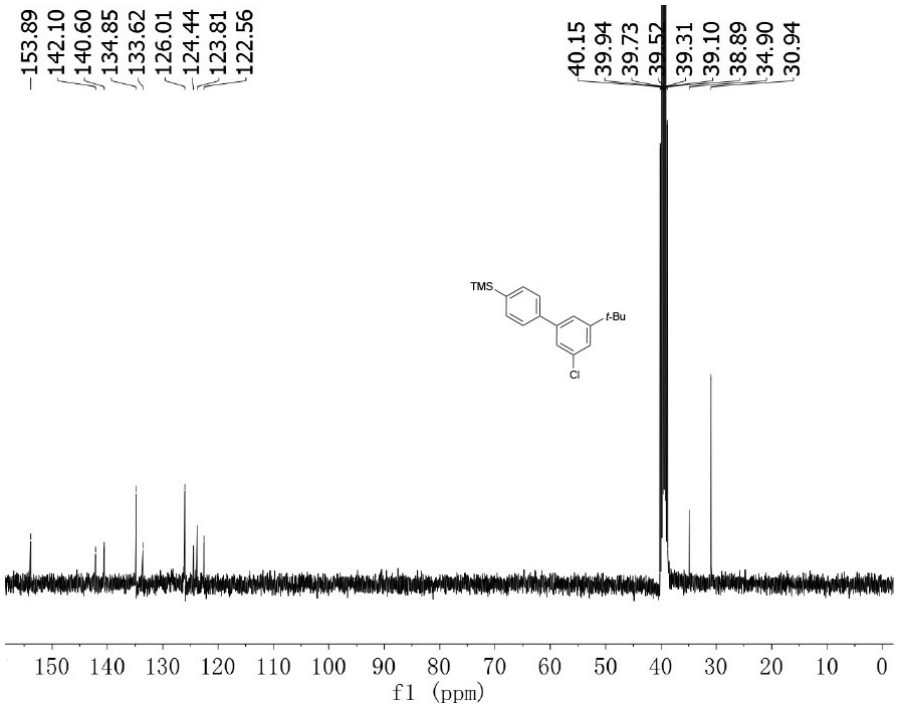

Fig. S9. ^{13}C NMR spectrum (101 MHz) of **3** in d_6-DMSO at room temperature.

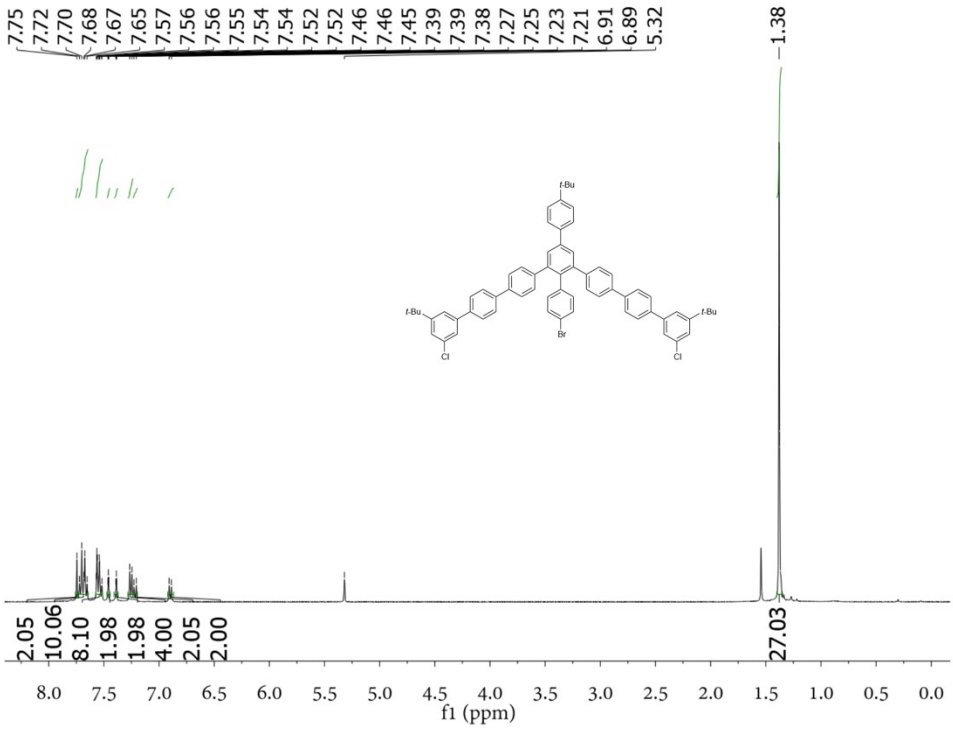

Fig. S10. ^{1}H NMR spectrum (400 MHz) of **6** in CD_2Cl_2 at room temperature.

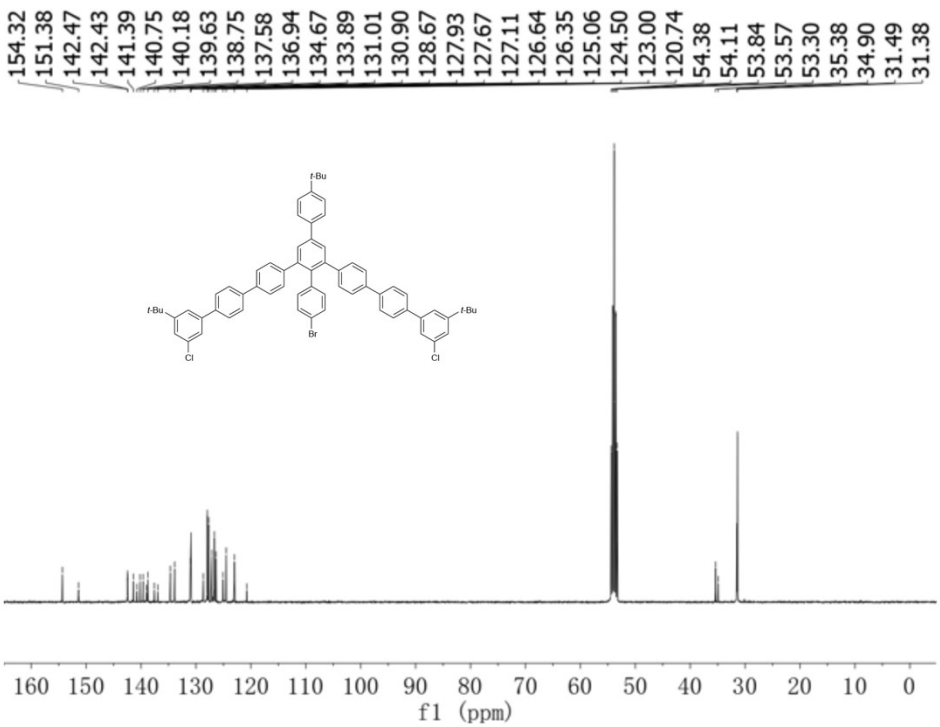

Fig. S11. ^{13}C NMR spectrum (101 MHz) of **6** in CD_2Cl_2 at room temperature.

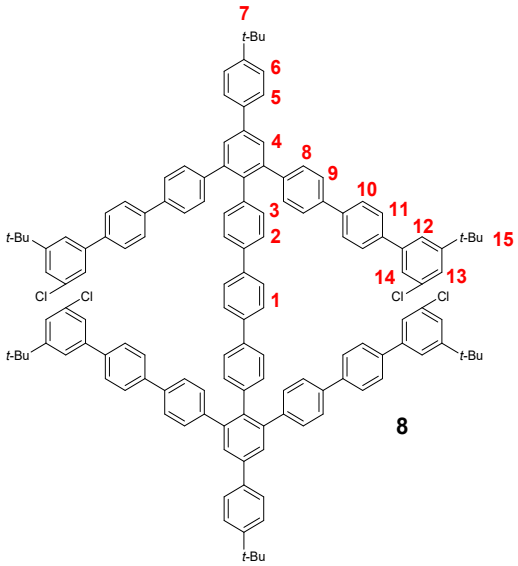

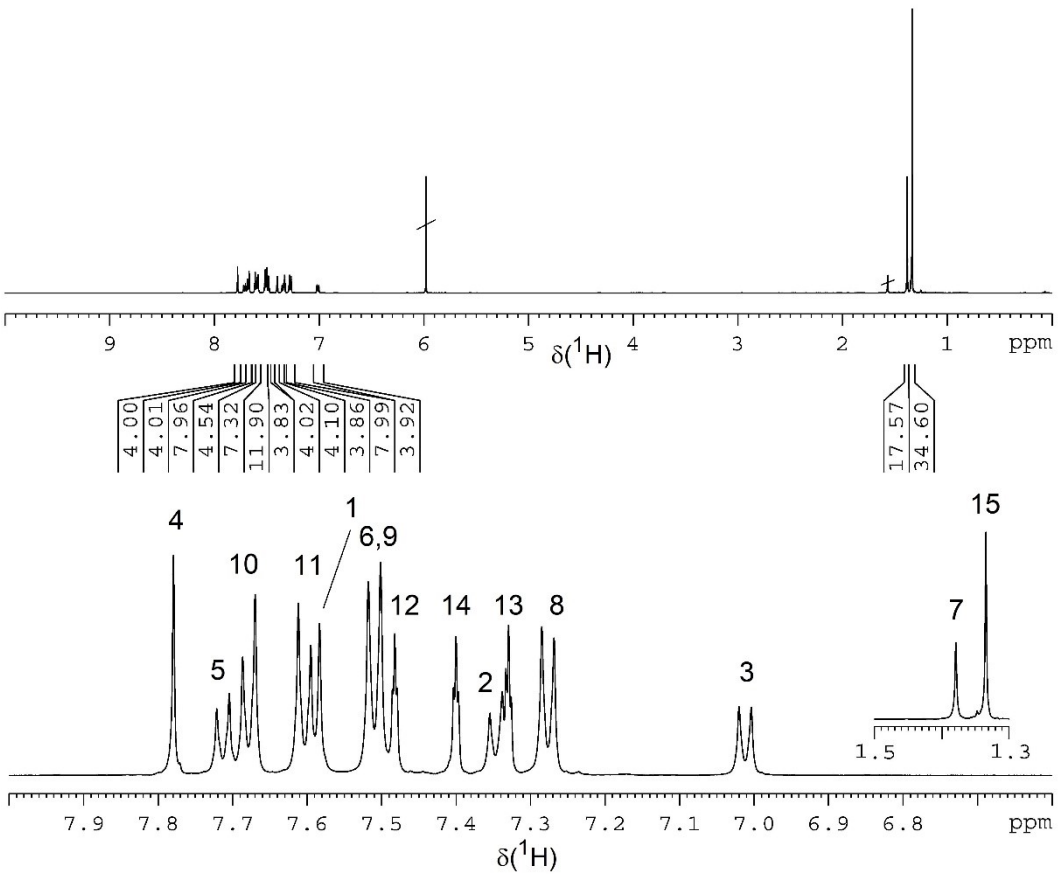

Fig. S12. ^1H NMR spectrum (500 MHz, $C_2D_2Cl_4$) of **8** and enlarged regions with signal assignment.

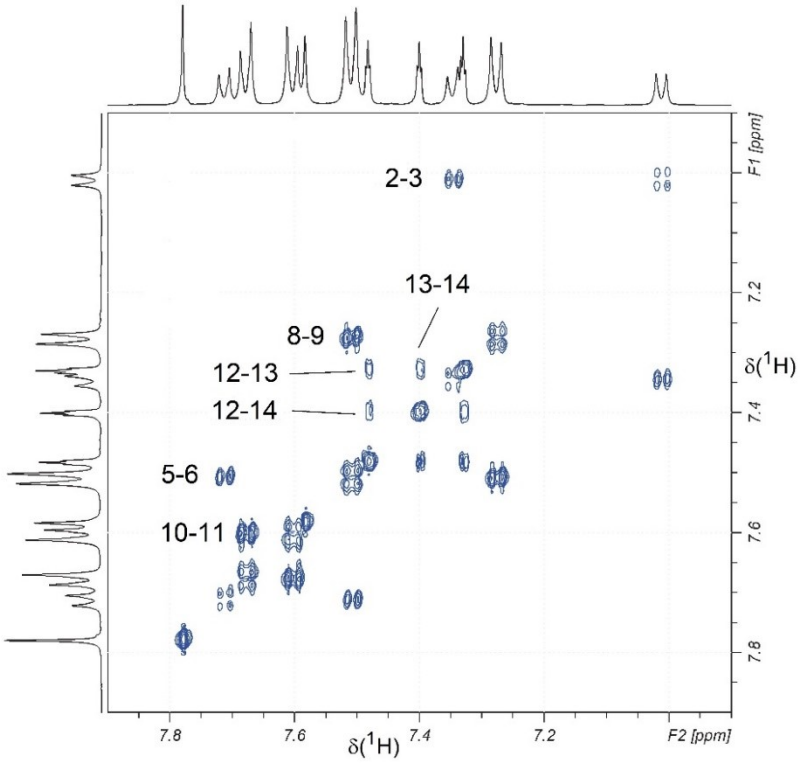

Fig. S13. COSY spectrum (region) of **8** with assignment of some correlations.

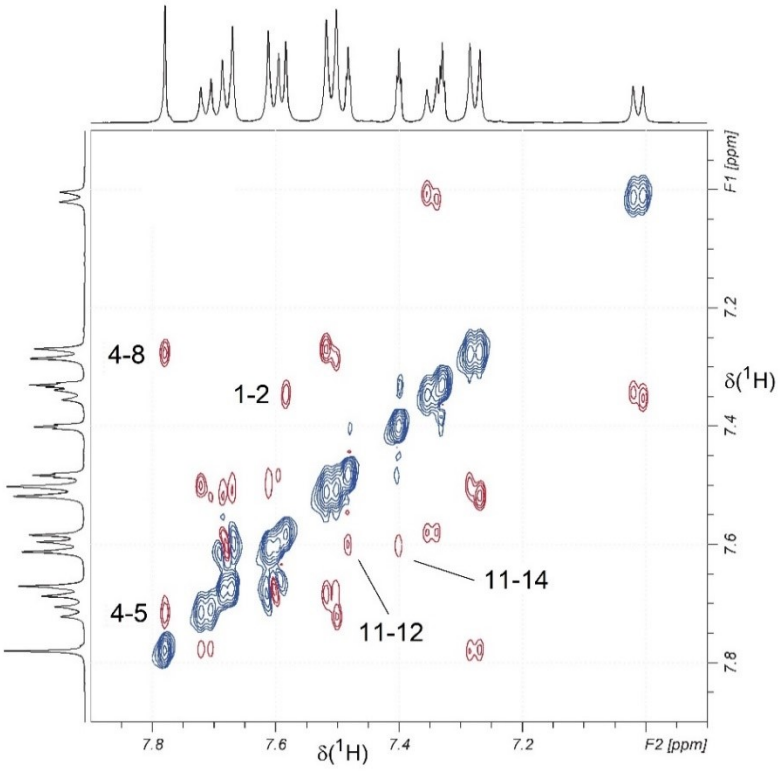

Fig. S14. ROESY spectrum (region) of **8** with assignment of some correlations.

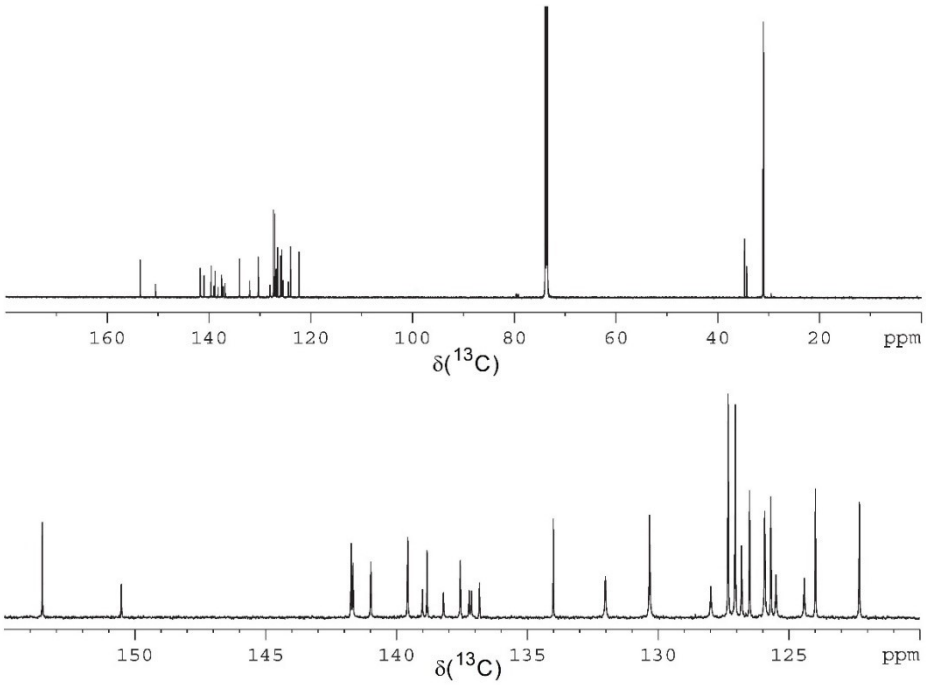

Fig. S15. ^{13}C NMR spectrum (125 MHz, $C_2D_2Cl_4$) of **8** and enlarged region of aromatic carbon signals.

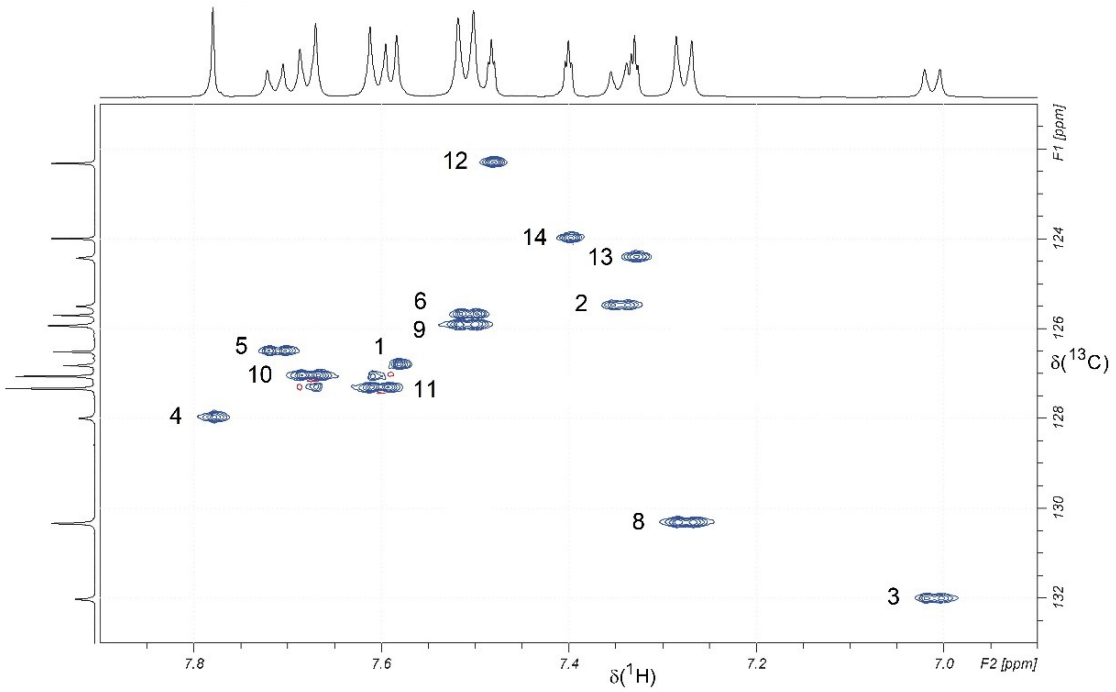

Fig. S16. HSQC spectrum (region) of **8** with assignment of aromatic CH signals. The projection at the F1 axis shows the DEPT135 spectrum.

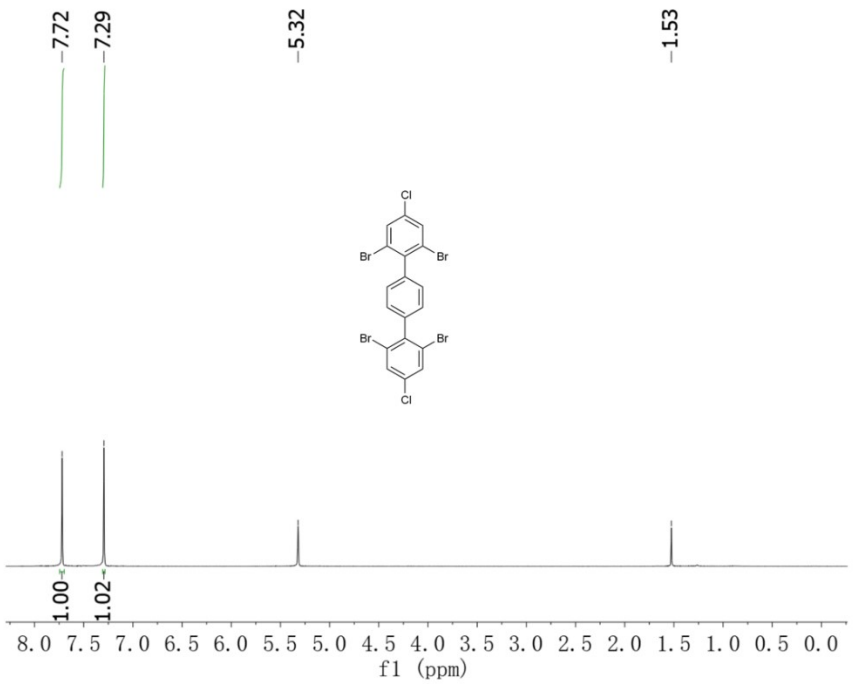

Fig. S17. ^{1}H NMR spectrum (400 MHz) of **11** in CD_2Cl_2 at room temperature.

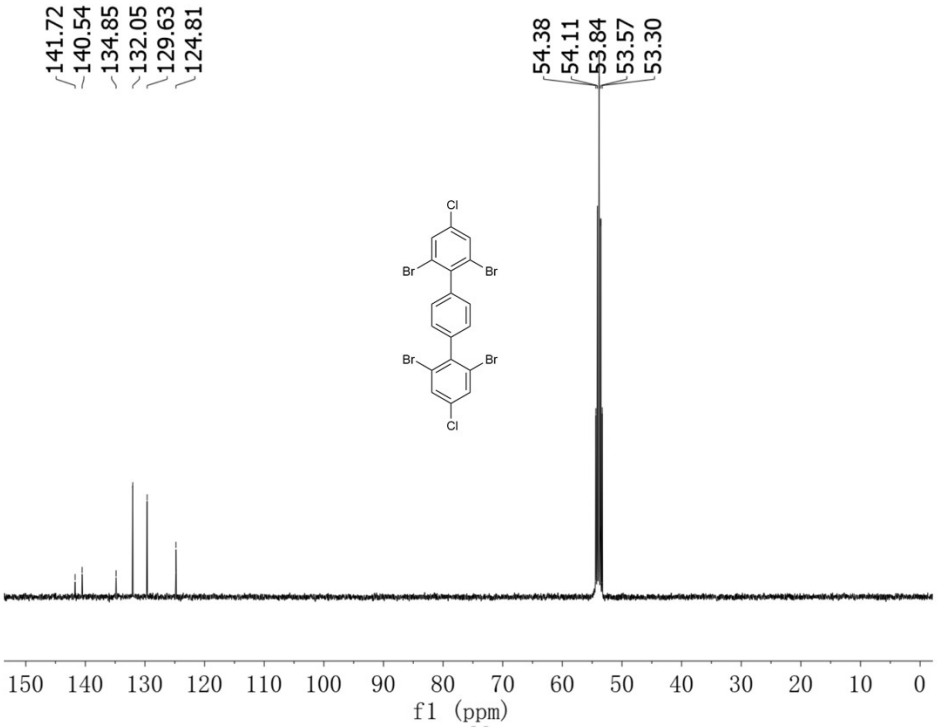

Fig. S18. ^{13}C NMR spectrum (101 MHz) of **11** in CD_2Cl_2 at room temperature.

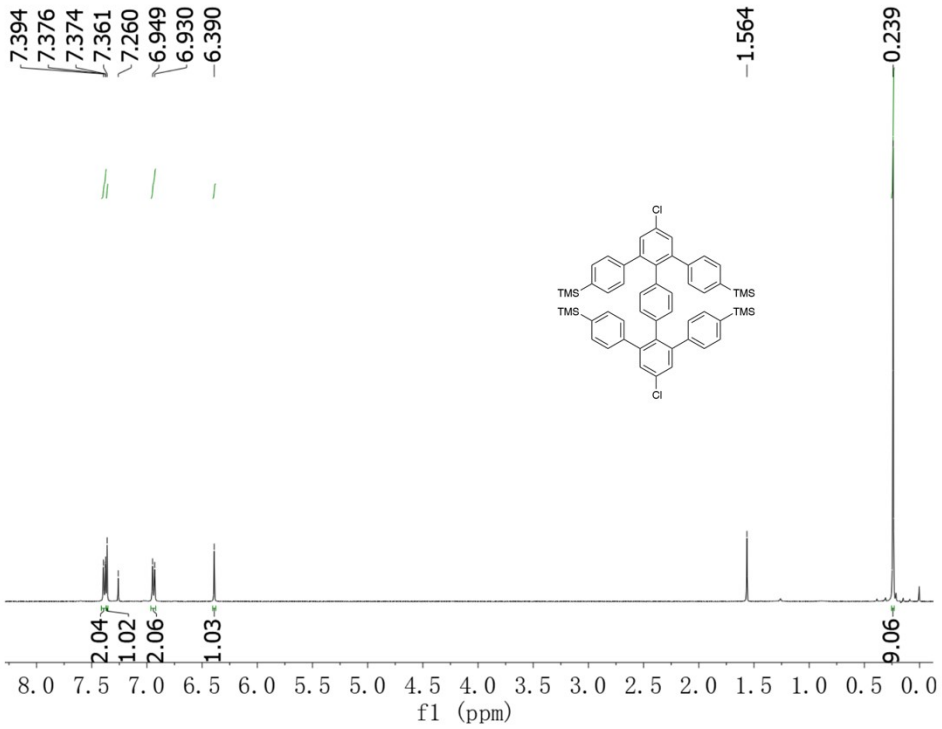

Fig. S19. ^{1}H NMR spectrum (400 MHz) of **13** in $CDCl_3$ at room temperature.

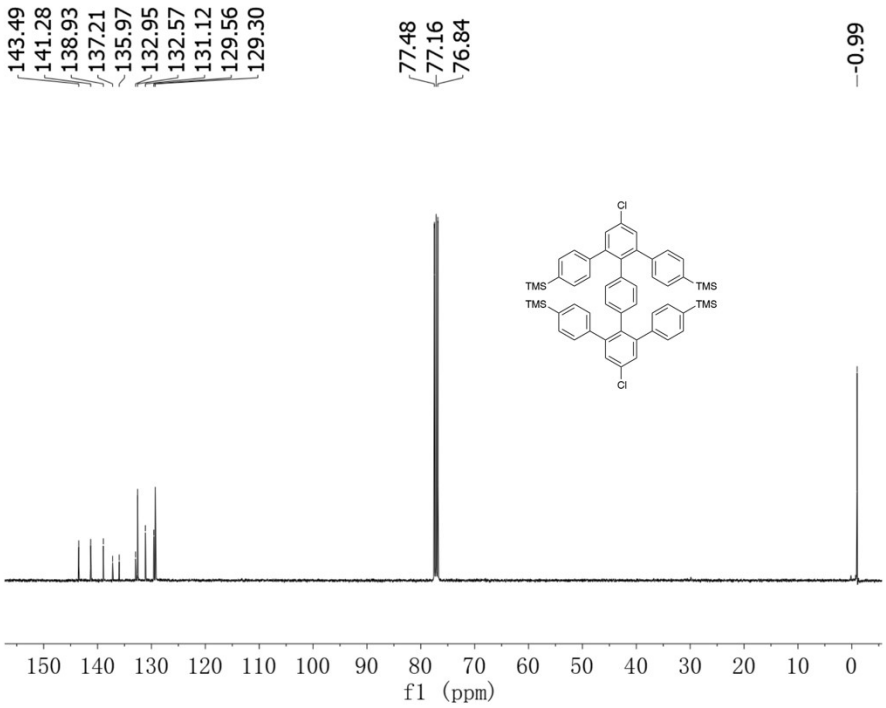

Fig. S20. ^{13}C NMR spectrum (101 MHz) of **13** in $CDCl_3$ at room temperature.

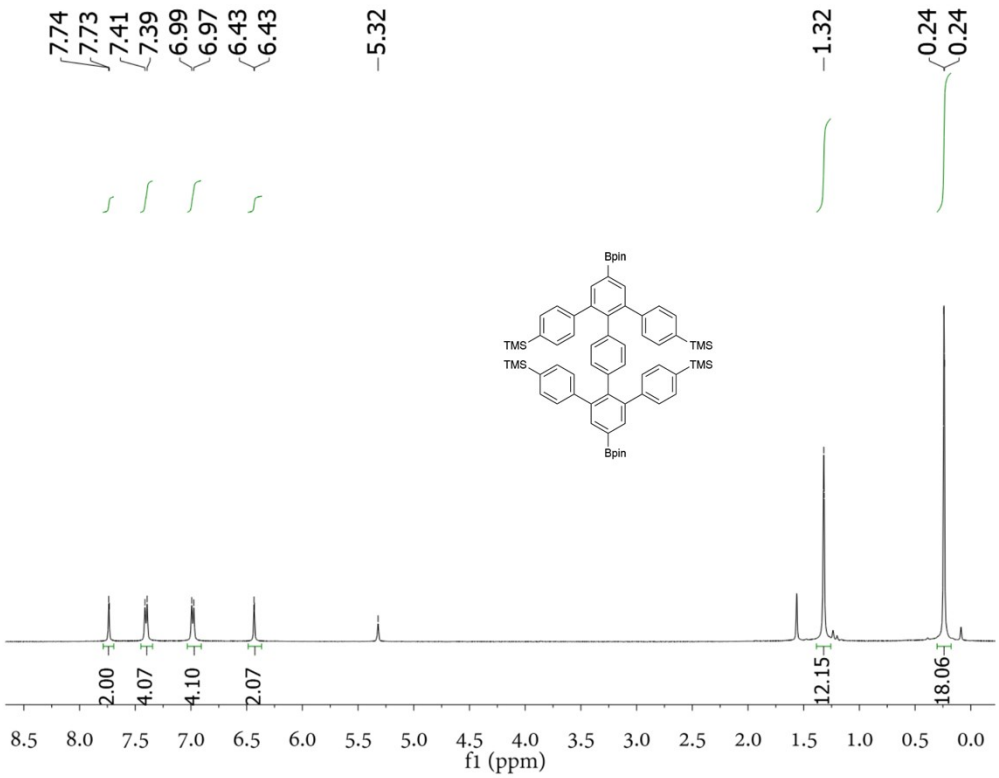

Fig. S21. ^{1}H NMR spectrum (400 MHz) of **14** in CD_2Cl_2 at room temperature.

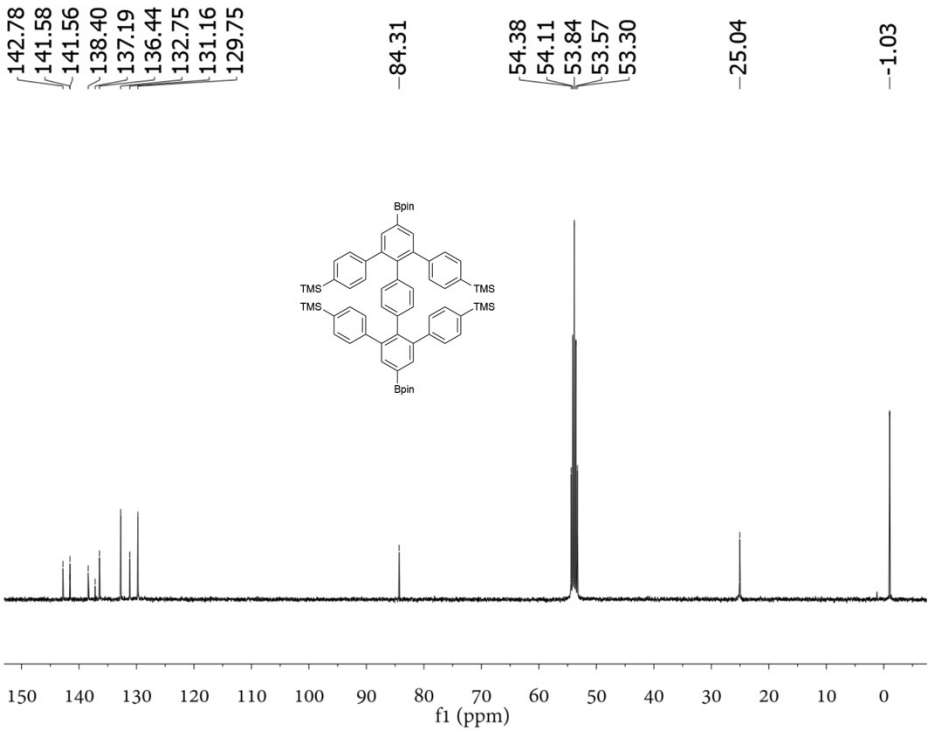

Fig. S22. ^{13}C NMR spectrum (101 MHz) of **14** in CD_2Cl_2 at room temperature.

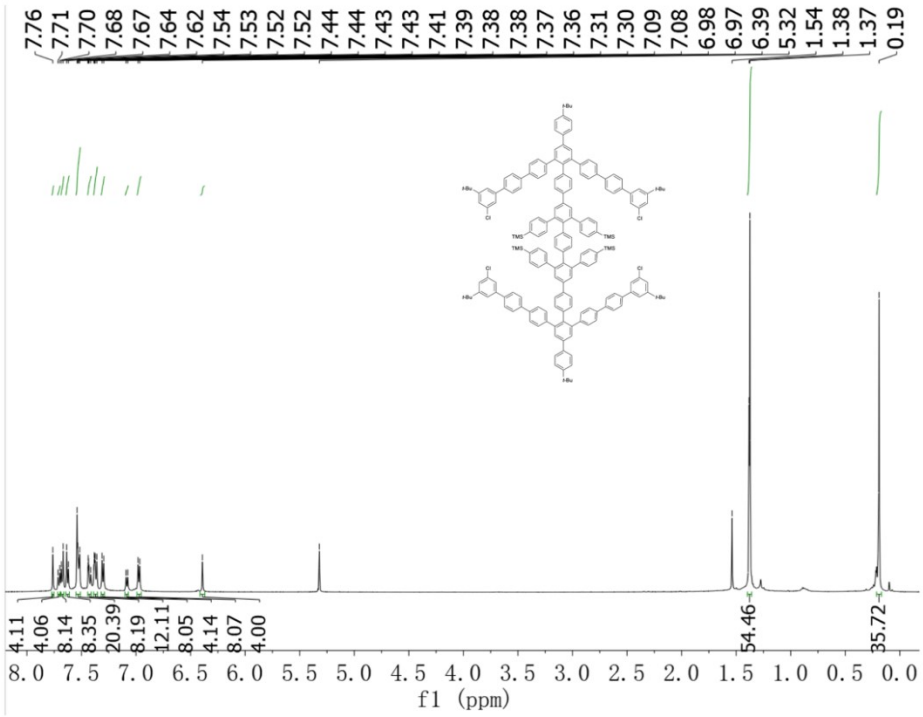

Fig. S23. ^{1}H NMR spectrum (500 MHz) of **15** in CD_2Cl_2 at room temperature.

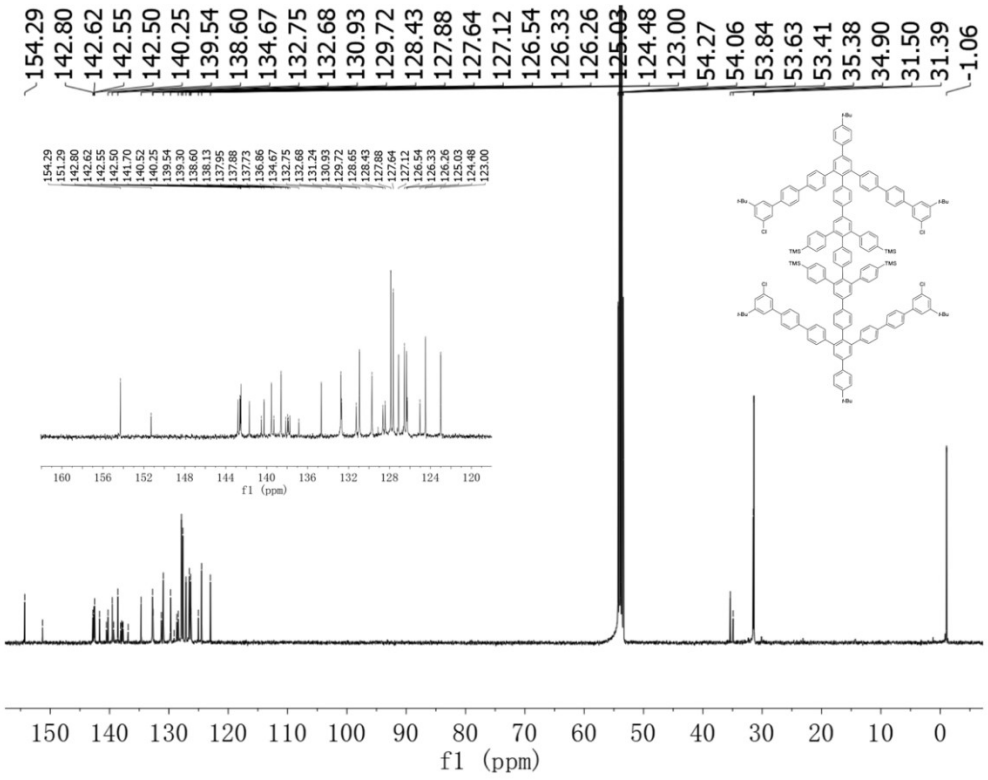

Fig. S24. ^{13}C NMR spectrum (125 MHz) of **15** in CD_2Cl_2 at room temperature.

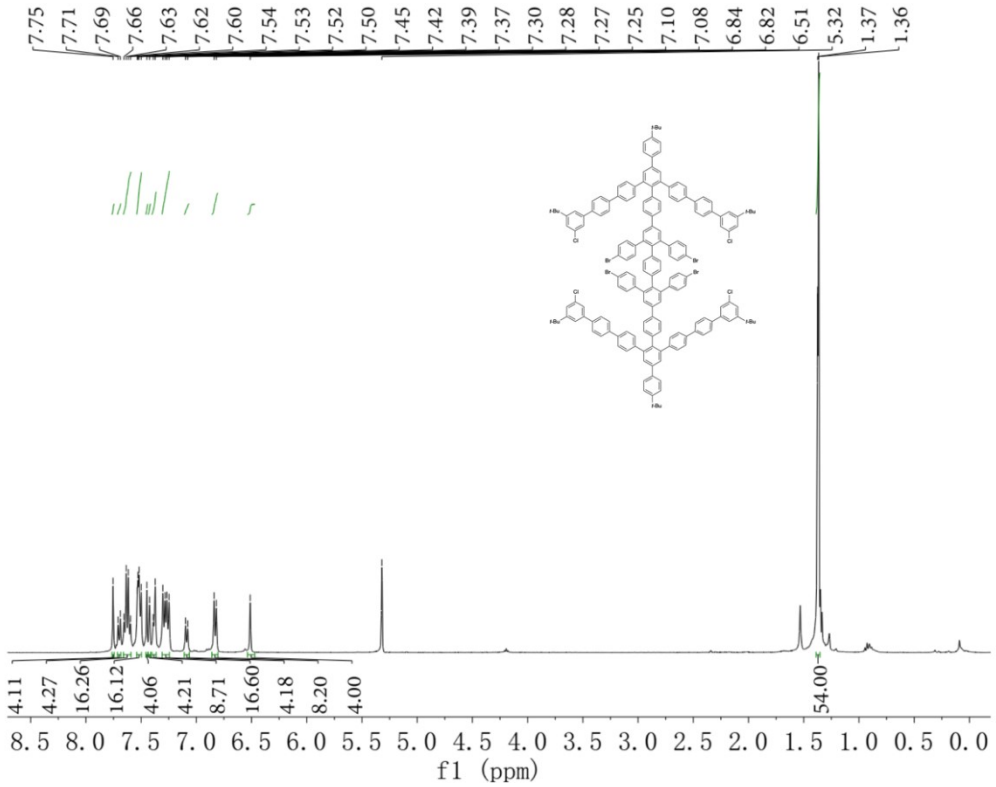

Fig. S25. ^{1}H NMR spectrum (400 MHz) of **16** in CD_2Cl_2 at room temperature.

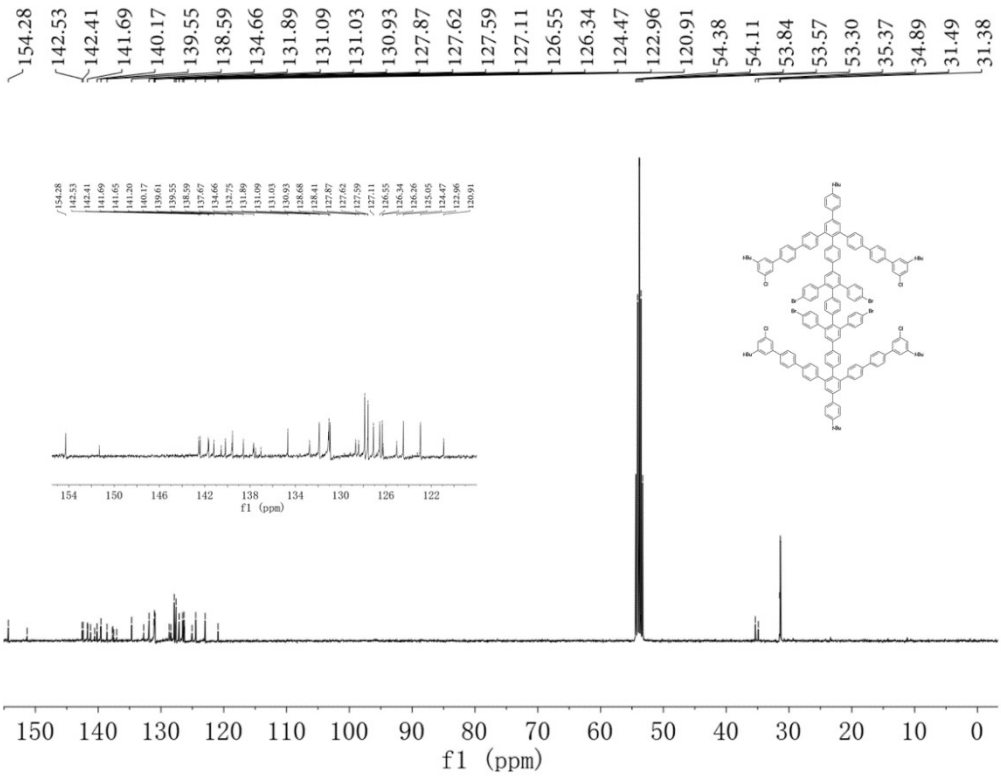

Fig. S26.^{13}C NMR spectrum (101 MHz) of **16** in CD_2Cl_2 at room temperature.

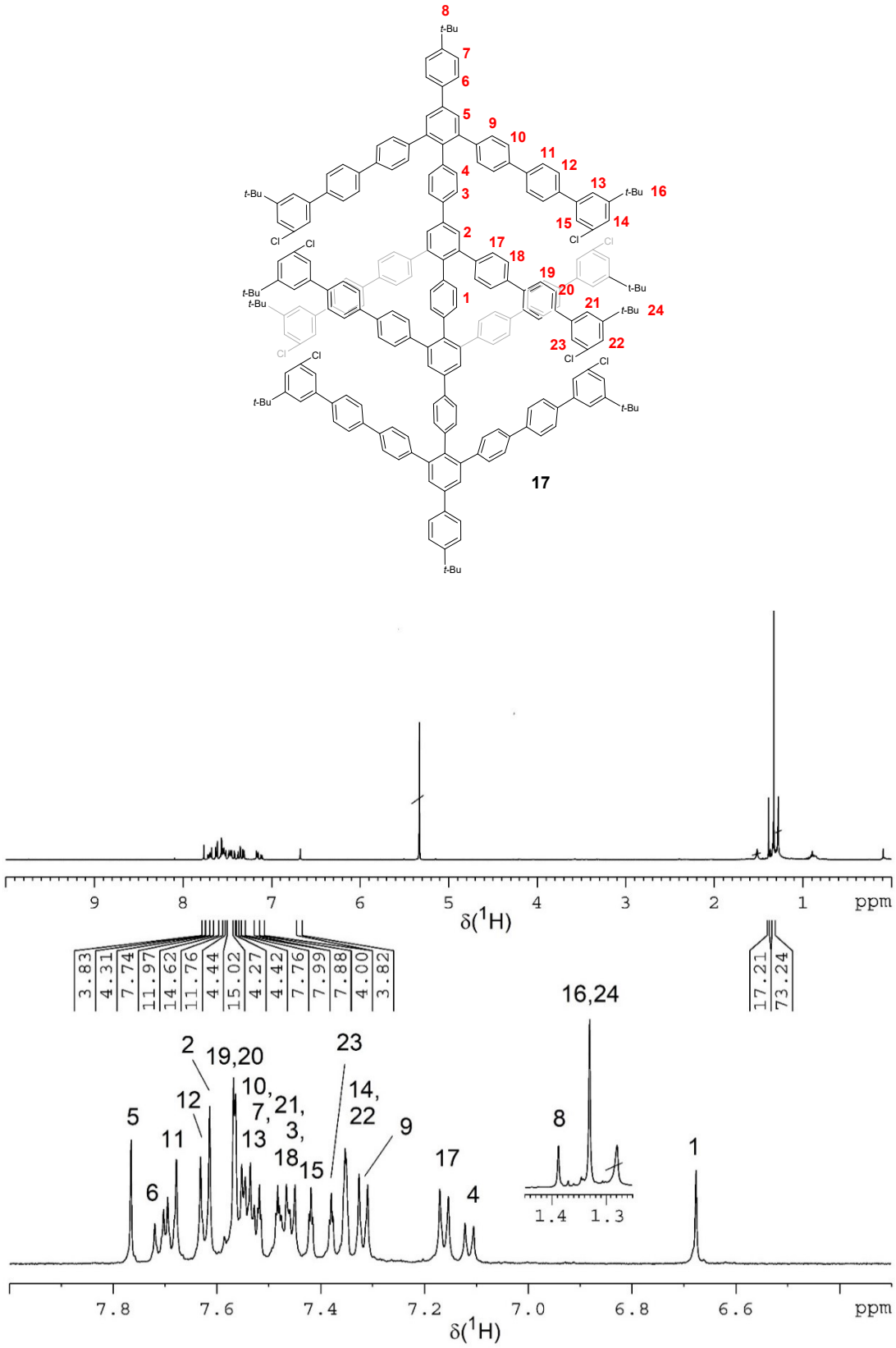

Fig. S27. ^{1}H NMR spectrum (500 MHz, CD_2Cl_2) of **17** and enlarged regions with signal assignment.

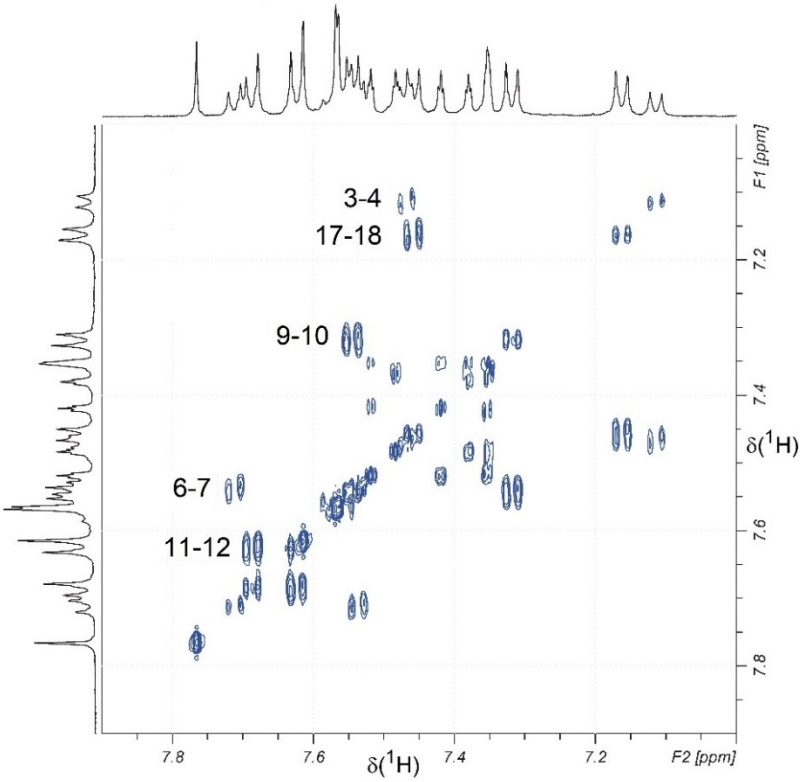

Fig. S28. COSY spectrum (region) of **17** with assignment of some correlations.

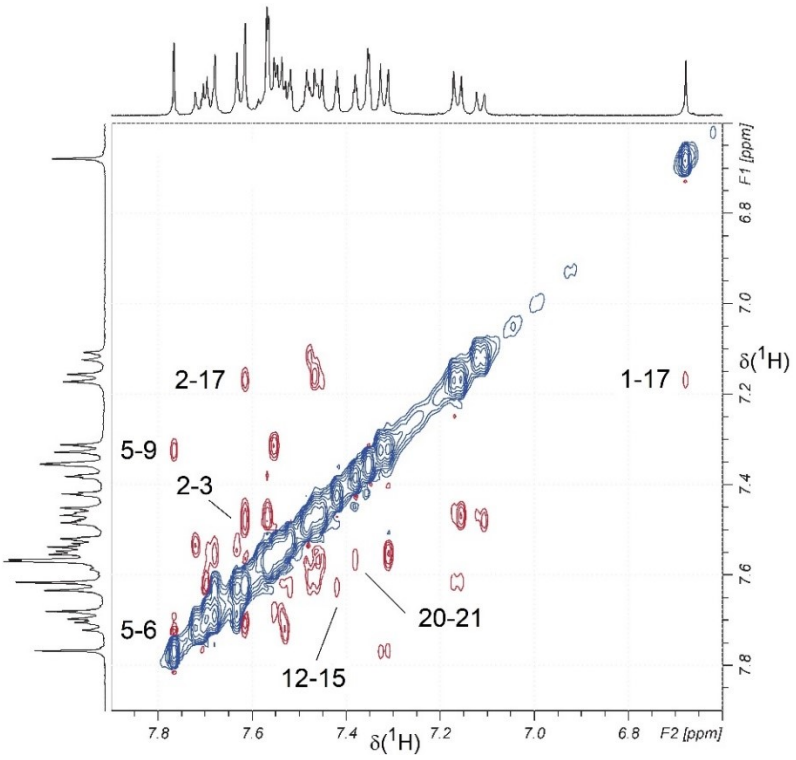

Fig. S29. ROESY spectrum (region) of **17** with assignment of some correlations.

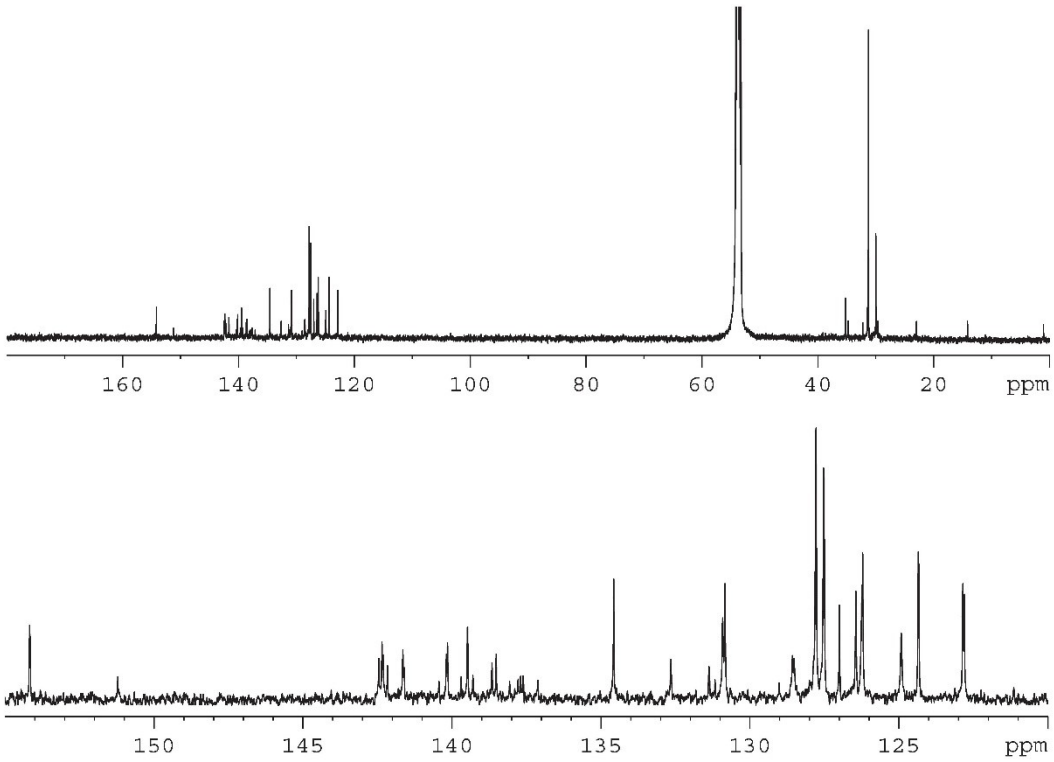

Fig. S30. ^{13}C NMR spectrum (125 MHz, CD_2Cl_2) of **17** and enlarged region of aromatic carbon signals.

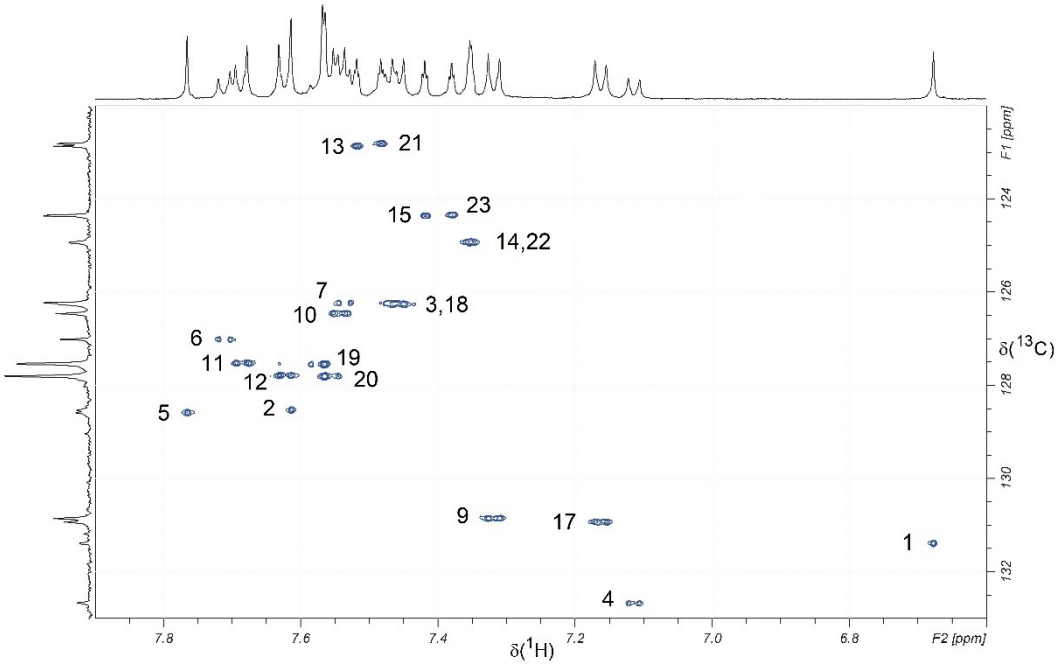

Fig. S31. HSQC spectrum (region) of **17** with assignment of aromatic CH signals.

7.2. NMR spectra of macrocycles **M** and **[2]CIM**

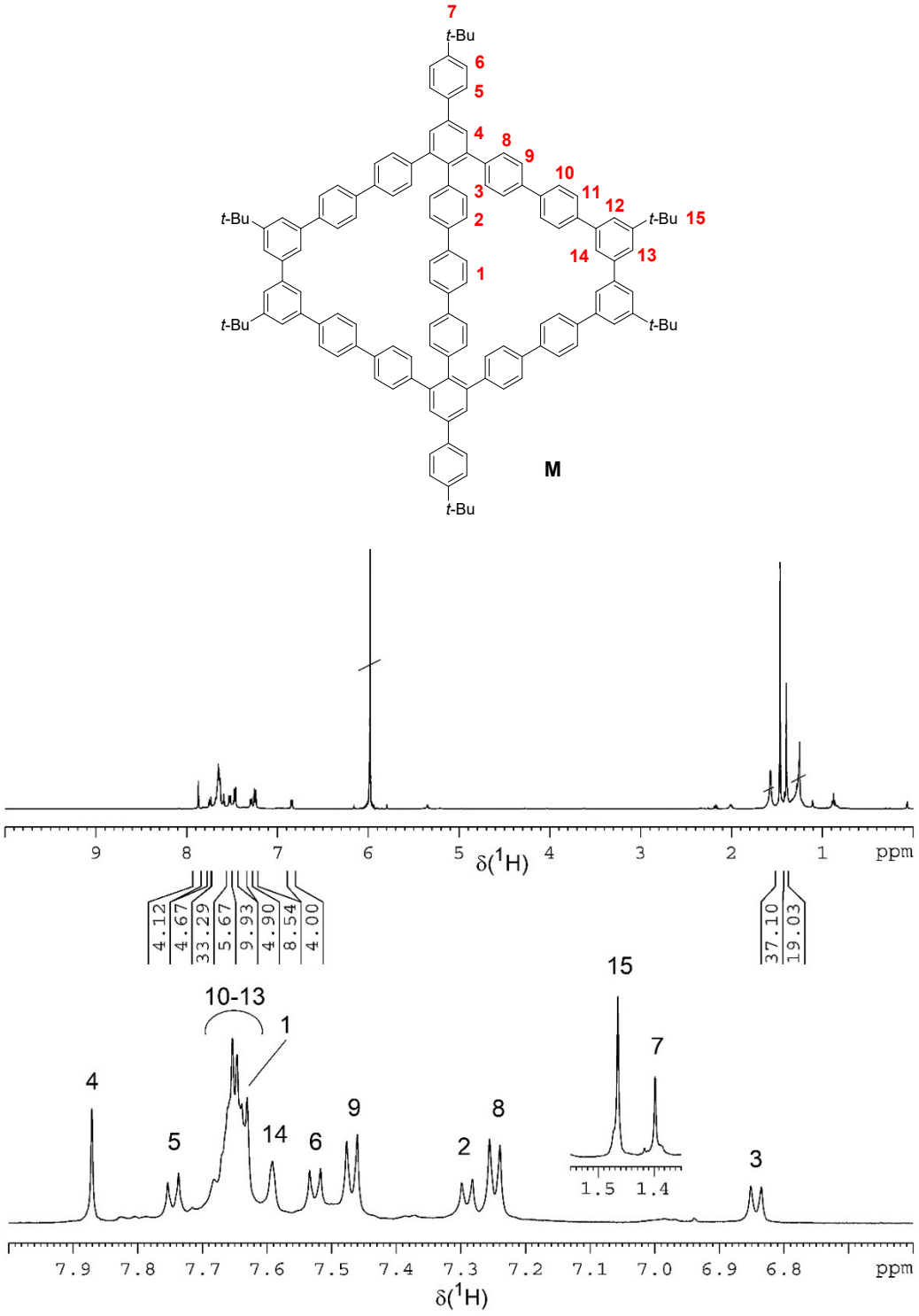

Fig. S32. ^{1}H NMR spectrum (500 MHz, $C_2D_2Cl_4$) of **M** and enlarged regions with signal assignment.

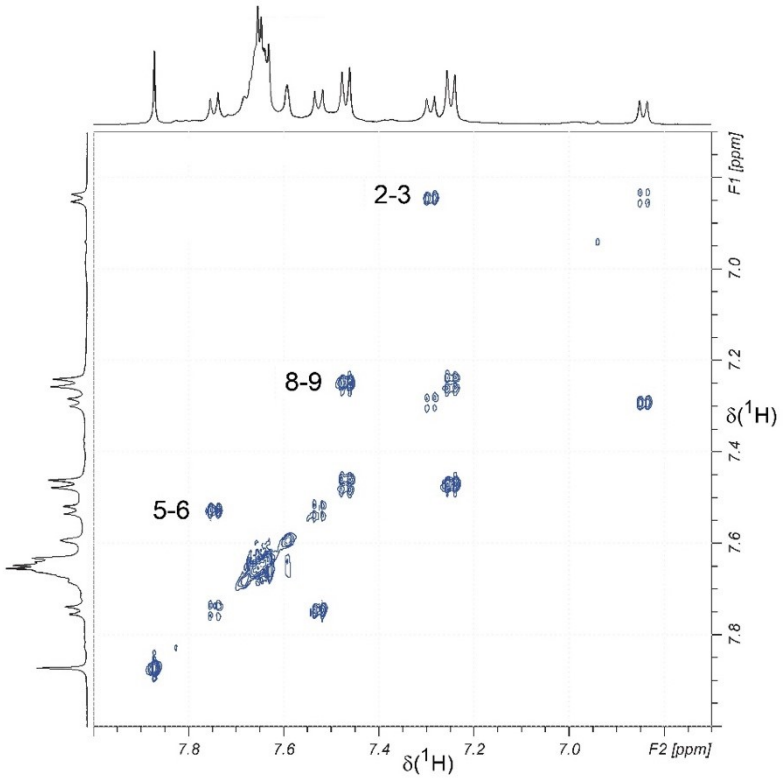

Fig. S33. COSY spectrum (region) of **M** with assignment of some correlations.

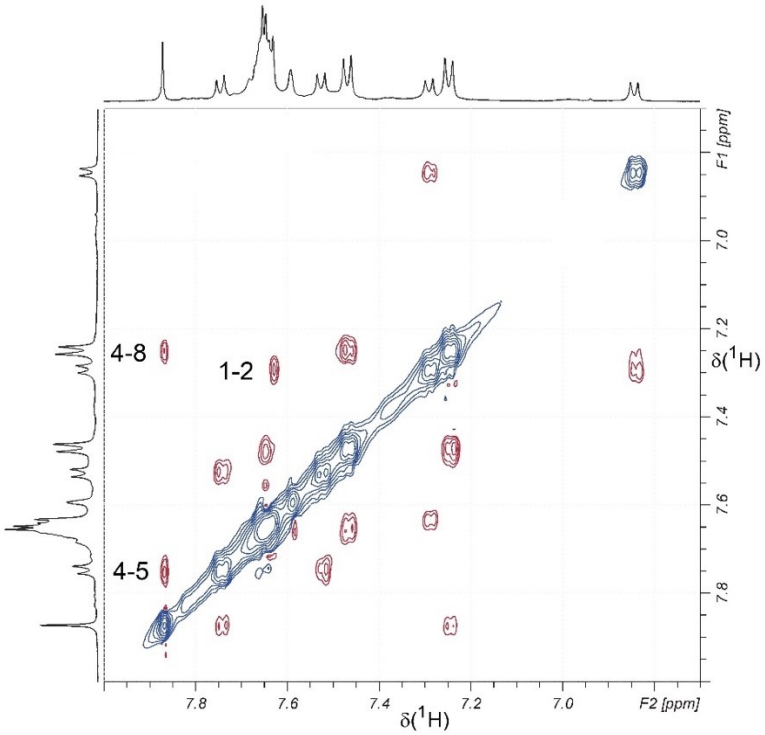

Fig. S34. ROESY spectrum (region) of **M** with assignment of some correlations.

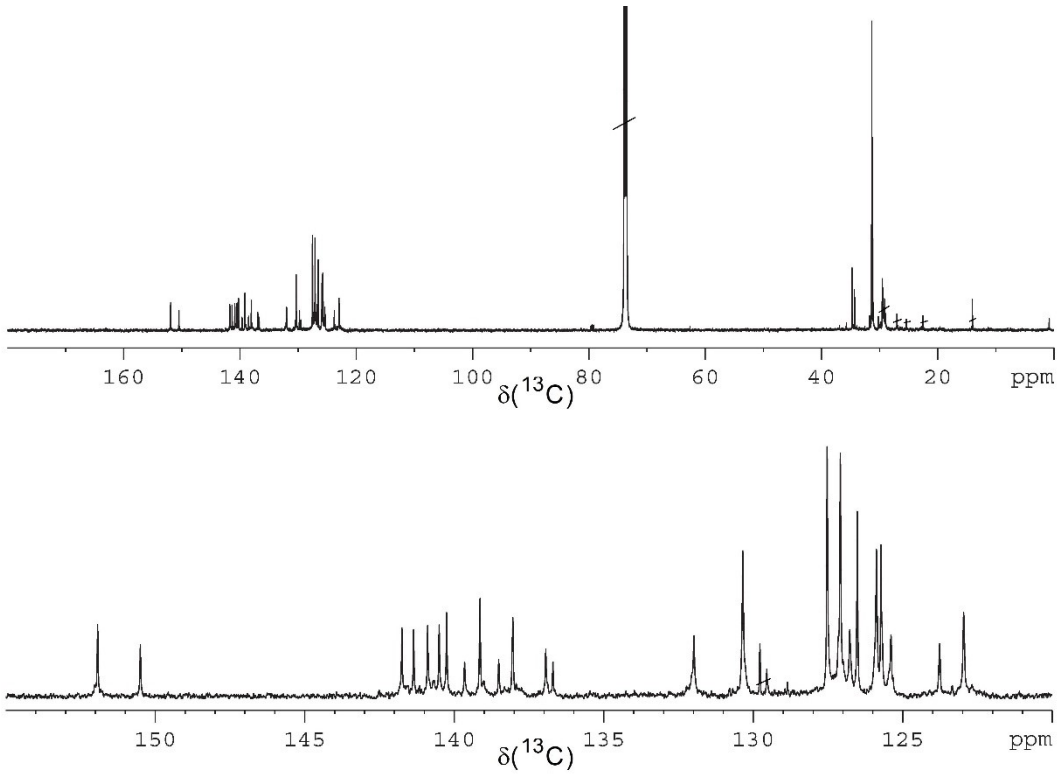

Fig. S35. ^{13}C NMR spectrum (125 MHz, $C_2D_2Cl_4$) of **M** and enlarged region of aromatic carbon signals.

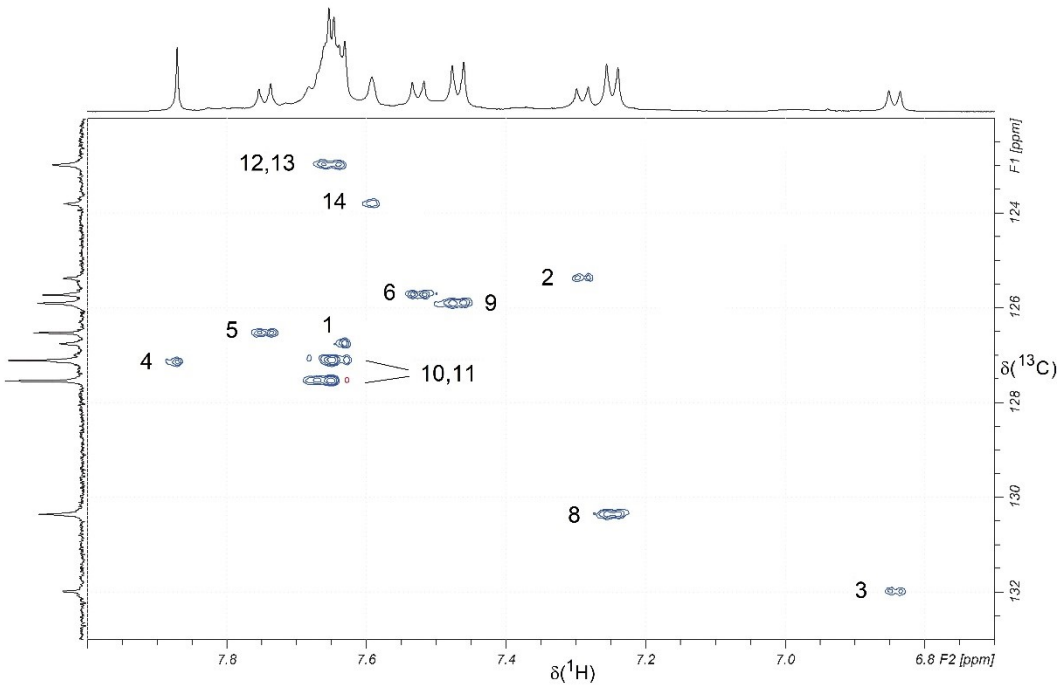

Fig. S36. HSQC spectrum (region) of **M** with assignment of aromatic CH signals. The projection at the F1 axis shows the DEPT135 spectrum.

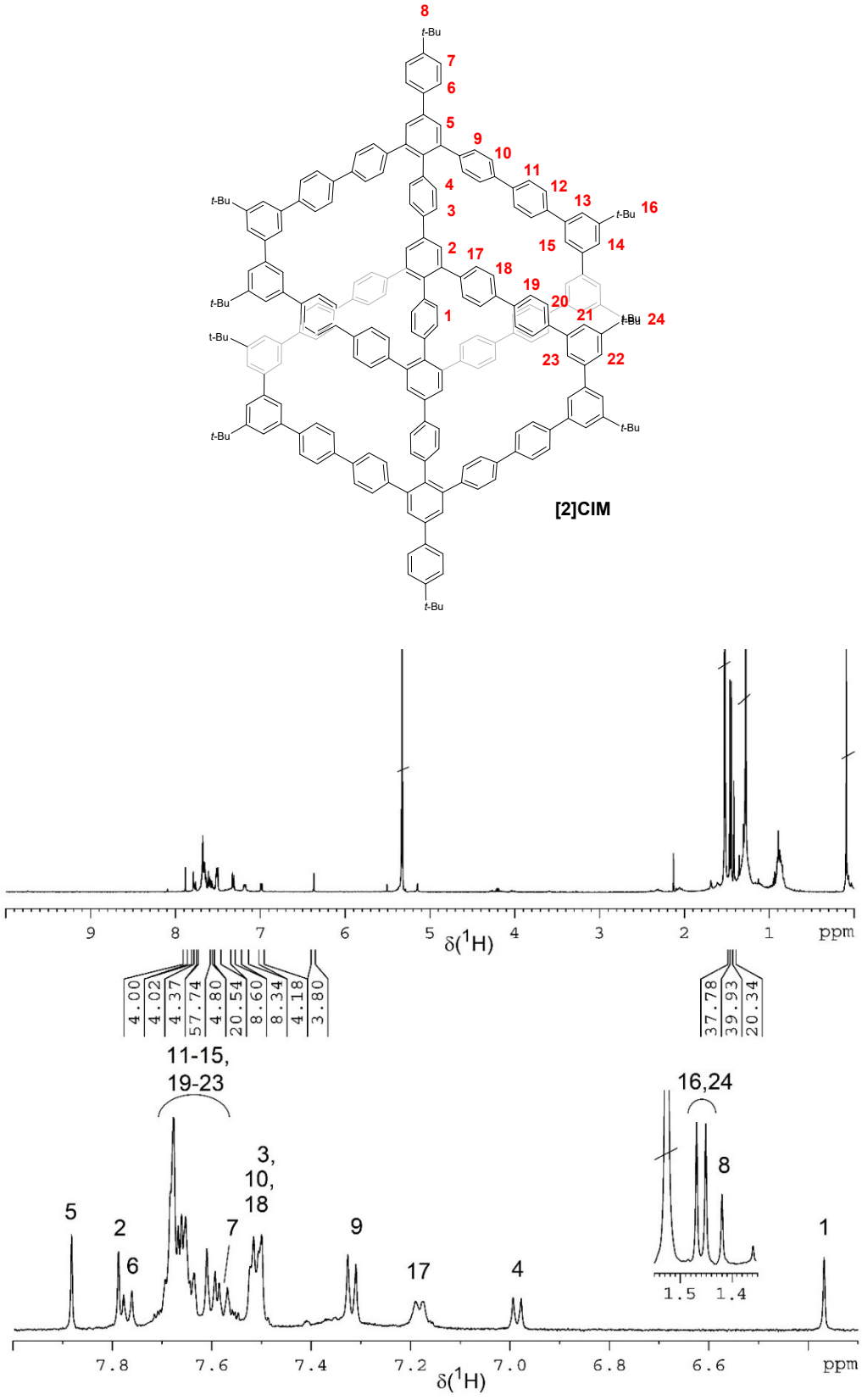

Fig. S37. ^{1}H NMR spectrum (500 MHz, CD_2Cl_2) of **[2]CIM** and enlarged regions with signal assignment.

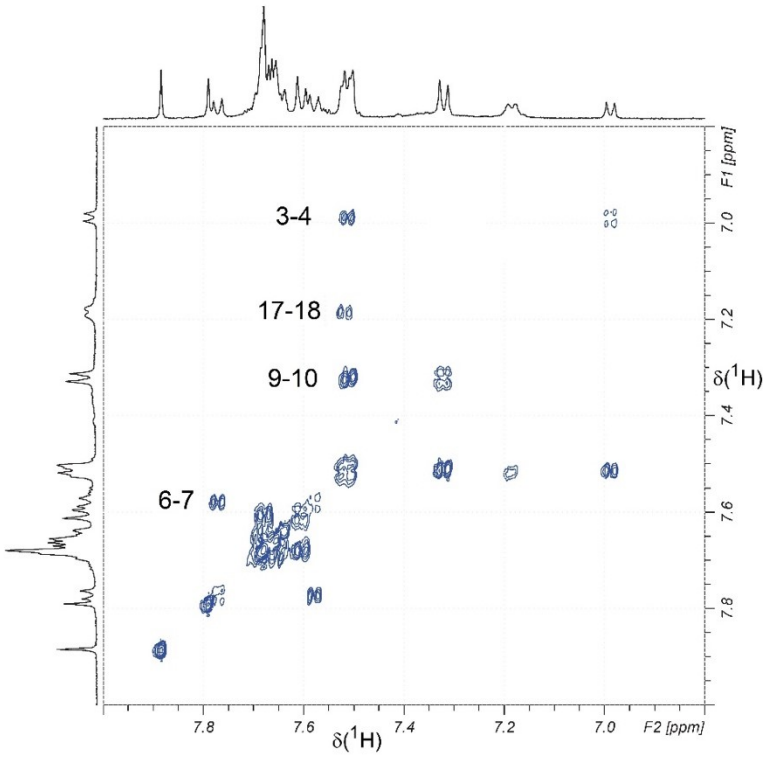

Fig. S38. COSY spectrum (region) of **[2]CIM** with assignment of some correlations.

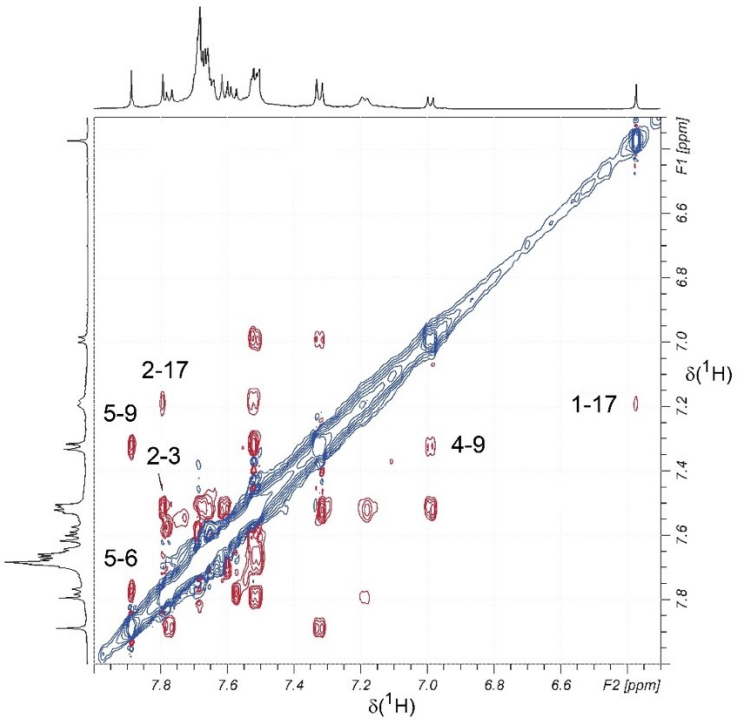

Fig. S39. ROESY spectrum (region) of **[2]CIM** with assignment of some correlations.

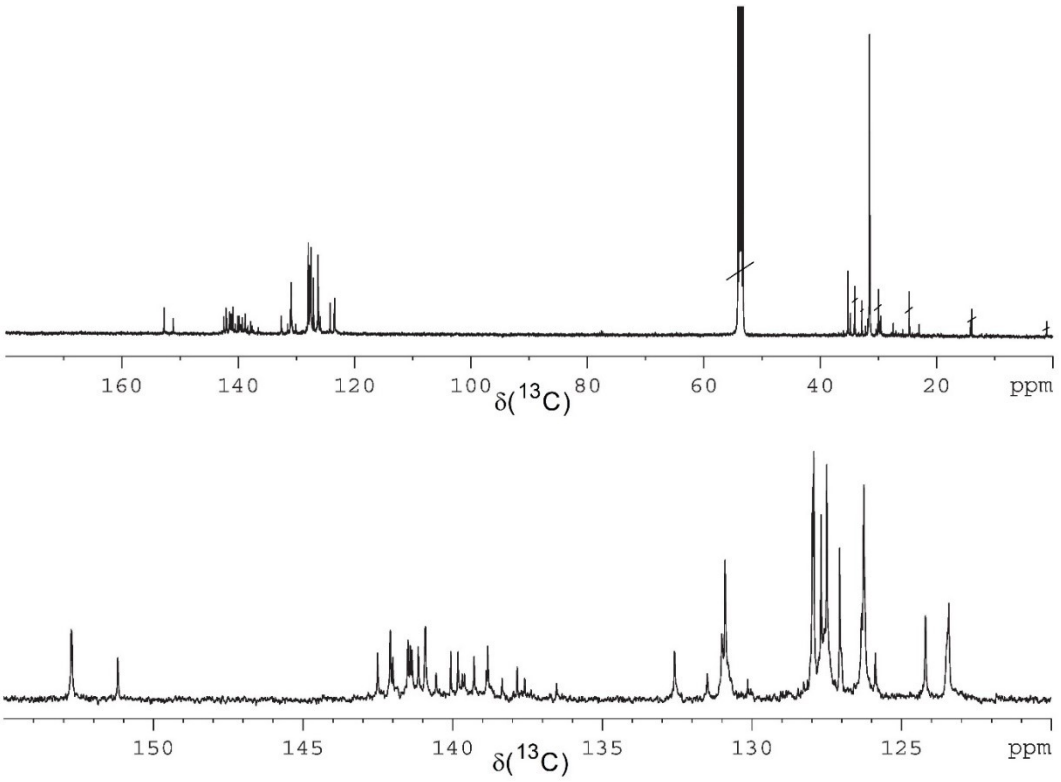

Fig. S40. ^{13}C NMR spectrum (125 MHz, CD_2Cl_2) of **[2]CIM** and enlarged region of aromatic carbon signals.

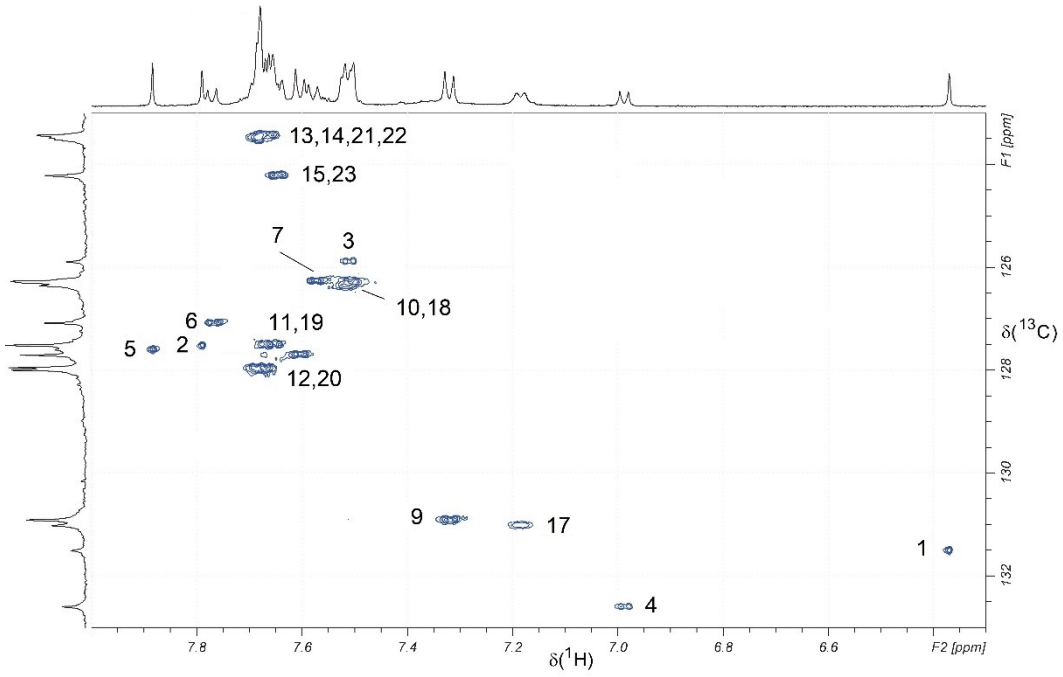

Fig. S41. HSQC spectrum (region) of **[2]CIM** with assignment of aromatic CH signals. The projection at the F1 axis shows the DEPT135 spectrum.

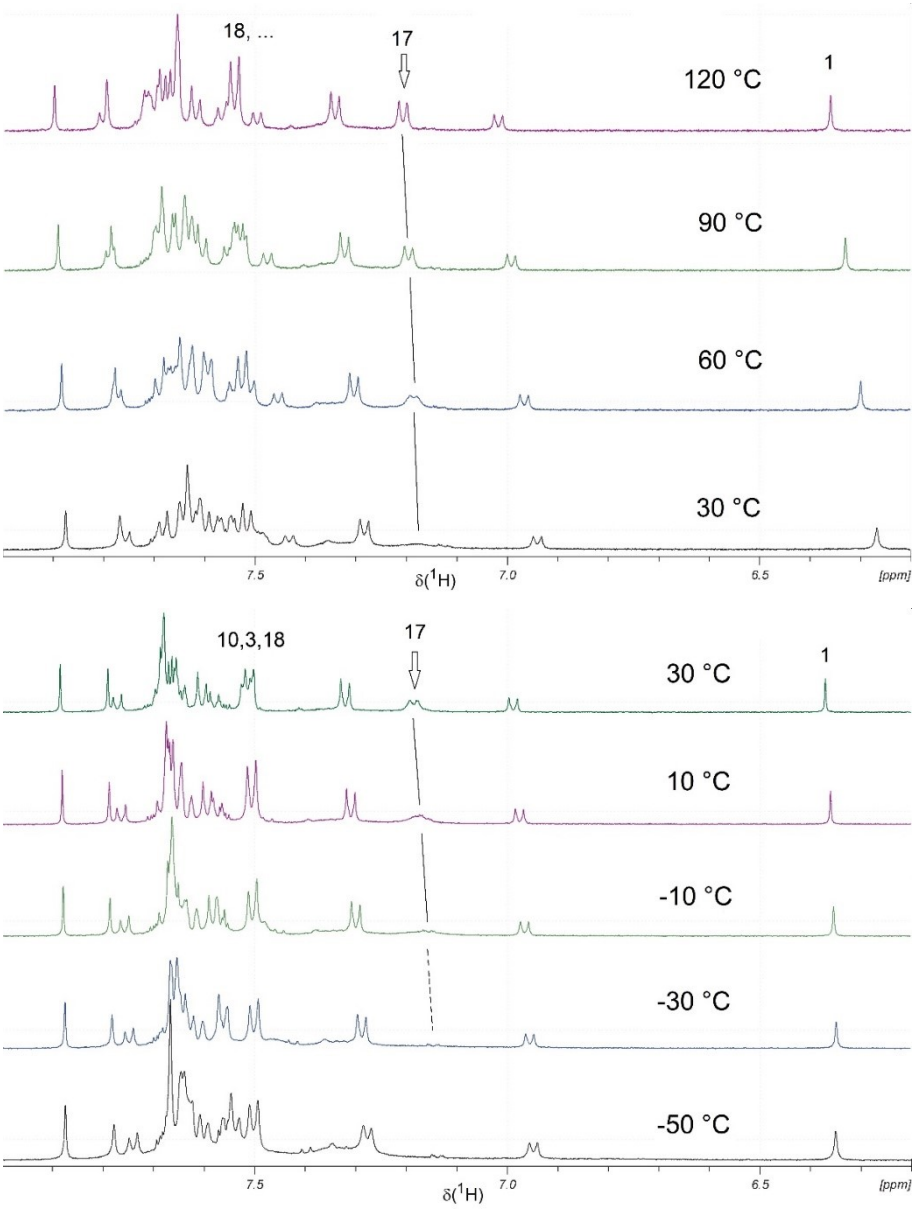

Fig. S42. Variable temperature ^{1}H NMR measurements on **[2]CIM**. The high temperature region was recorded from a solution in $C_2D_2Cl_4$ (top), the low temperature spectra were measured in CD_2Cl_2. While the linewidth of the signal from the central phenyl ring (H_1) does not change significantly, the neighbouring four *para*-substituted phenyl rings show line broadening due to decreased rotation rate with decreasing temperature. This can be well followed for H_{17}, while the signal of H_{18} is overlaid by other signals. Note: The rate is solvent dependent, as can be concluded from the comparison of spectra recorded at 30 °C in both solvents.

7.3. High-resolution mass spectroscopy (HR-MS) spectra.

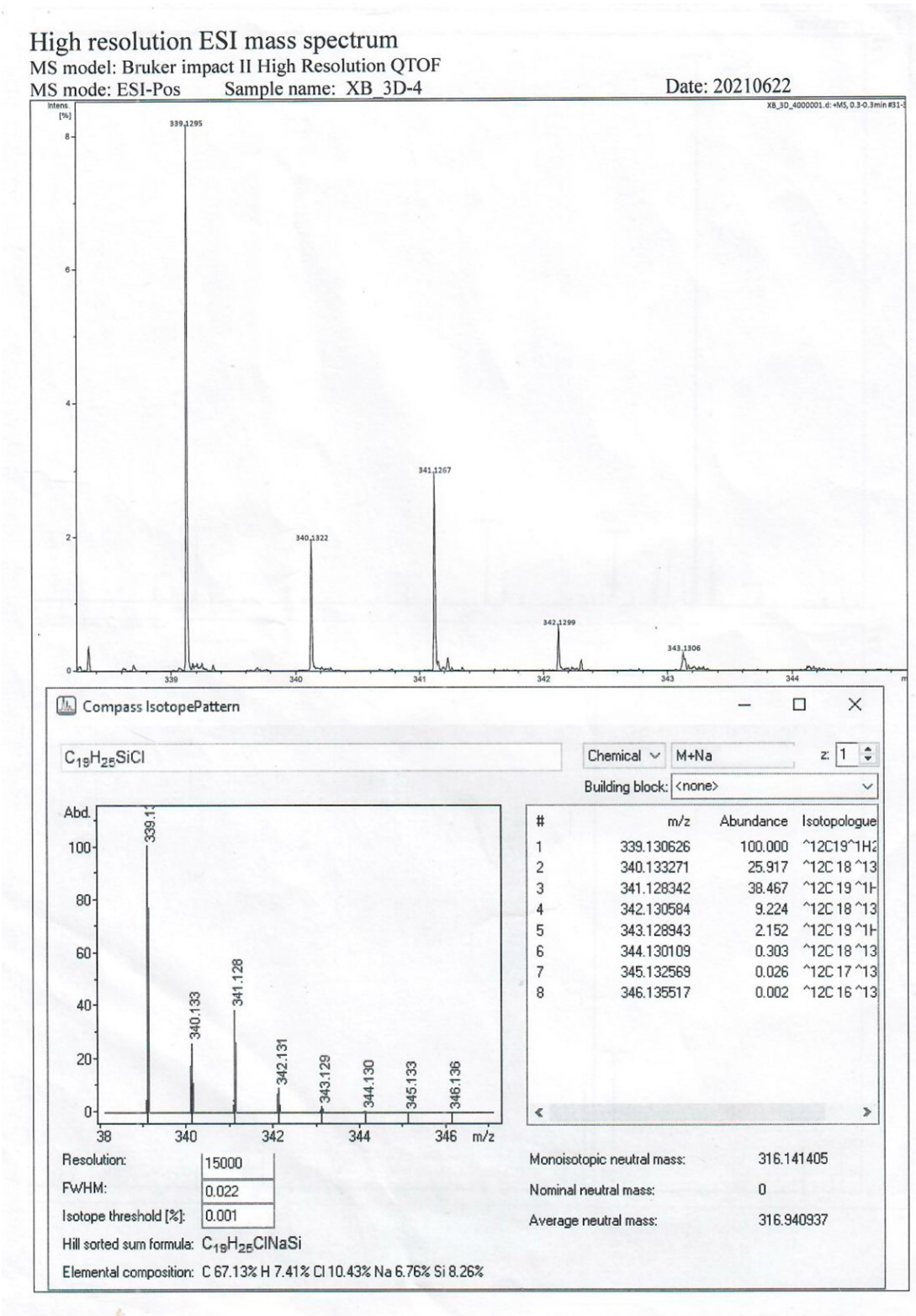

Fig. S43. High-resolution mass spectrum (ESI) of **3**.

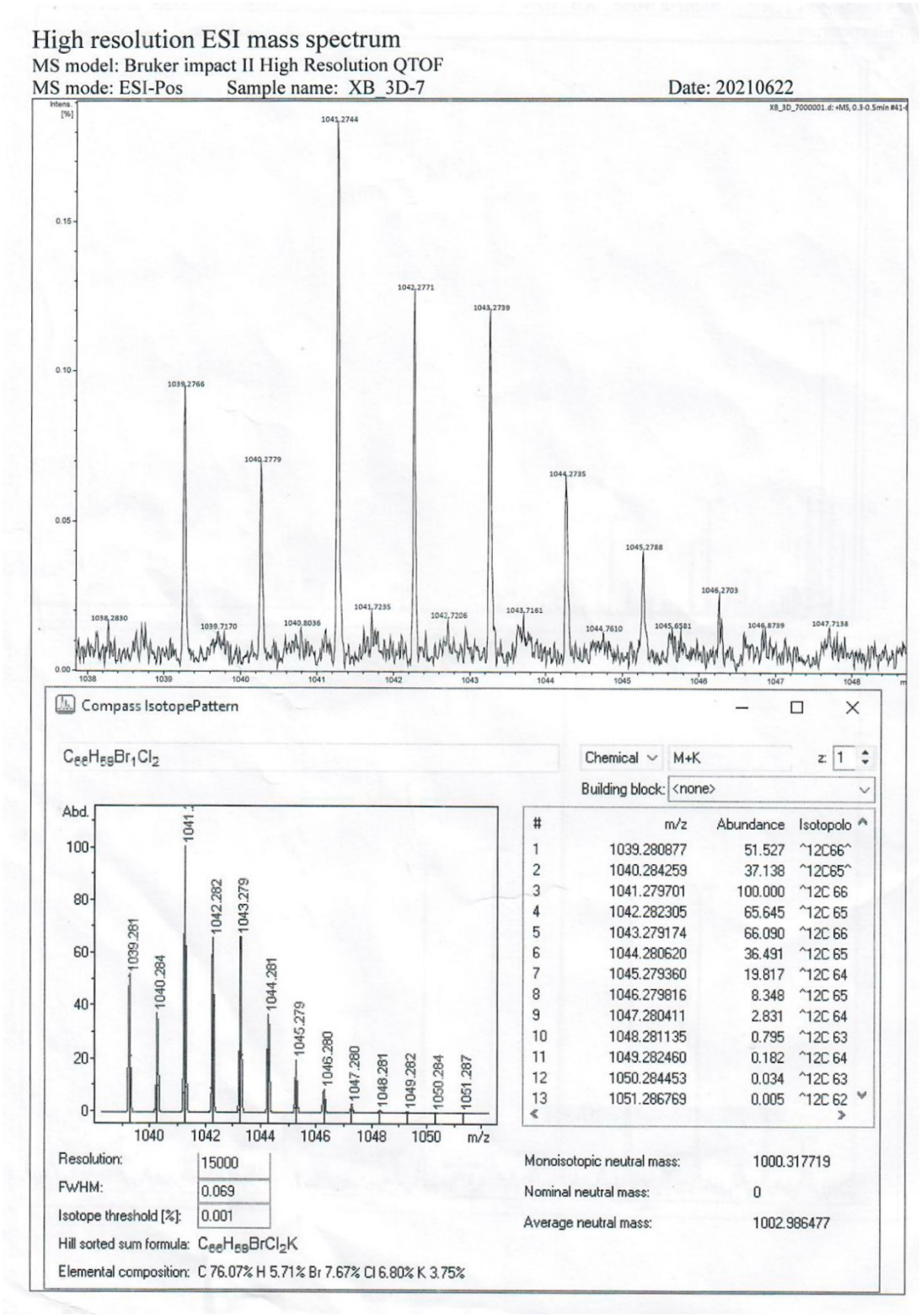

Fig. S44. High-resolution mass spectrum (ESI) of **6**.

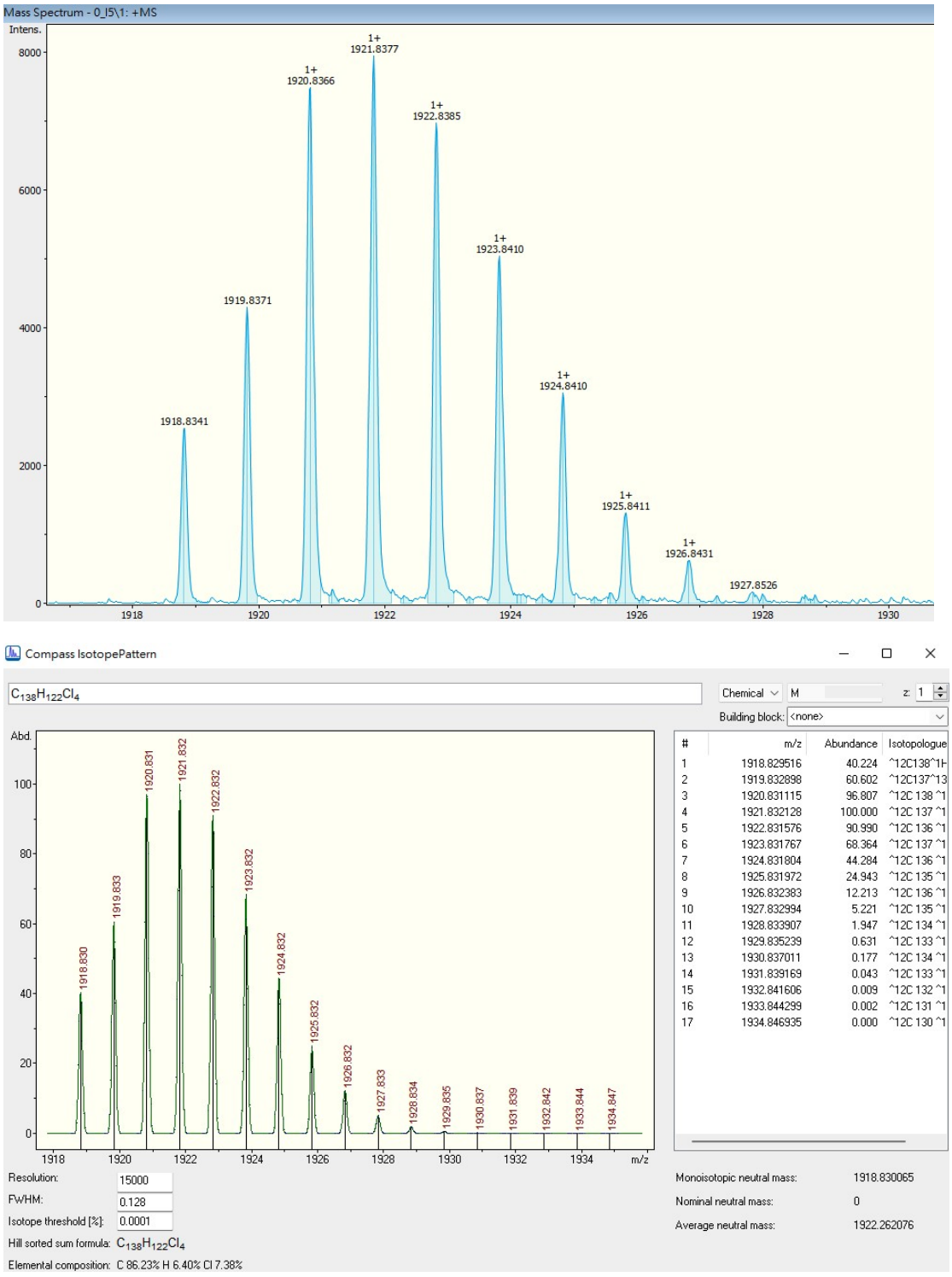

#	m/z	Abundance	Isotopologue
1	1918.829516	40.224	^12C138^1H
2	1919.832898	60.602	^12C137^13
3	1920.831115	96.807	^12C 138 ^1
4	1921.832128	100.000	^12C 137 ^1
5	1922.831576	90.990	^12C 136 ^1
6	1923.831767	68.364	^12C 137 ^1
7	1924.831804	44.284	^12C 136 ^1
8	1925.831972	24.943	^12C 135 ^1
9	1926.832383	12.213	^12C 136 ^1
10	1927.832994	5.221	^12C 135 ^1
11	1928.833907	1.947	^12C 134 ^1
12	1929.835239	0.631	^12C 133 ^1
13	1930.837011	0.177	^12C 134 ^1
14	1931.839169	0.043	^12C 133 ^1
15	1932.841606	0.009	^12C 132 ^1
16	1933.844299	0.002	^12C 131 ^1
17	1934.846935	0.000	^12C 130 ^1

Fig. S45. HR-MALDI-TOF mass spectrum of **6**.

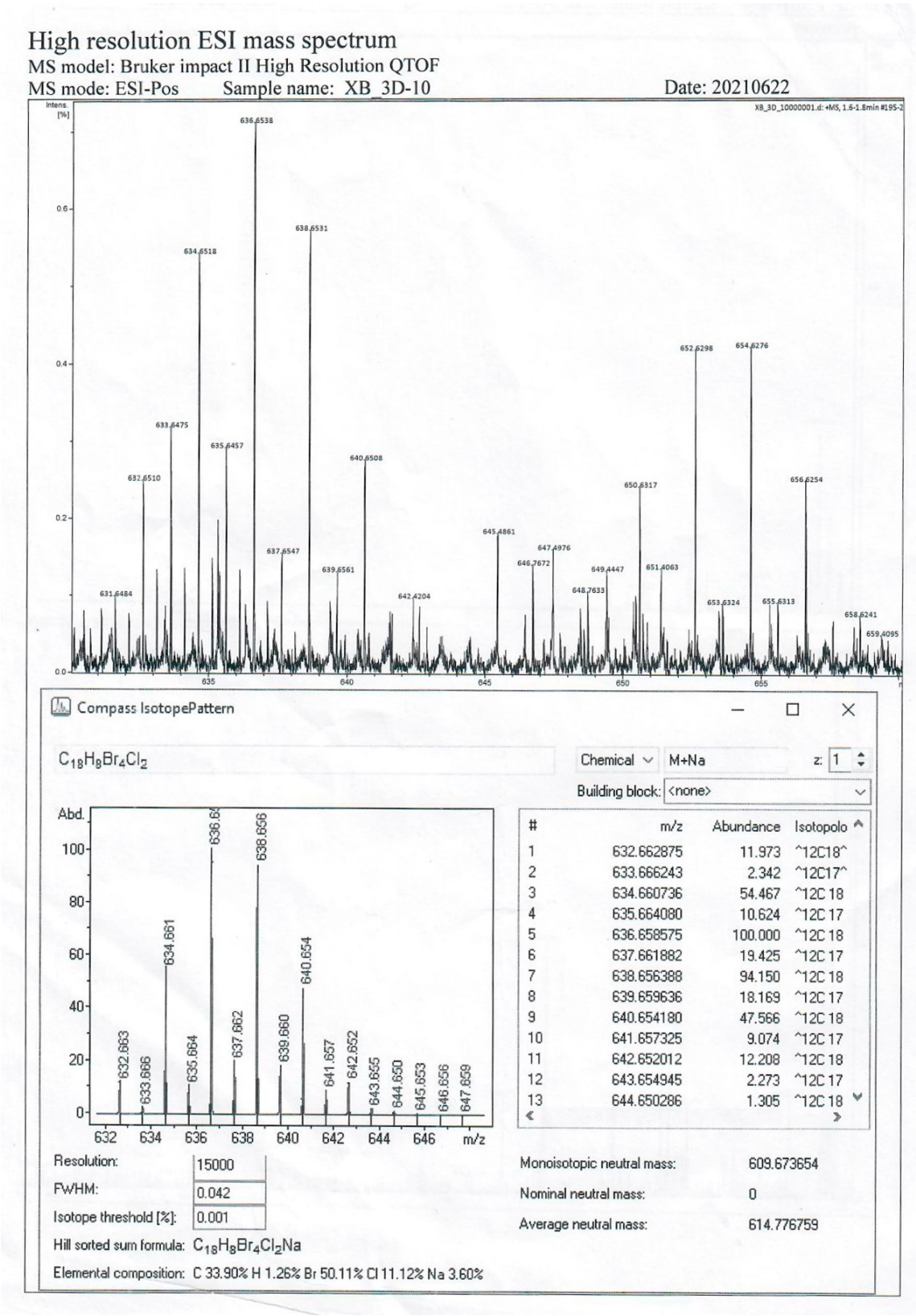

#	m/z	Abundance	Isotopolo
1	632.662875	11.973	^12C18^
2	633.666243	2.342	^12C17^
3	634.660736	54.467	^12C 18
4	635.664080	10.624	^12C 17
5	636.658575	100.000	^12C 18
6	637.661882	19.425	^12C 17
7	638.656388	94.150	^12C 18
8	639.659636	18.169	^12C 17
9	640.654180	47.566	^12C 18
10	641.657325	9.074	^12C 17
11	642.652012	12.208	^12C 18
12	643.654945	2.273	^12C 17
13	644.650286	1.305	^12C 18

Fig. S46. High-resolution mass spectrum (ESI) of **11**.

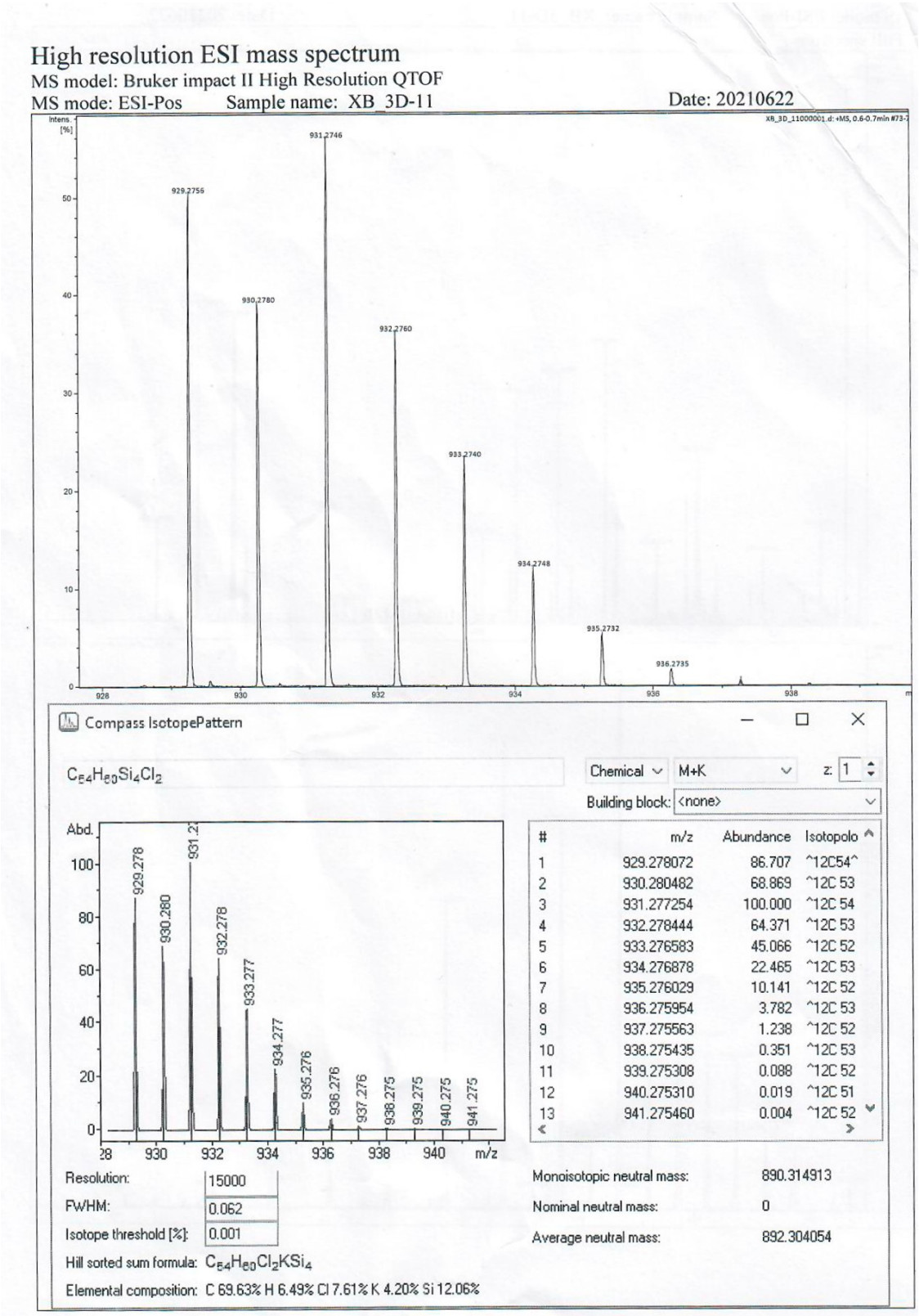

Fig. S47. High-resolution mass spectrum (ESI) of **13**.

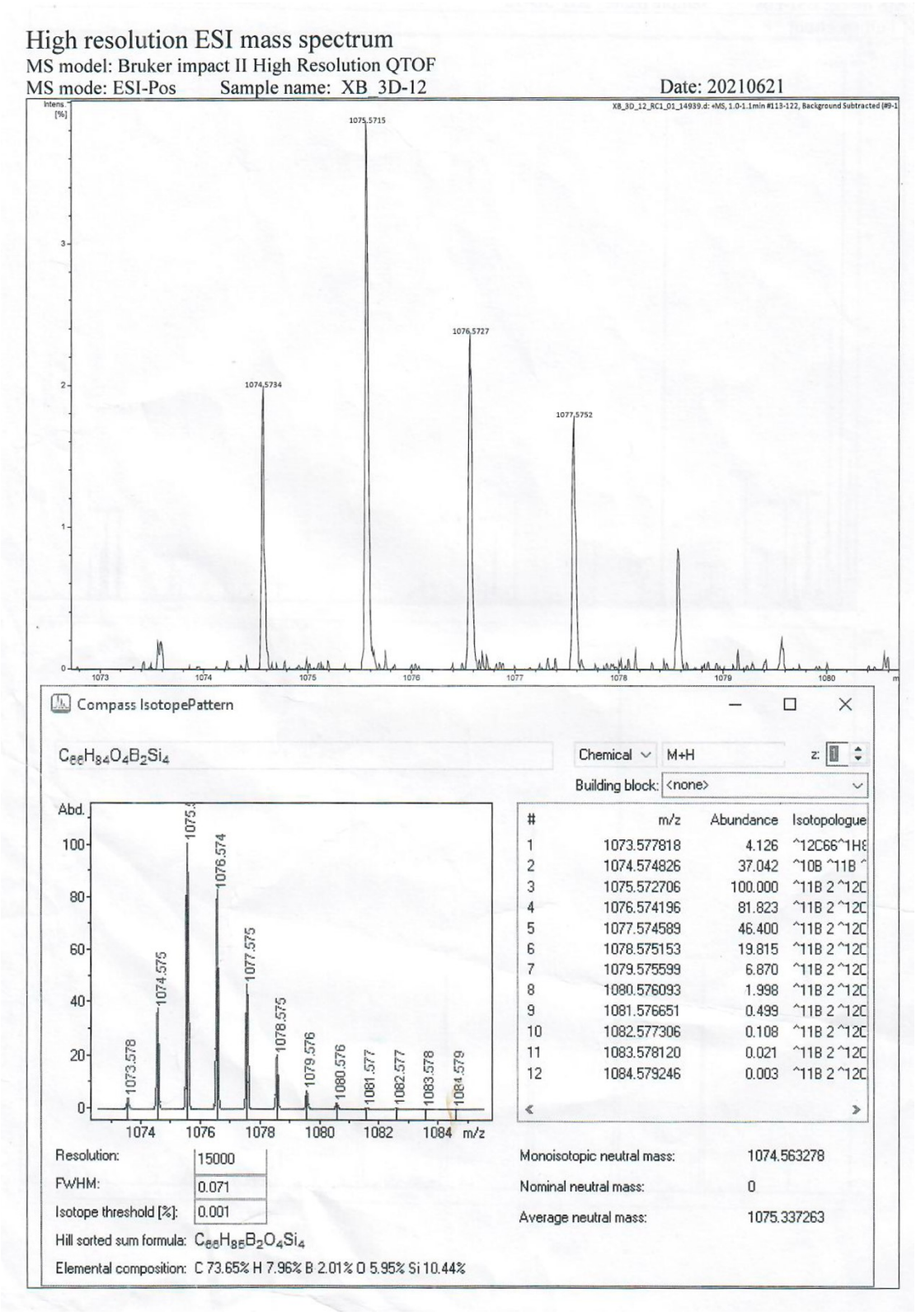

Fig. S48. High-resolution mass spectrum (ESI) of **14**.

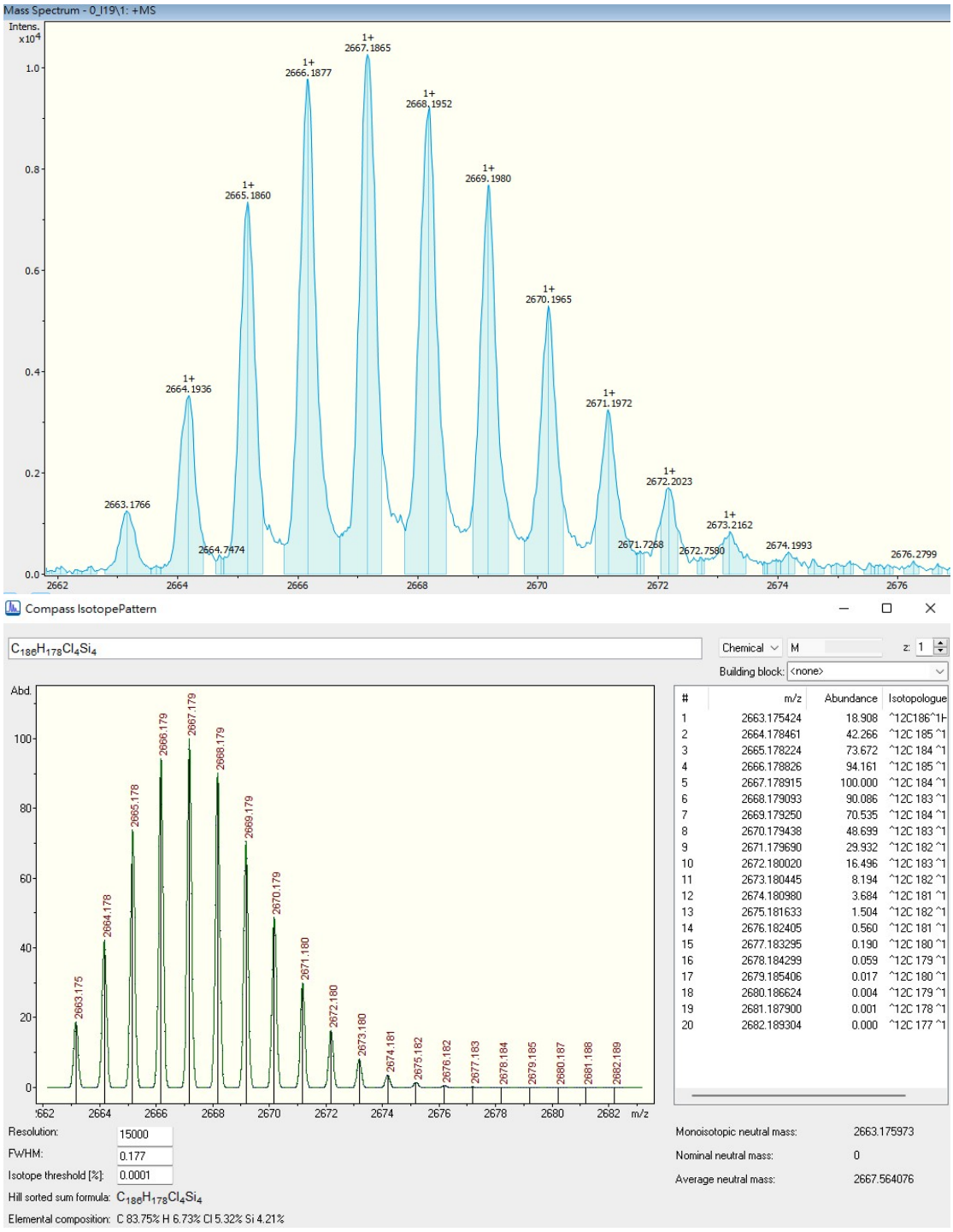

Fig. S49. HR-MALDI-TOF mass spectrum of compound **15**.

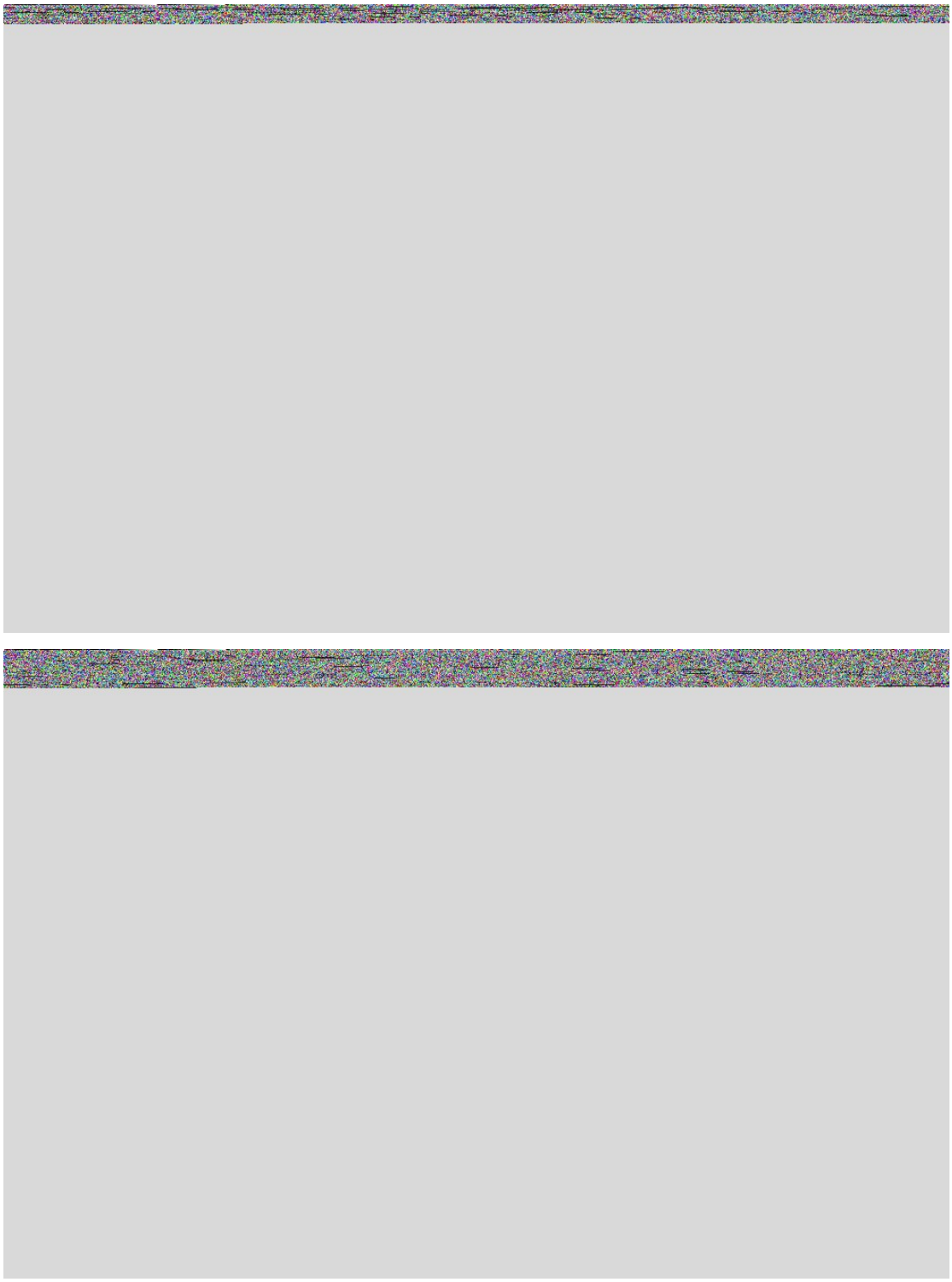

Fig. S50. HR-MALDI-TOF mass spectrum of compound **8**.

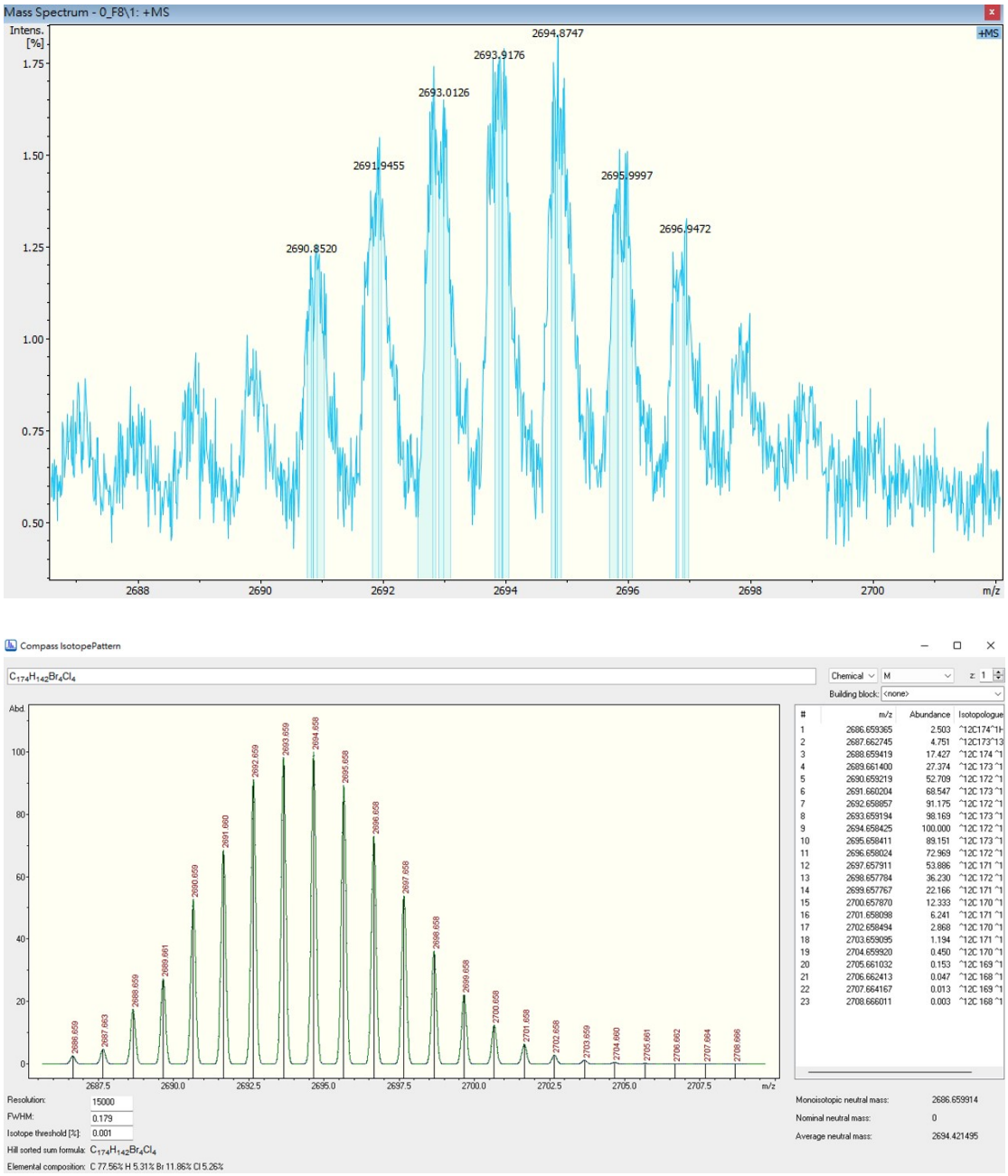

Fig. S51. HR-MALDI-TOF mass spectrum of compound **16.**

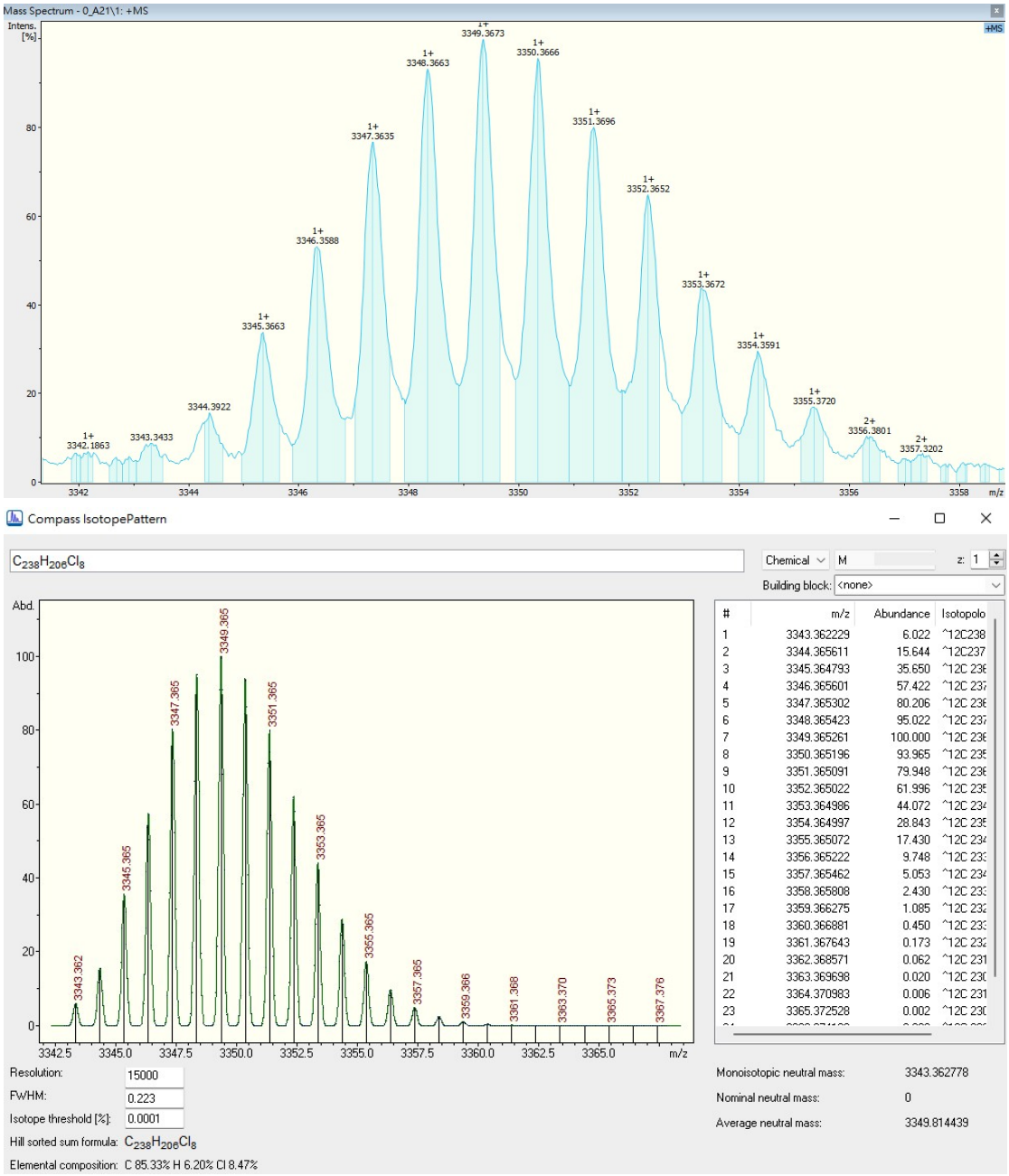

Fig. S52. HR-MALDI-TOF mass spectrum of compound **17.**

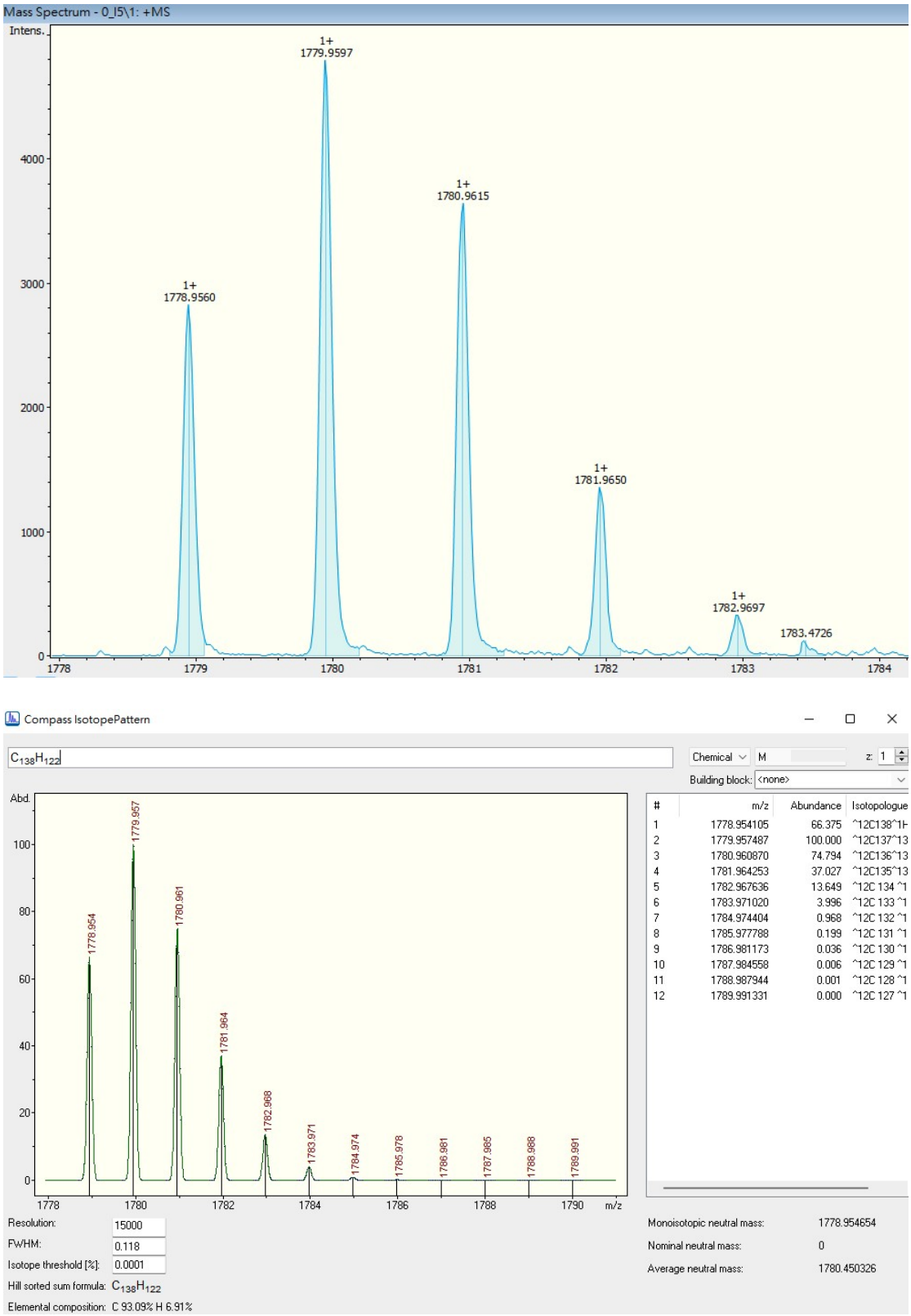

Fig. S53. HR-MALDI-TOF mass spectrum of compound **M.**

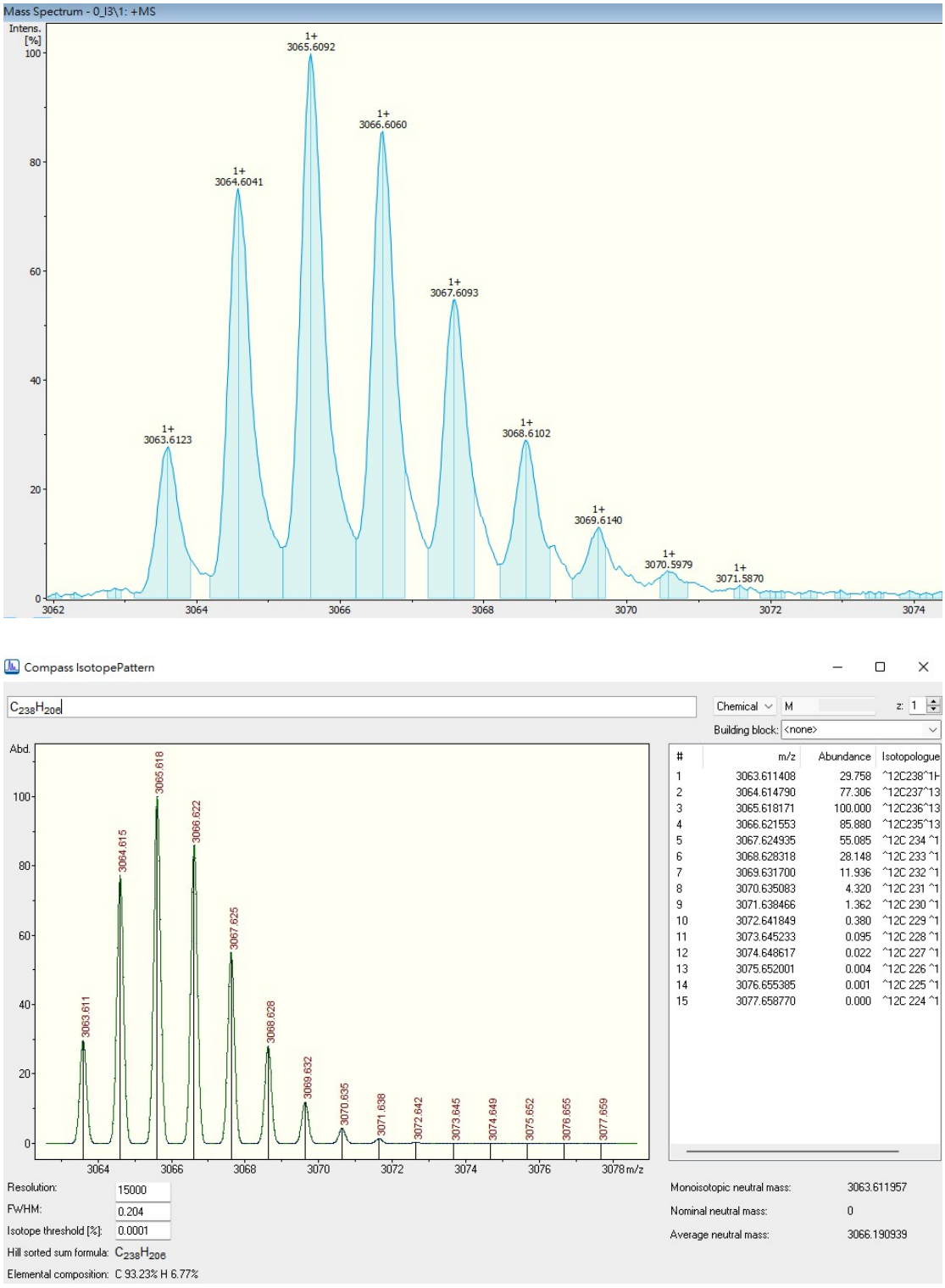

Fig. S54. HR-MALDI-TOF mass spectrum of compound **[2]CIM**.

8. Powder X-Ray Diffraction

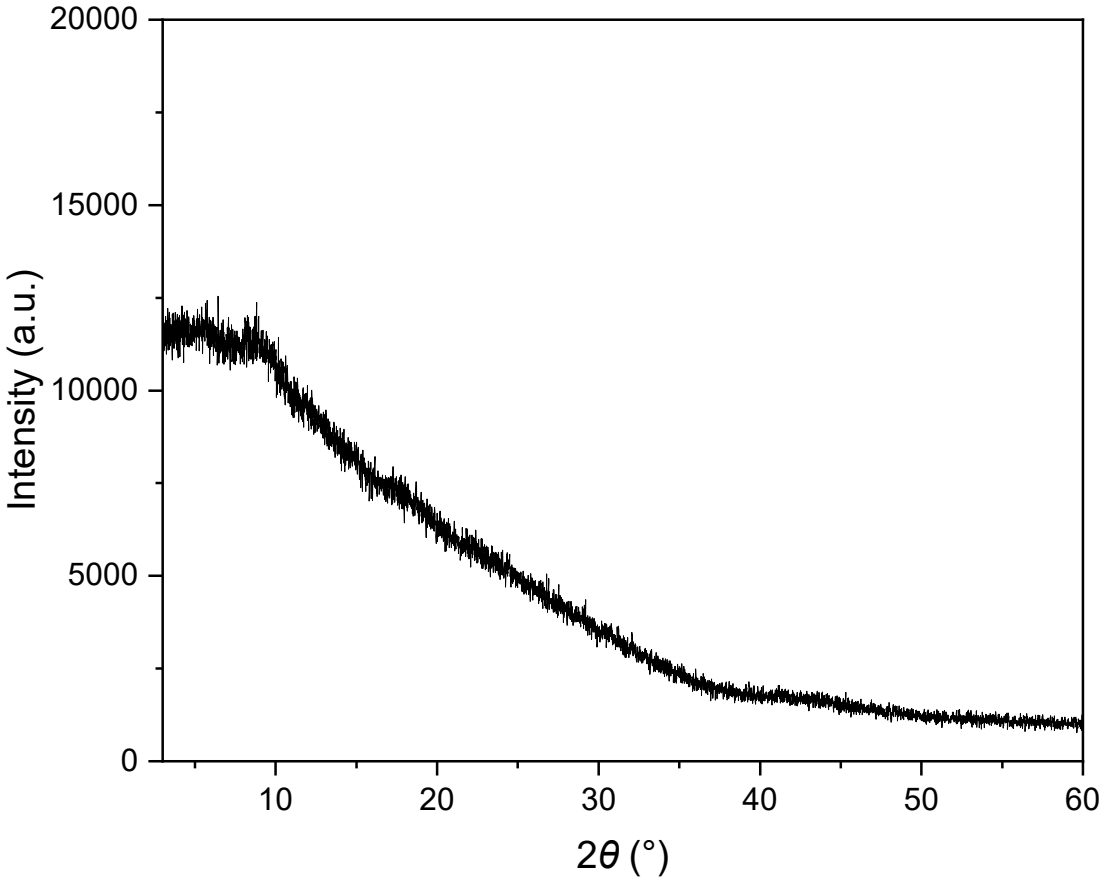

Fig. S55. Powder X-ray diffraction spectrum of **[2]CIM**.

9. Gas Sorption

Table S2. Gases used in the here presented studies.

Gas	Formula	CAS	Supplier	Quality
Nitrogen	N_2	7727-37-9	Air Liquide	5.0 (99.999%)
Argon	Ar	7440-37-1	Air Liquide	4.8 (99.998%)
Ethane	C_2H_6	74-84-0	Air Liquide	3.5 (99.5%)
Ethylene	C_2H_4	74-85-1	Air Liquide	3.5 (99.5%)
Acetylene	C_2H2	74-86-2	Air Liquide	3.5 (99.5%)

Non-ideality factors

To express the deviation of the behaviour of a real gas from the ideal one, the so-called non-ideality factor α was calculated and implemented in the parameter files of the operating software of the Quantachrome IQ2 and IQ3 systems used during the here presented studies. Two methods have been taken into account to calculate the non-ideality factors and the average of both values was used for the corresponding measurements.

Method 1: Berthelot-Equation[5]

$$pV(1 + \alpha p) = nRT$$

with

$$\alpha = \frac{9}{128}\frac{1}{p_c}\frac{T_c}{T}\left(6\left(\frac{T_c}{T}\right)^2 - 1\right)$$

α: non-ideality factor
p: pressure
p_c: critical pressure
V: volume
R: gas constant
T: temperature
T_c: critical temperature

Method 2: van der Waals Equation[6]

$$\left(p + \frac{a}{V_m^2}\right)\left(V_m - b\right) = RT$$

with

$$a = \frac{27\left(RT_c\right)^2}{64p_c}$$

and

$$b = \frac{RT_c}{8p_c}$$

a: van der Waals parameter (internal pressure)
b: van der Waals parameter (co-volume)
p: pressure
p_c: critical pressure
V_m: molar volume
R: gas constant
T: temperature
T_c: critical temperature

Since the co-volume b defines the deviation for ideal behaviour at high pressures. The van-der-Waals parameter a is equivalent to the non-ideality factor and taken into account exclusively.

Values for the critical pressure, critical temperature and boiling points have been extracted from the *NIST Chemistry WebBook, SRD 69* of the National Institute of Standards and Technology.[7]

Table S3. Selected physical properties and non-ideality factors.

Gas	bp (K)	T (K)[a]	crit. T (K)	crit. P (Torr)	non-ideality ($\times 10^{-5} \cdot Torr^{-1}$)		
					Berthelot	vdW	average

C_2H_6	184.6	193.15	305.3	36753	4.23	2.33	3.28
C_2H_6	184.6	213.15	305.3	36753	3.10	1.87	2.48
C_2H_6	184.6	233.15	305.3	36753	2.33	1.52	1.92
C_2H_6	184.6	253.15	305.3	36753	1.78	1.26	1.52
C_2H_6	184.6	273.15	305.3	36753	1.39	1.05	1.22
C_2H_6	184.6	283.15	305.3	36753	1.23	0.97	1.10
C_2H_6	184.6	298.15	305.3	36753	1.04	0.86	0.95
C_2H_4	169	273.15	282.5	37953	1.04	0.85	0.94
C_2H_4	169	283.15	282.5	37953	0.92	0.78	0.85
C_2H_4	169	298.15	282.5	37953	0.77	0.96	0.73
C_2H_2	189	273.15	308.3	46039	1.04	0.85	0.94
C_2H_2	189	283.15	308.3	46039	1.02	0.79	0.90
C_2H_2	189	298.15	308.3	46039	0.86	0.70	0.78

[a] Measurement temperature. [b] Sublimation point.

Selectivity Calculations

The adsorption behaviour of two gases in comparison was investigated using two different selectivity models. The ideal adsorbed solution theory (IAST)[8] considers the spreading pressure and is thus taking the competing character of two gases for the selective binding sites into account. The IAST is defined by a series of equations which have to be solved numerically. The numerical solution was accomplished using 3P instruments' 3p sim software (version 1.1.0.9).

The experimental isotherms possessing a type I like behaviour have been fitted with the non-linear Tóth equation:

$$q_{eq} = q_{max} \frac{K \cdot p}{\left(1 + (K \cdot p)^t\right)^{\frac{1}{t}}}$$

With: p: pressure

q_{eq}: experimental uptake (mmol·g^{-1})

$q_{max:}$ maximum uptake (mmol·g^{-1})

K: affinity constant (1·bar^{-1})

t: heterogeneity (or Tóth) parameter (dimensionless)

Since gases with lower adsorption tendencies differ from a typical type I like behaviour, other isotherm models had to be used for them. Isotherms with a non-linear yet non-pronounce type I like behaviour have been fitted using the non-linear Tóth equation with $t = 1$ which is known as Langmuir adsorption isotherm:

$$q_{eq} = q_{max} \frac{K \cdot p}{1 + (K \cdot p)}$$

with: p: pressure

q_{eq}: experimental uptake (mmol·g^{-1})

$q_{max:}$ maximum uptake (mmol·g^{-1})

K: affinity constant (1·bar^{-1})

Linear isotherms can be thus interpreted as Langmuir isotherms with $q_{max} \rightarrow \infty$, which transfers the Langmuir isotherm to a standard Henry isotherm:

$$q_{eq} = K \cdot p$$

with: p: pressure

q_{eq}: experimental uptake (mmol·g^{-1})

K: affinity constant (1·bar^{-1})

For this purpose, the max. uptake was set to 1000 mmol·g^{-1}

The parameters obtained by the described fittings where then applied in the IAST-theory to calculate the selectivity $S_{A/B}$ of gas A over gas B by:

$$S_{A/B} = \frac{x_A / y_A}{x_B / y_B}$$

with: x_i: molar fraction of compound i in the adsorbed phase

Y_i: molar fraction of compound i in the gas phase

For pressures of $p \rightarrow 0$, the IAST-selectivity can be seen as a frontier selectivity which is commonly known as Henry selectivity with the simplified Tóth equation:

$$q_{eq} = q_{max} \cdot K \cdot p$$

By the definition of Henry's law, this means the Henry constant K_H is now defined as:

$$K_H = q_{max} \cdot K$$

And the Henry selectivity S_H of a gas A over gas B can be now calculated as the quotient of the corresponding Henry constants.

While the IAST-selectivity is considering the competition of two gases and thus gives insights in the bulk behaviour of an adsorbent, the Henry selectivity is only taking the most selective binding sites into account.

N_2-Sorption at 77 K

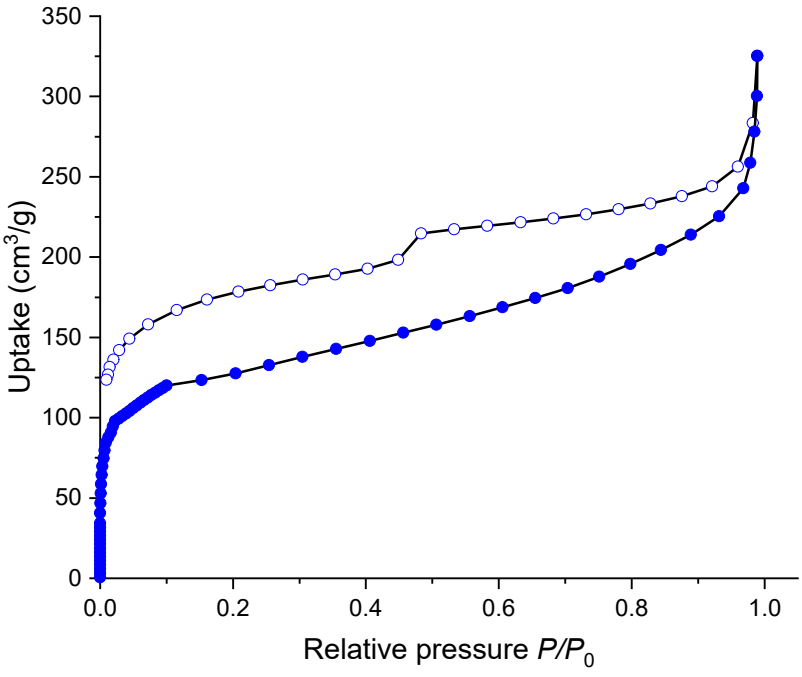

Fig. S56. Nitrogen sorption isotherm of **[2]CIM** at 77 K. Filled circles: adsorption; empty circles: desorption.

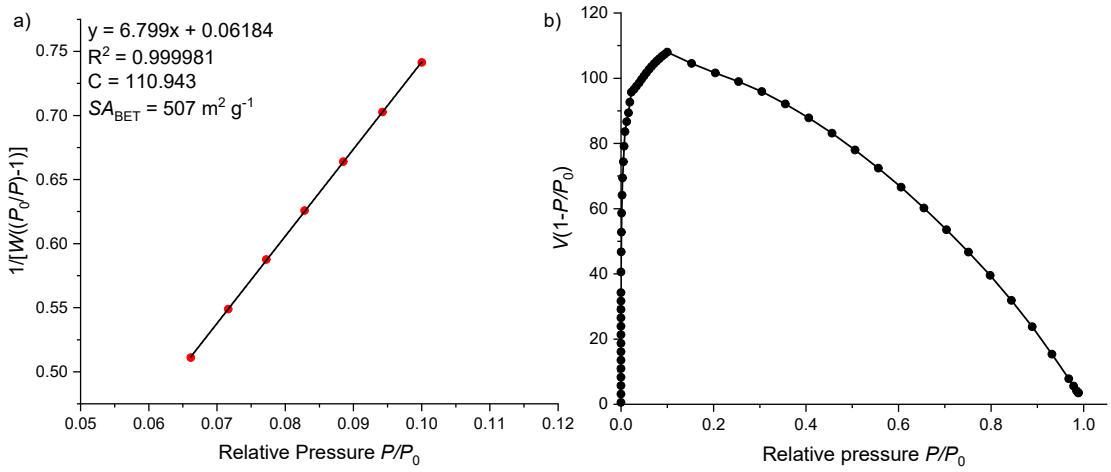

Fig. S57. (a) BET-plot and (b) corresponding Rouquerol-plot of **[2]CIM** at 77 K.

Ar-Sorption at 87 K

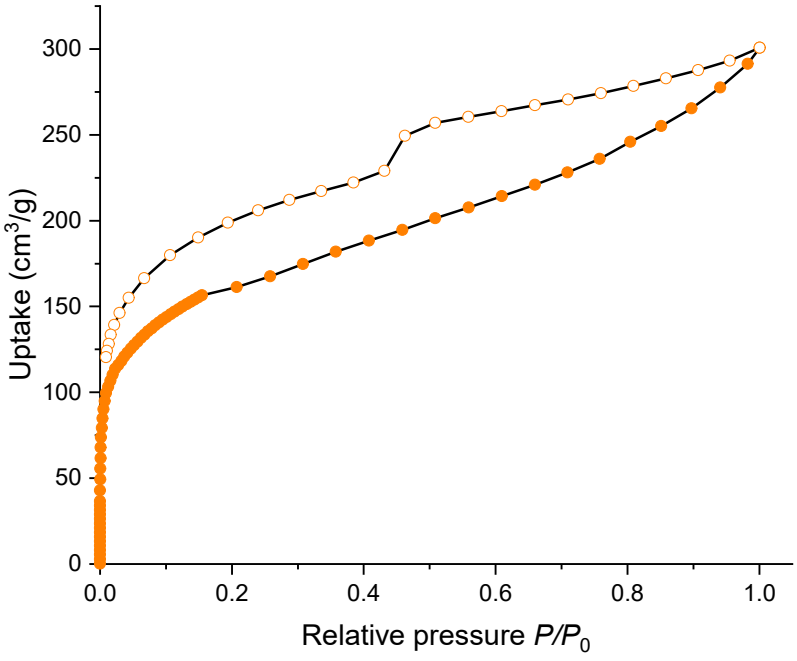

Fig. S58. Argon sorption isotherm of **[2]CIM** at 87 K. Filled circles: adsorption; empty circles: desorption.

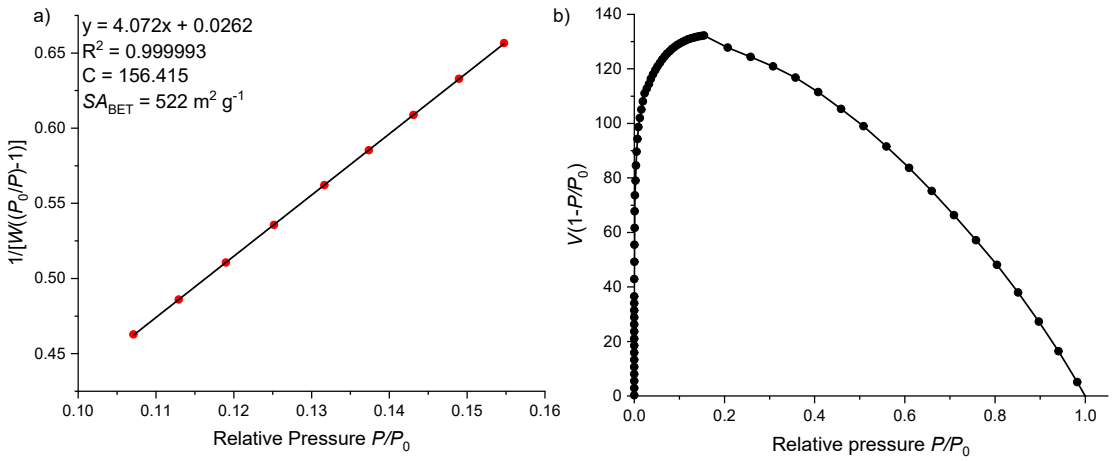

Fig. S59. (a) BET-plot and (b) corresponding Rouquerol-plot of **[2]CIM** at 87 K.

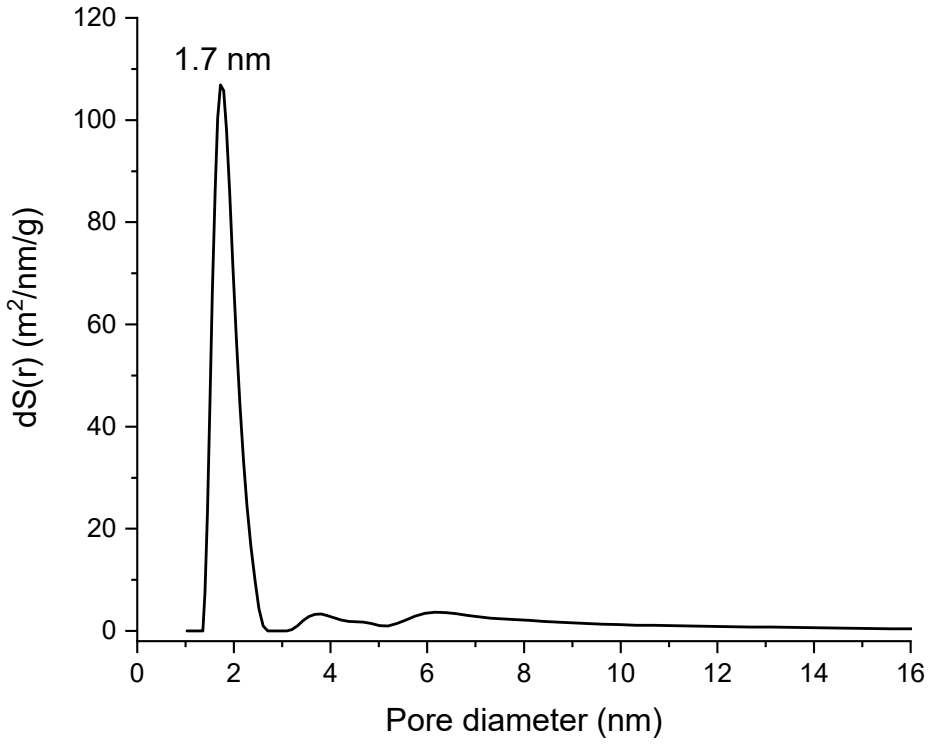

Fig. S60. QSDFT pore size distribution (cyclindr.spher. pores on carbon adsorption branch) of **[2]CIM** from nitrogen sorption at 77 K. Fitting error: 1.512%.

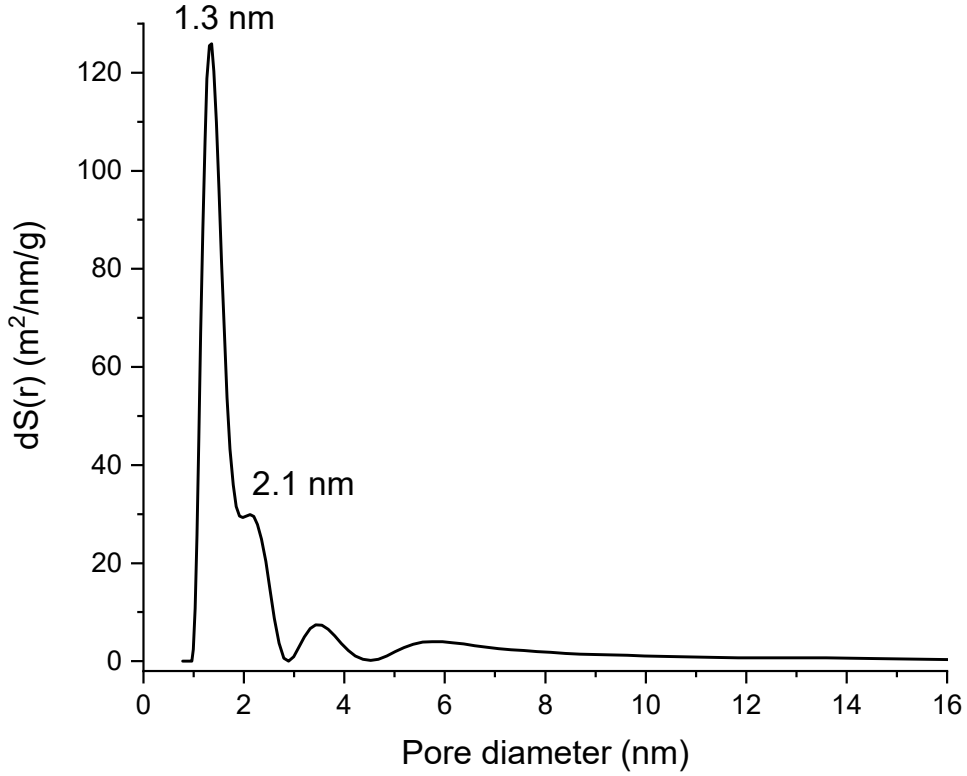

Fig. S61. QSDFT pore size distribution (cyclindr. spher. pores on carbon adsorption branch) of **[2]CIM** from argon sorption at 87 K. Fitting error: 0.476%.

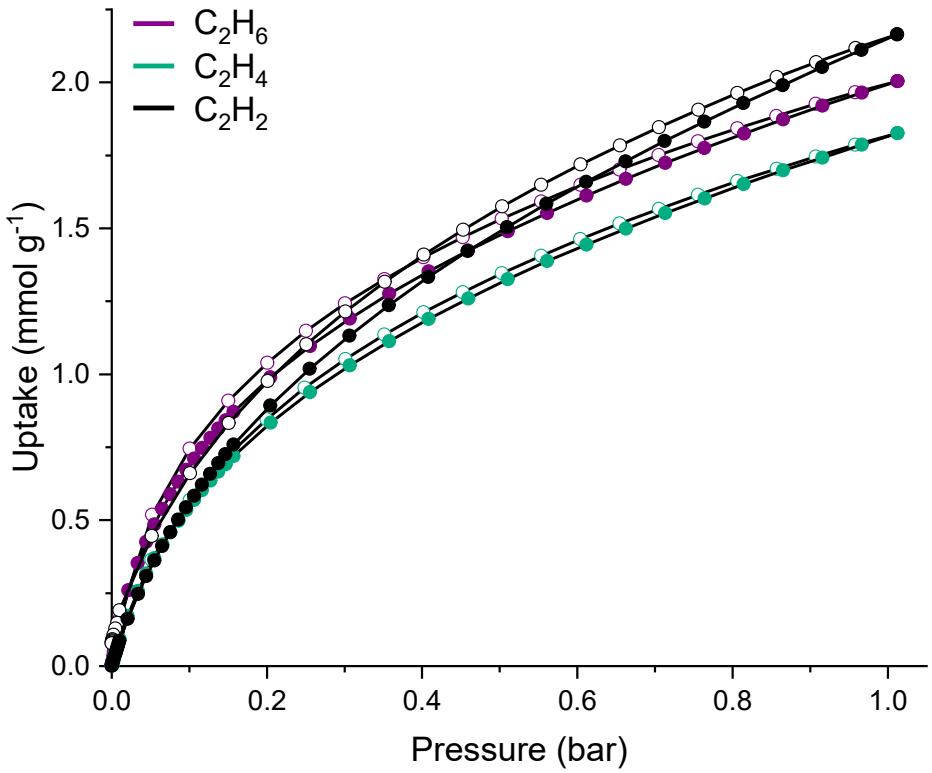

Fig. S62. C_2H_6 (purple), C_2H_4 (cyan) and C_2H_2 (black) sorption isotherms of **[2]CIM** at 273 K. Full circles: adsorption; empty circles: desorption.

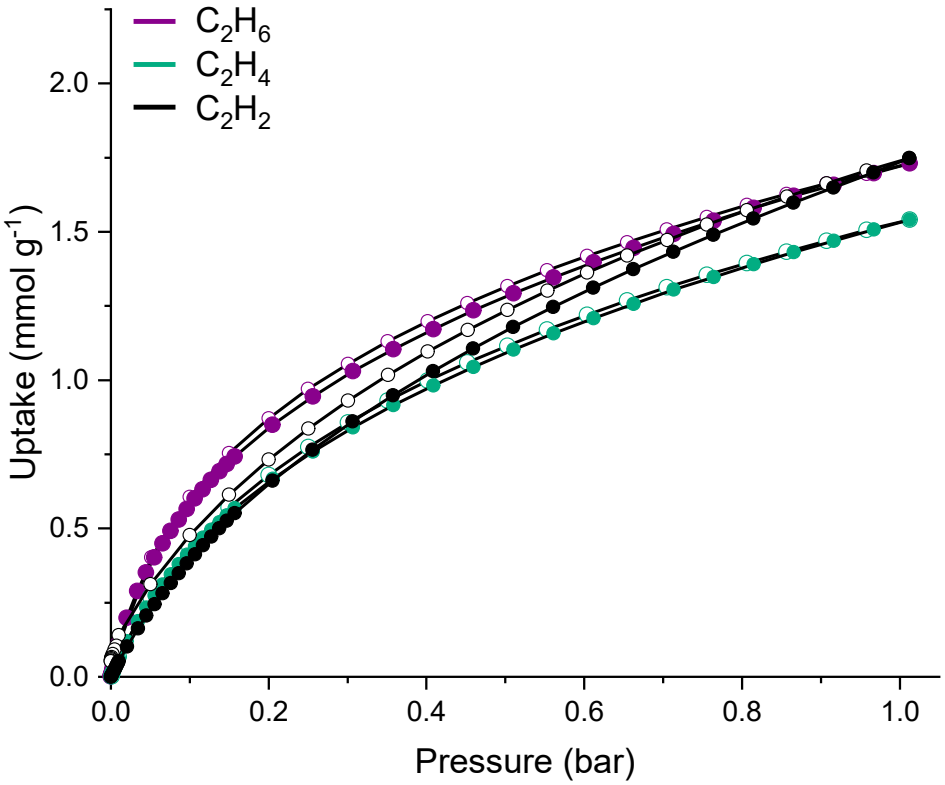

Fig. S63. C_2H_6 (purple), C_2H_4 (cyan) and C_2H_2 (black) sorption isotherms of **[2]CIM** at 283 K. Full circles: adsorption; empty circles: desorption.

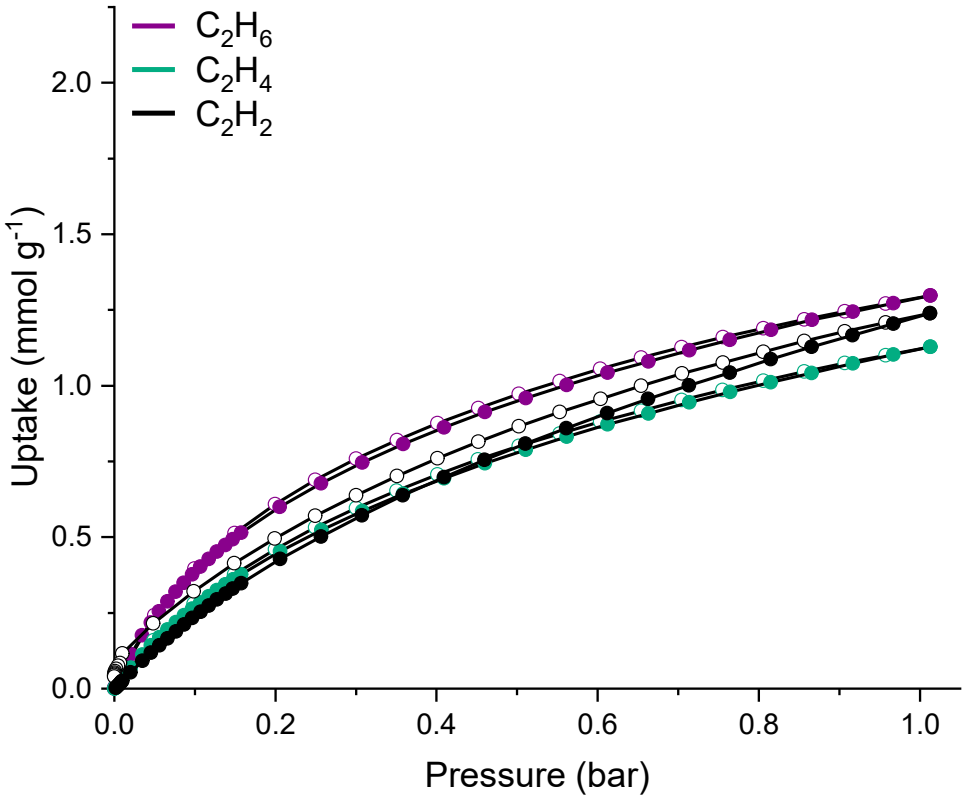

Fig. S64. C_2H_6 (purple), C_2H_4 (cyan) and C_2H_2 (black) sorption isotherms of **[2]CIM** at 298 K. Full circles: adsorption; empty circles: desorption.

Gas sorption selectivities

Table S4. Fitting and IAST parameters of non-linear Tóth isotherms of **[2]CIM** at various temperatures.

Gas	Temp. [K]	**Affinity const. *K* [1/bar]**	**Max. uptake *q*max [mmol/g]**	**Heterogenity Parameter *t***	**R^2**
C_2H_6	273	4.952865	7.984603	0.3306	0.999755
	283	4.716529	5.681336	0.3800	0.999836
	298	2.545839	3.439726	0.4952	0.999933
C_2H_4	273	2.535248	6.954115	0.3902	0.999870
	283	1.792697	5.348184	0.4532	0.999929
	298	1.285712	3.463307	0.5526	0.999960
C_2H_2	273	1.276067	11.558082	0.3831	0.999929
	283	0.832033	8.671581	0.4555	0.999956
	298	0.641077	5.083795	0.5837	0.999941

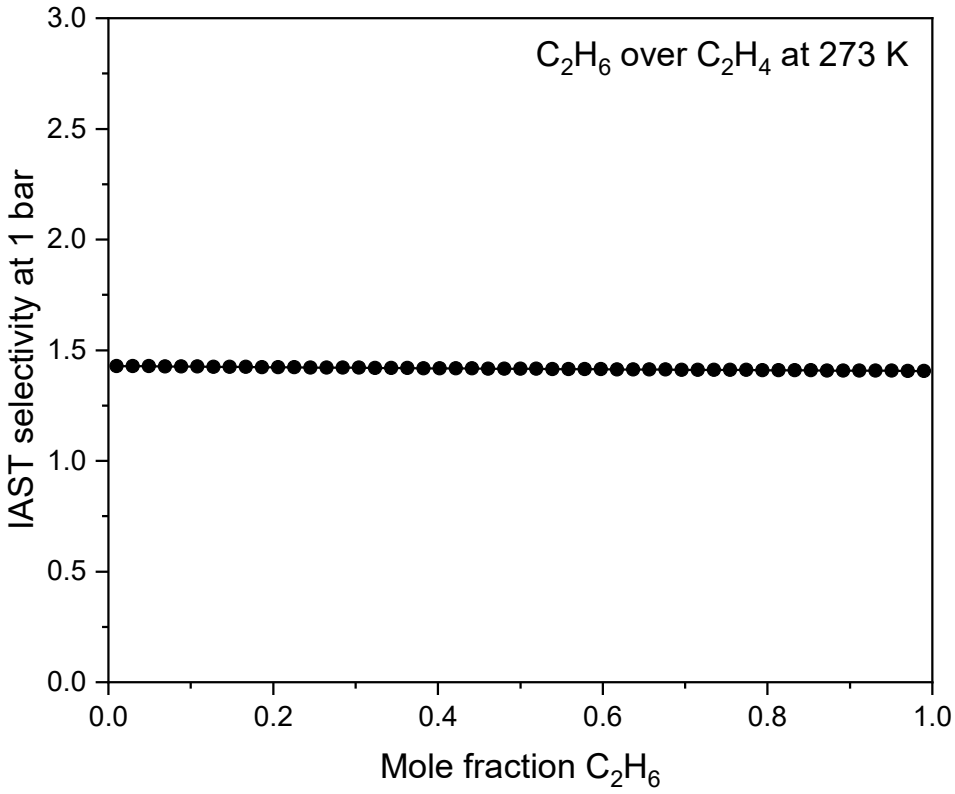

Fig. S65. IAST selectivity curve of **[2]CIM** for C_2H_6 over C_2H_4 at different mole ratios at 273 K and 1 bar.

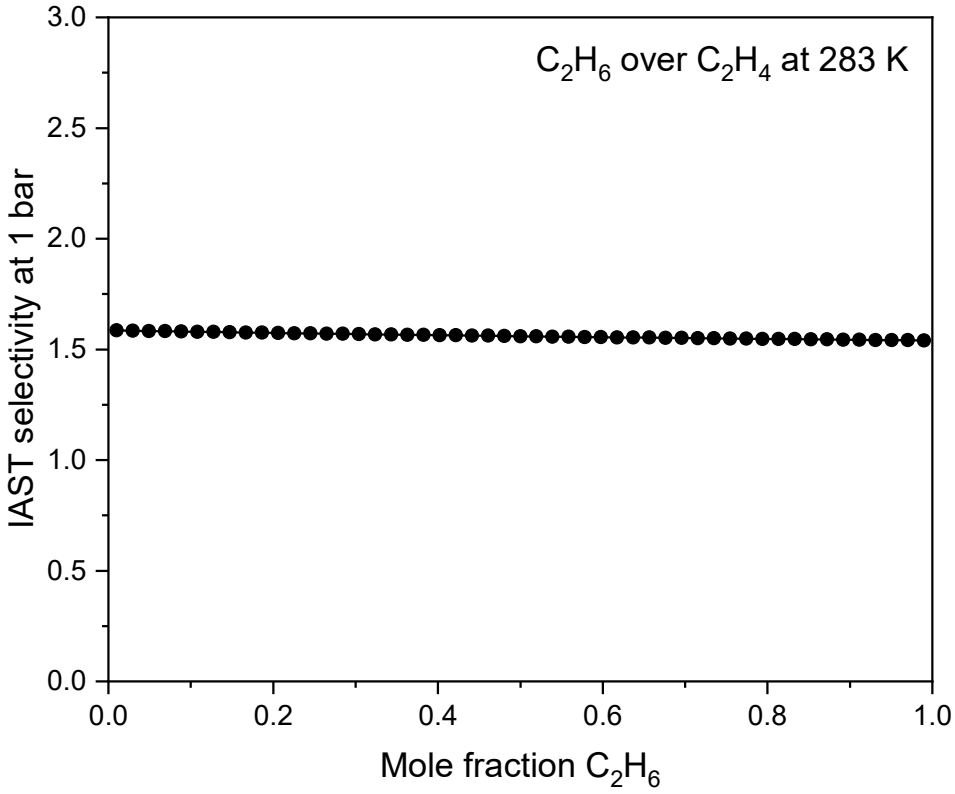

Fig. S66. IAST selectivity curve of **[2]CIM** for C_2H_6 over C_2H_4 at different mole ratios at 283 K and 1 bar.

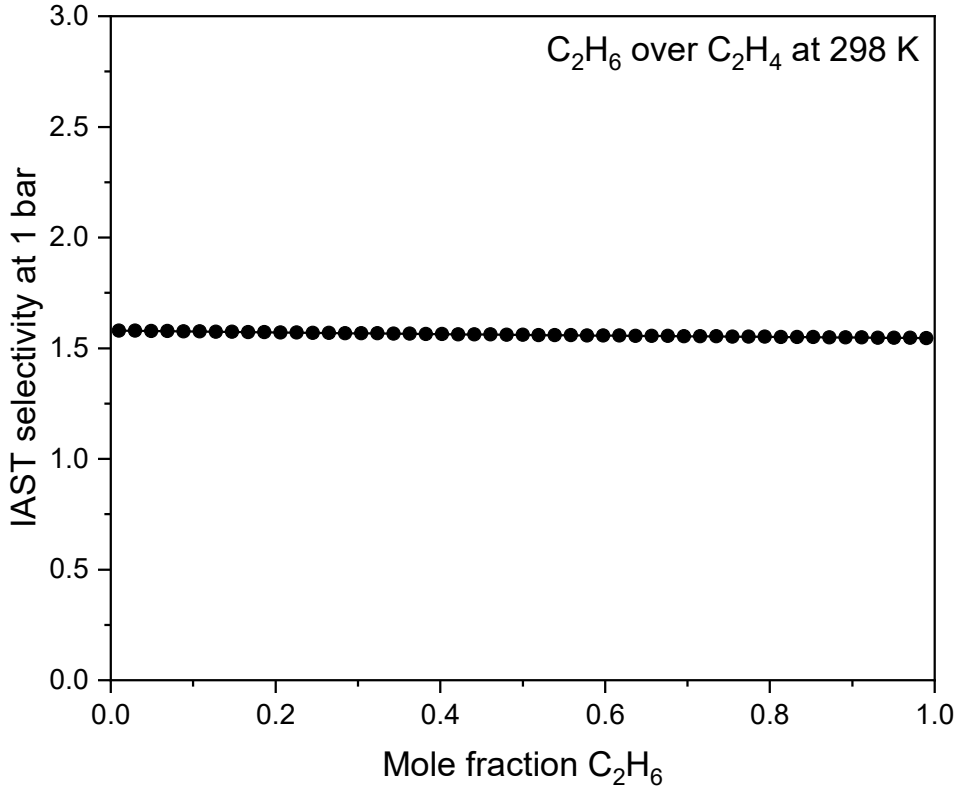

Fig. S67. IAST selectivity curve of **[2]CIM** for C_2H_6 over C_2H_4 at different mole ratios at 298 K and 1 bar.

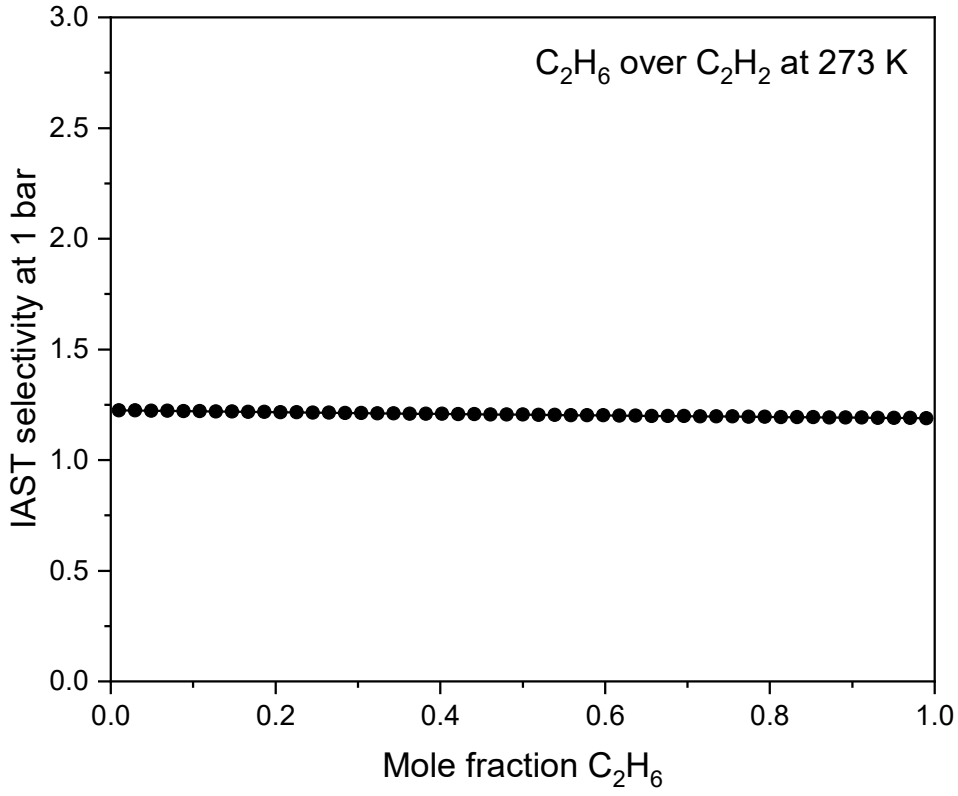

Fig. S68. IAST selectivity curve of **[2]CIM** for C_2H_6 over C_2H_2 at different mole ratios at 273 K and 1 bar.

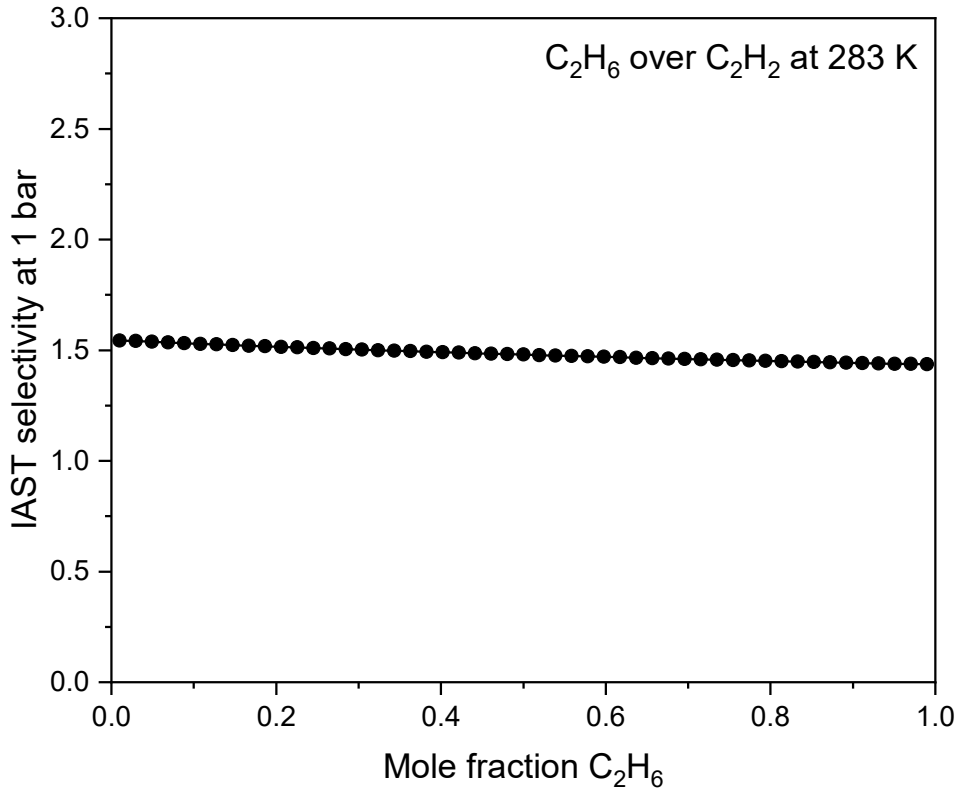

Fig. S69. IAST selectivity curve of **[2]CIM** for C_2H_6 over C_2H_2 at different mole ratios at 283 K and 1 bar.

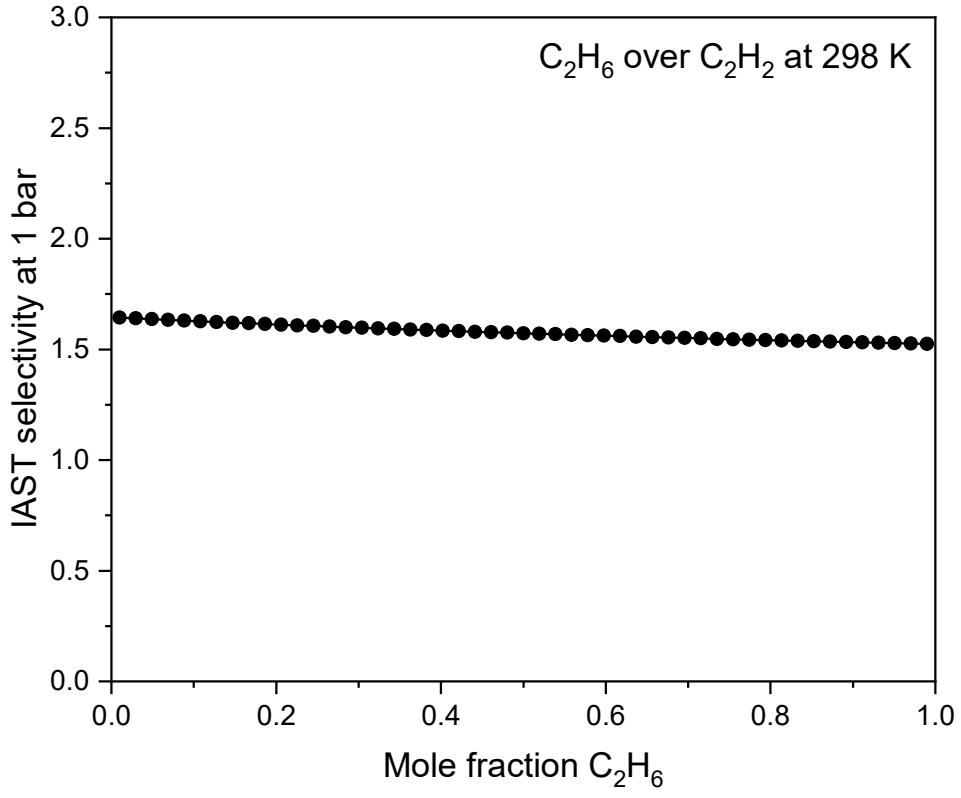

Fig. S70. IAST selectivity curve of **[2]CIM** for C_2H_6 over C_2H_2 at different mole ratios at 298 K and 1 bar.

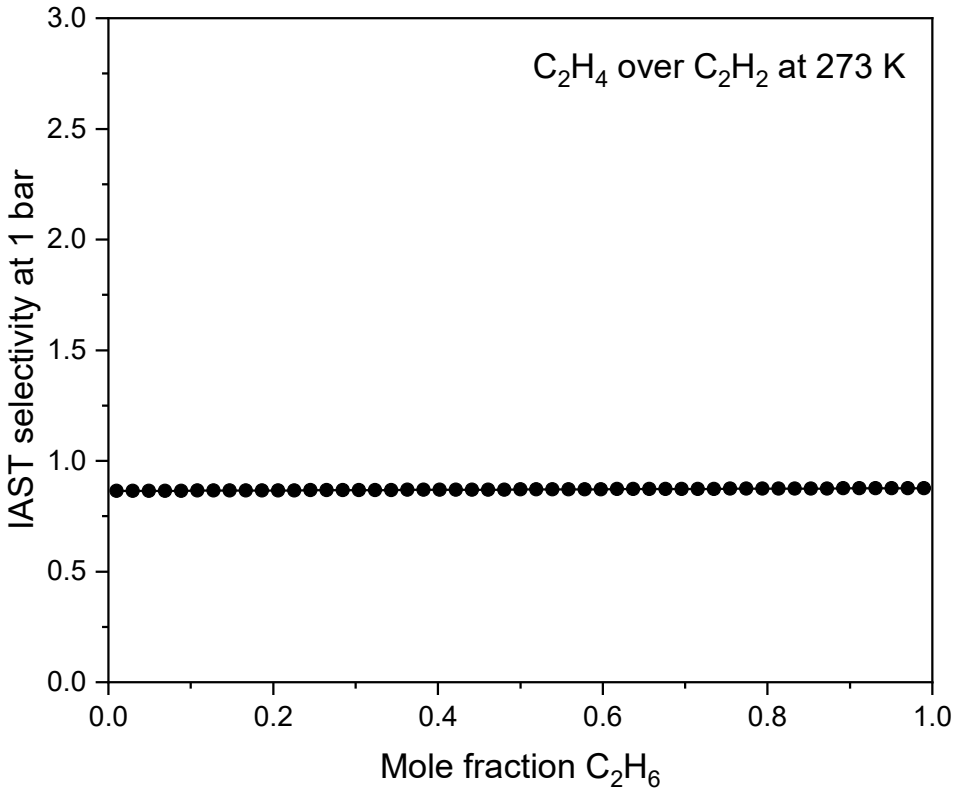

Fig. S71. IAST selectivity curve of **[2]CIM** for C_2H_4 over C_2H_2 at different mole ratios at 273 K and 1 bar.

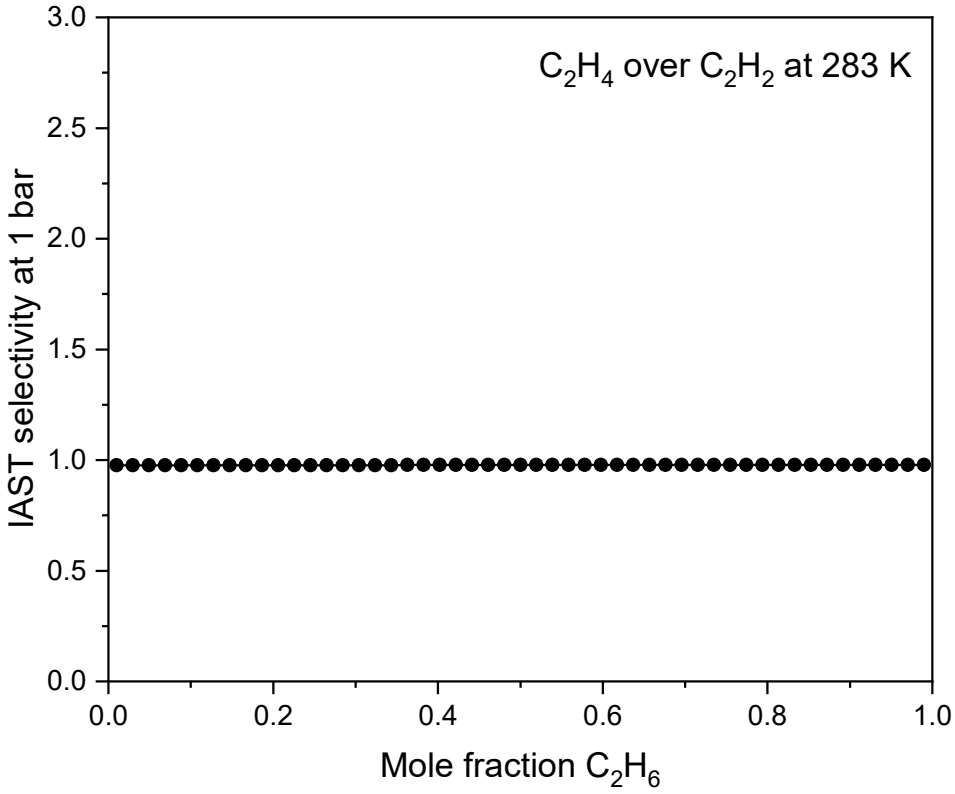

Fig. S72. IAST selectivity curve of **[2]CIM** for C_2H_4 over C_2H_2 at different mole ratios at 283 K and 1 bar.

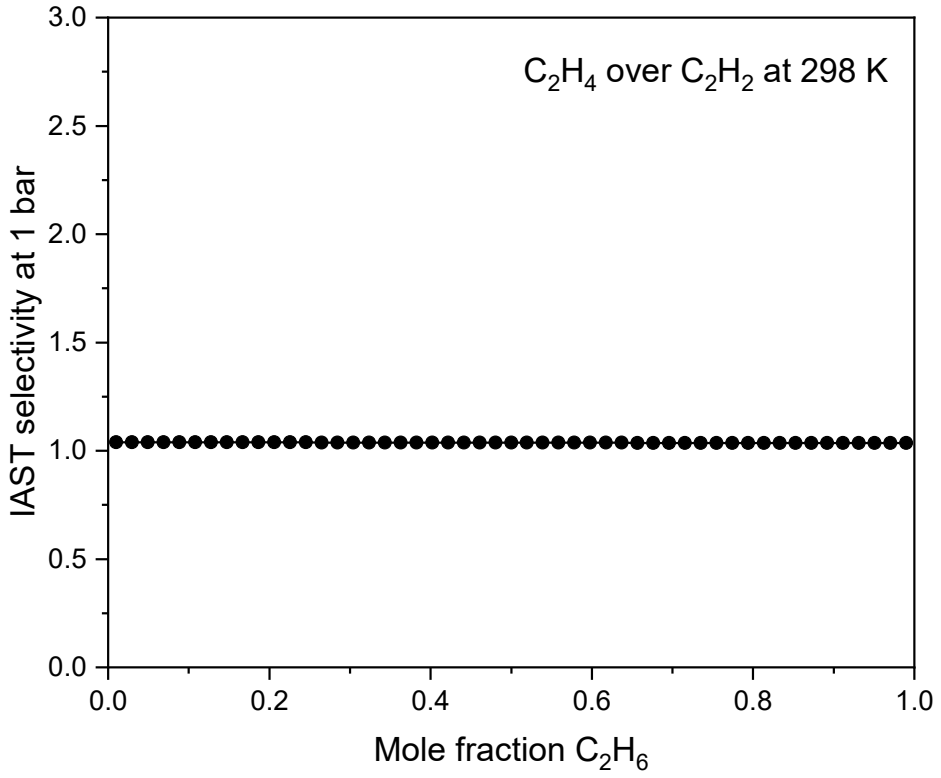

Fig. S73. IAST selectivity curve of **[2]CIM** for C_2H_4 over C_2H_2 at different mole ratios at 298 K and 1 bar.

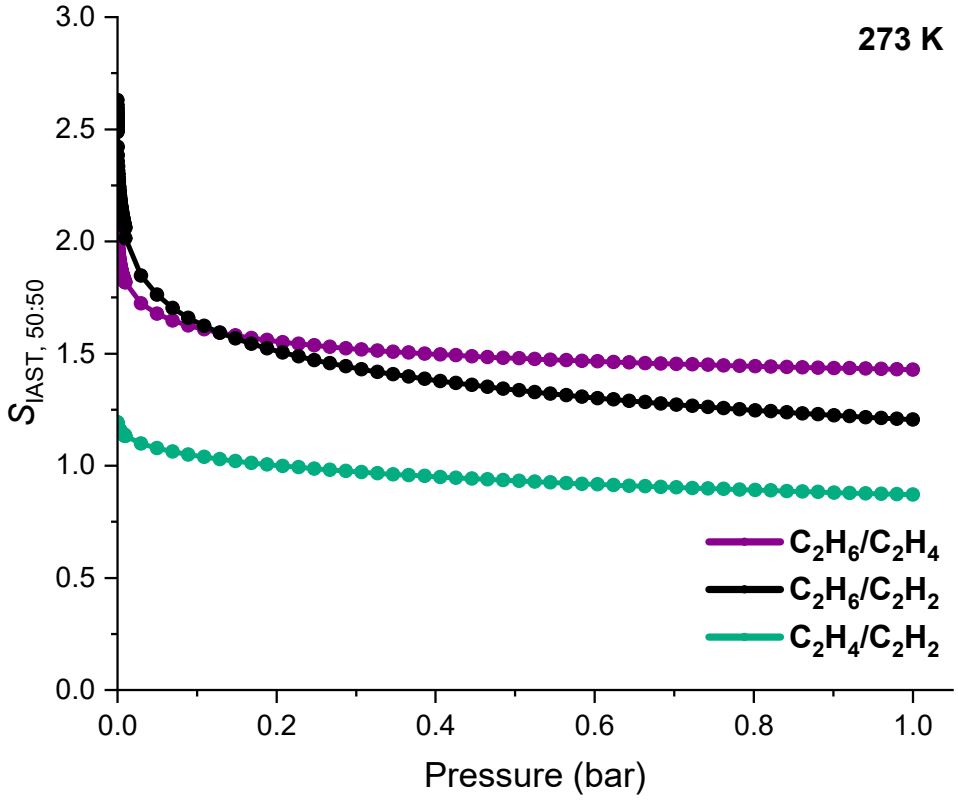

Fig. S74. Pressure dependent IAST selectivities (50:50 mixtures) of **[2]CIM** of ethane over ethylene (purple), ethane over acetylene (black) and ethylene over acetylene (green) at 273 K.

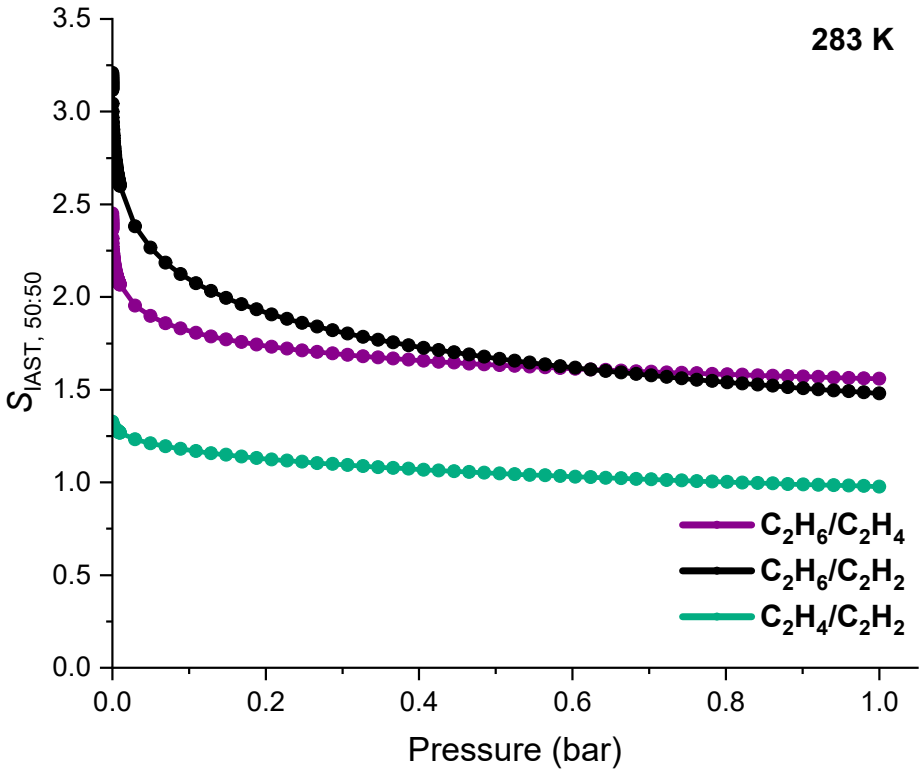

Fig. S75. Pressure dependent IAST selectivities (50:50 mixtures) of **[2]CIM** of ethane over ethylene (purple), ethane over acetylene (black) and ethylene over acetylene (green) at 283 K.

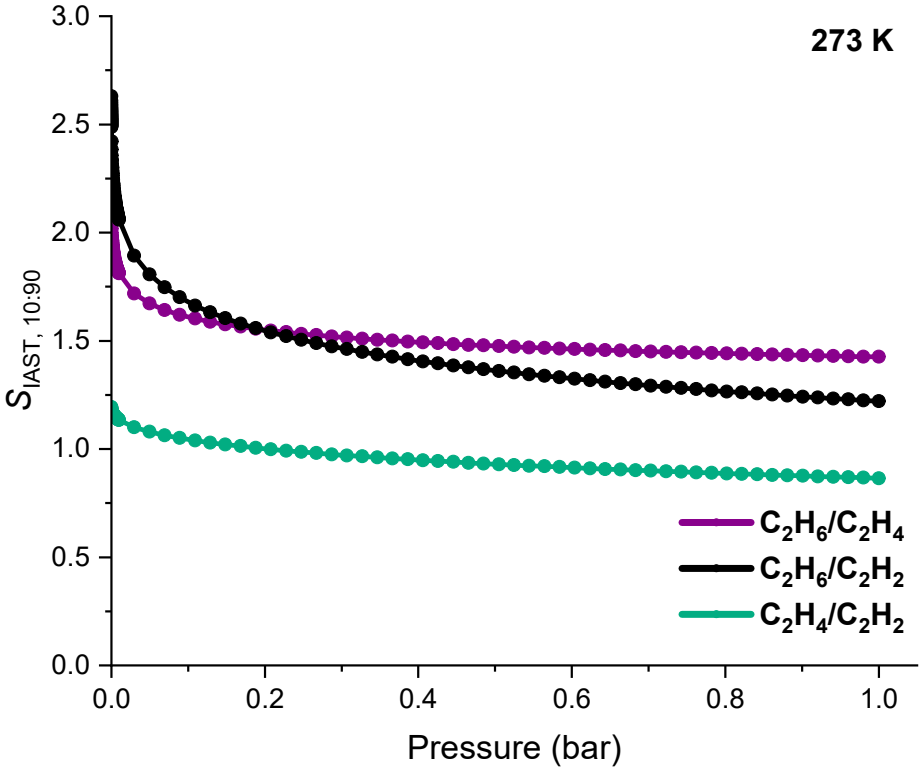

Fig. S76. Pressure dependent IAST selectivities (10:90 mixtures) of **[2]CIM** of ethane over ethylene (purple), ethane over acetylene (black) and ethylene over acetylene (green) at 273 K.

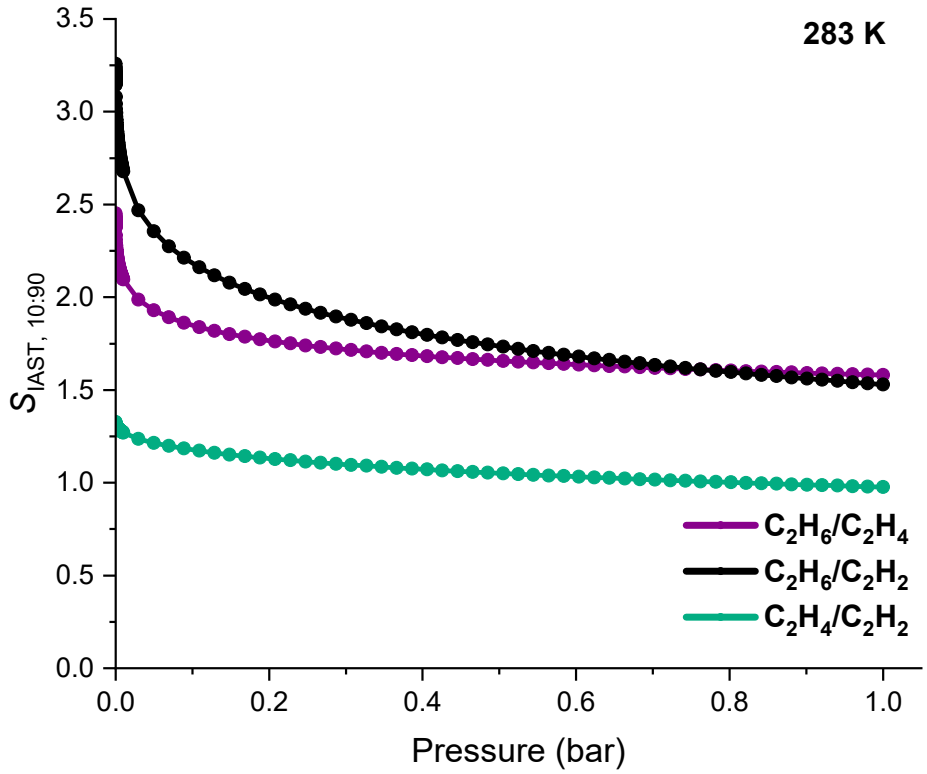

Fig. S77. Pressure dependent IAST selectivities (10:90 mixtures) of **[2]CIM** of ethane over ethylene (purple), ethane over acetylene (black) and ethylene over acetylene (green) at 283 K.

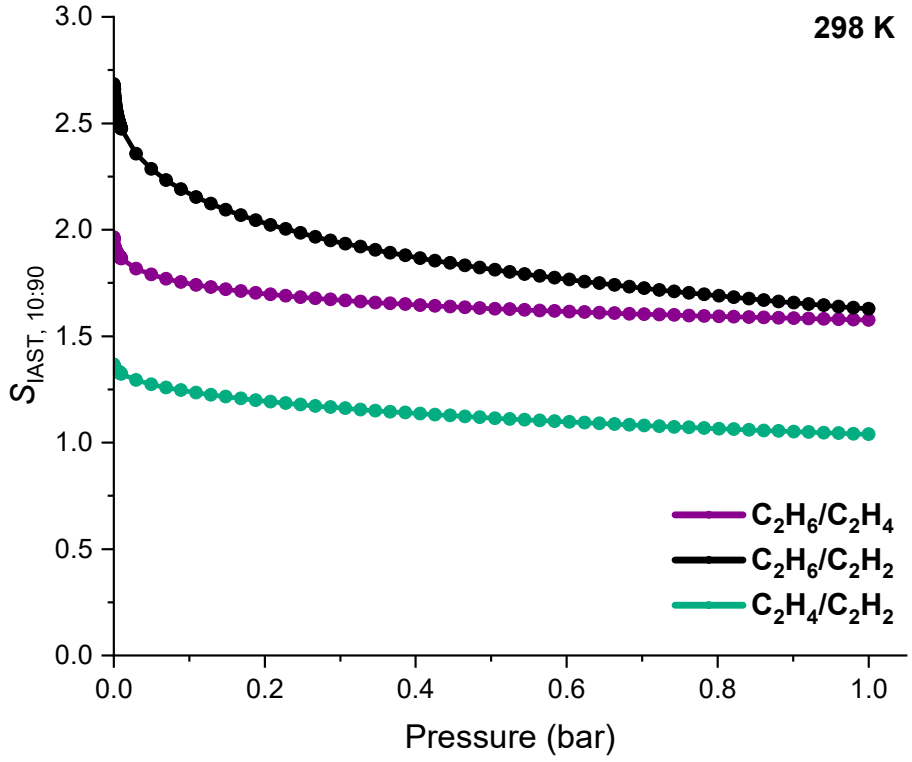

Fig. S78. Pressure dependent IAST selectivities (10:90 mixtures) of **[2]CIM** of ethane over ethylene (purple), ethane over acetylene (black) and ethylene over acetylene (green) at 298 K.

10. Supplementary references

1 Ikemoto, K., Kobayashi, R., Sato, S. & Isobe, H. Synthesis and Bowl-in-bowl Assembly of a Geodesic Phenylene Bowl. *Angew. Chem. Int. Ed.* **56**, 6511-6514 (2009).

2 Lei, S., Ver Heyen, A., De Feyter, S., Surin, M., Lazzaroni, R., Rosenfeldt, S., Ballauff, M., Lindner, P., Mössinger, D. & Höger, S. Two-Dimensional Oligo(phenylene-ethynylene-butadiynylene)s: All-Covalent Nanoscale Spoked Wheels. *Chem. Eur. J.* **15**, 2518-2535 (2009).

3 Shimizu, M., Tatsumi, H., Mochida, K., Oda, K. & Hiyama, T. 2008. Silicon-Bridge Effects on Photophysical Properties of Silafluorenes. *Chem. Asian J.* **3**, 1238-1247 (2008).

4 Frisch, M. J. et al. Gaussian 16, Revision B.01, Gaussian, Inc., Wallingford CT, 2016.

5 Saturno, A. F. Daniel Berthelot's equation of state. *J. Chem. Educ.* **39**, 464 (1962).

6 Kontogeorgis, G. M., Privat, R. & Jaubert, J.-N. Taking Another Look at the van der Waals Equation of State–Almost 150 Years Later. *J. Chem. Eng. Data* **64**, 4619-4637 (2019).

7 Mallard, P. J. L. a. W. G. *NIST Chemistry WebBook, NIST Standard Reference Database Number 69, National Institute of Standards and Technology, Gaithersburg MD, 20899, https://doi.org/10.18434/T4D303, (retrieved February 8, 2022).*

8 Myers, A. L. & Prausnitz, J. M. Thermodynamics of mixed-gas adsorption. *AlChE J.* **11**, 121-127 (1965).